

**A STUDY ON DATA-DRIVEN IMPEDANCE
MATCHING IN FOUR CHANNELS BILATERAL
TELEOPERATION**

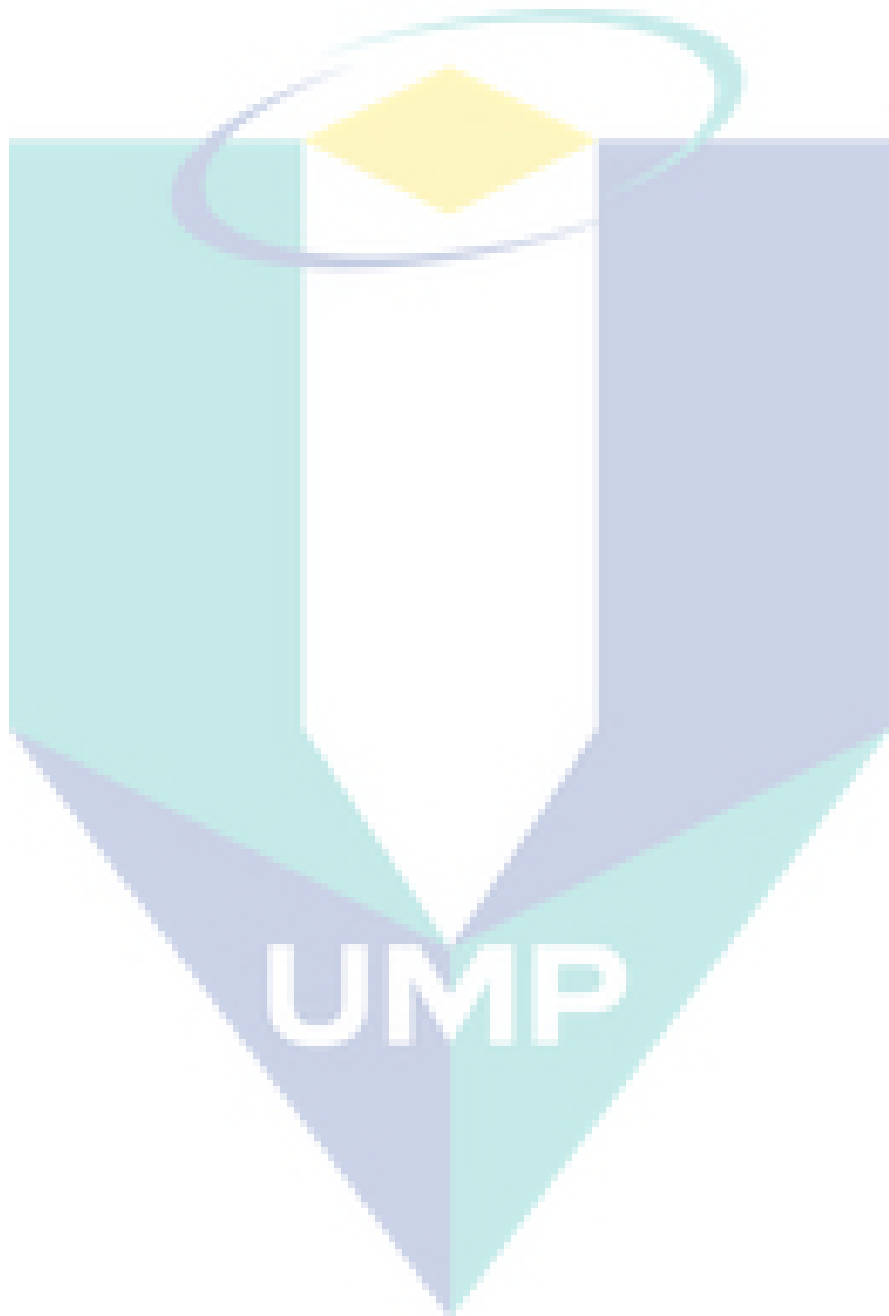
The logo of the University of Malaysia Pahang (UMP) is a shield-shaped emblem. It features a yellow diamond at the top, a white vertical stripe in the center, and a teal and blue background. The letters 'UMP' are prominently displayed in white at the bottom of the shield.

**MOHD SYAKIRIN BIN RAMLI
HAMZAH BIN AHMAD
SAIFUDIN BIN RAZALI
NUR AQILAH BINTI OTHMAN
MOHD RAZALI BIN DAUD
ADDIE IRAWAN BIN HASHIM
MOHD NIZAM BIN MD ISA**


**RESEARCH VOTE NO:
RDU1703139**

**Faculty of Electrical & Electronics Engr. Tech.
Universiti Malaysia Pahang**

2019



Abstract



A STUDY ON DATA DRIVEN IMPEDANCE MATCHING IN FOUR-CHANNELS BILATERAL TELEOPERATION

(*Keywords: data-driven, model-free tuning, PID control, impedance matching, fictitious signals*)

A teleoperator system comprised of dual robots namely the master robot controlled by the human operators, and remote slave robots which tracks the motion of master, where it concurrently transmits the environment's force back to the human operator. Problems arose when there exists a mismatch in terms of system dynamics between master and slave manipulators, which consequently yields to a distorted transparency between both sides of the systems. Therefore, there is a need to overcome the said mismatch pattern in the overall closed-loop architecture. The main objective of this research is to design and develop control algorithms to drive both sides of the master and slave system to attain symmetrical impedance between them. By ensuring that both sides are symmetry, a good transparency is feasible. The proposed techniques was to introduce an equalizer or controller connected to the master manipulator. Then, by utilizing the model-free approach, namely the Fictitious-Reference-Iterative-Tuning (FRIT), the controller can then be properly tuned to obtain a good control performance. This project focused on the computational modeling where the proposed impedance matching algorithms have been investigated and analyzed utilizing the Matlab (Simulink) Software.

There are several possible applications that can employ the control algorithms derived from this project. Obviously, underwater tele-robotics may find the proposed technique is beneficial since the model-free approach which dealt mainly on the measured input-output data in tuning procedure, can help to overcome the uncertainty that exists in the underwater environment. Besides, we also had investigated and analyzed the feasibility of this technique when working with multi-slave manipulators configuration. Hence, this open the opportunity for applications that utilize the multi-robots configurations such as in automotive or manufacturing industries.

In general, it was found that a symmetric impedance between the master and slave manipulators attainable with the utilization of equalizer in the form of Laguerre network connected in feedback-loop to the master manipulator. This was also applicable for the case of single-master-multiple-slaves system, but additional

passive decomposition algorithm must also be employed to treat the multi-slaves manipulators into the Locked and Shape subsystems.

Key researchers:

Dr. Mohd Syakirin bin Ramli

Assoc. Prof. Dr. Hamzah bin Ahmad

Assoc. Prof. Dr. Razali bin Daud

Dr. Addie Irawan bin Hashim

Dr. Saifudin bin Razali

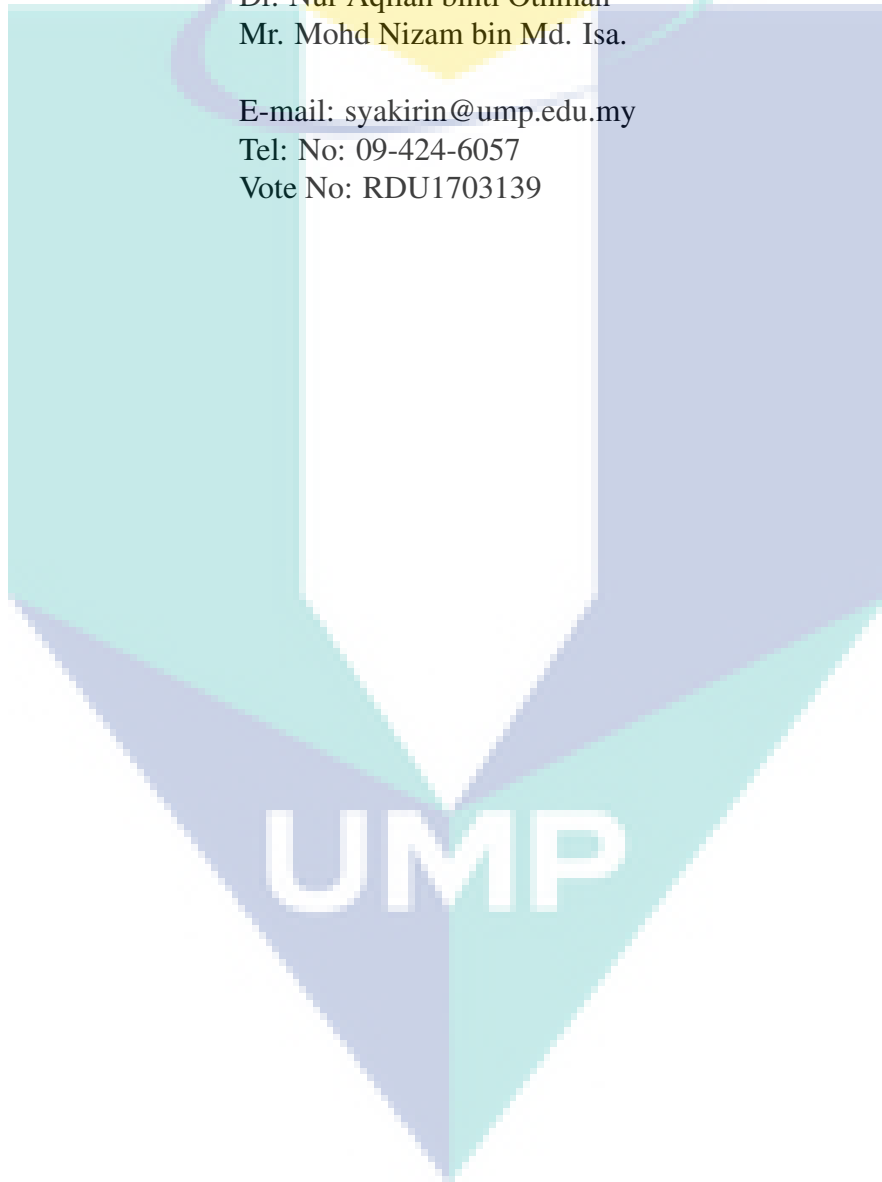
Dr. Nur Aqilah binti Othman

Mr. Mohd Nizam bin Md. Isa.


E-mail: syakirin@ump.edu.my

Tel: No: 09-424-6057

Vote No: RDU1703139



Abstrak



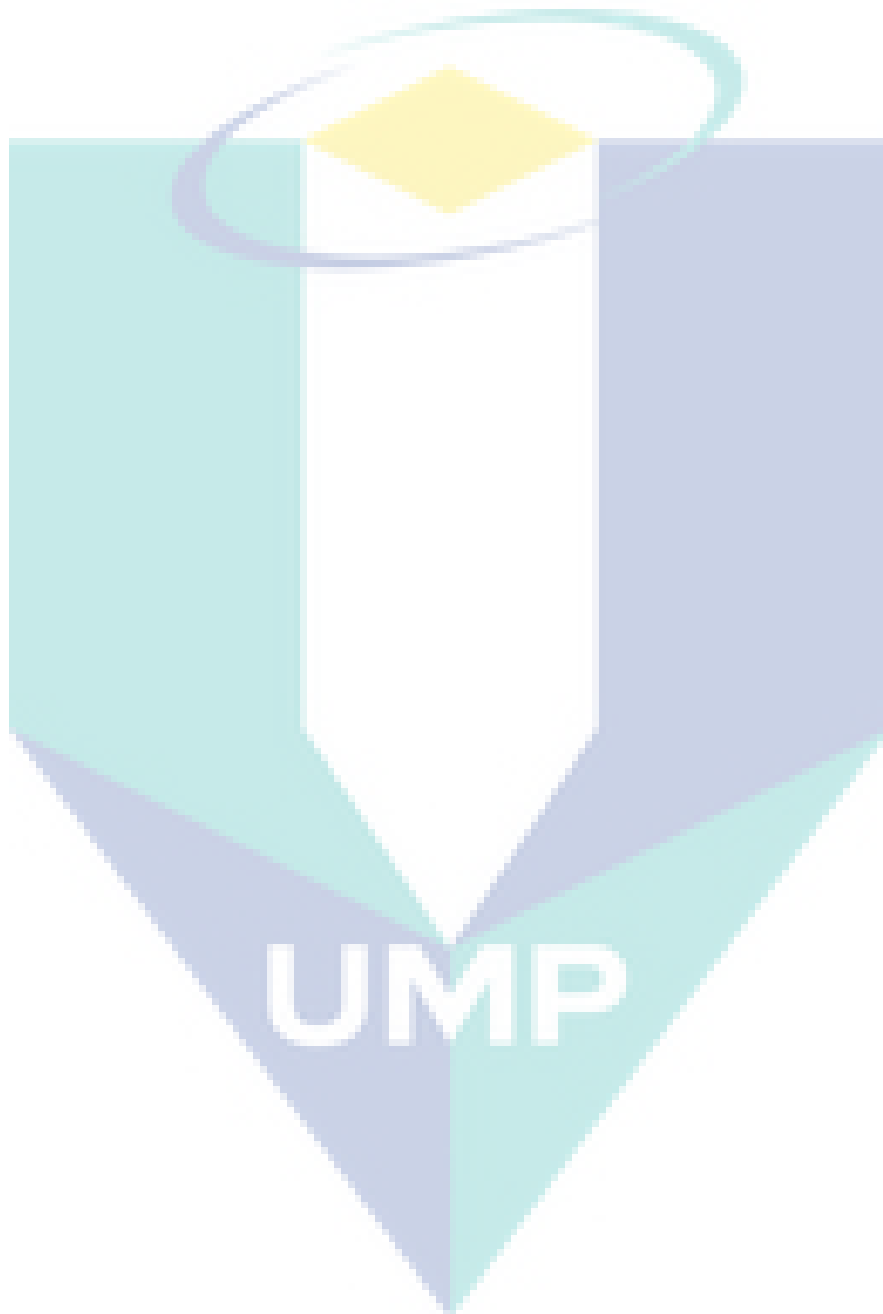
A STUDY ON DATA DRIVEN IMPEDANCE MATCHING IN FOUR-CHANNELS BILATERAL TELEOPERATION

Sistem teleoperator terdiri daripada dual robot iaitu robot induk yang dikendalikan oleh pengendali manusia, dan robot hamba jarak jauh yang mengesan pergerakan tuan, di mana ia secara bersamaan mengirimkan kekuatan persekitaran kembali kepada pengendali manusia. Masalah timbul apabila terdapat ketidakcocokan dalam hal dinamika sistem antara manipulator induk dan hamba, yang mengakibatkan ketelusan yang terpesong antara kedua-dua belah sistem. Oleh itu, terdapat keperluan untuk mengatasi pola ketidakcocokan tersebut dalam keseluruhan seni bina gelung tertutup. Objektif utama penyelidikan ini adalah untuk merancang dan mengembangkan algoritma kawalan untuk mendorong kedua-dua sisi sistem induk dan hamba untuk mencapai impedans simetris di antara mereka. Dengan memastikan bahawa kedua-dua belah pihak adalah simetri, ketelusan yang baik dapat dilaksanakan. Teknik yang dicadangkan adalah memperkenalkan suatu penyama atau pengawal yang disambungkan ke manipulator induk. Kemudian, dengan menggunakan pendekatan bebas model, iaitu Fictitious-Reference-Iterative-Tuning (FRIT), pengawal kemudian dapat ditala dengan sempurna untuk mendapatkan prestasi kawalan yang baik. Projek ini memfokuskan pada pemodelan komputasi di mana algoritma pencocokan impedans yang dicadangkan telah diselidiki dan dianalisis menggunakan Perisian Matlab (Simulink).

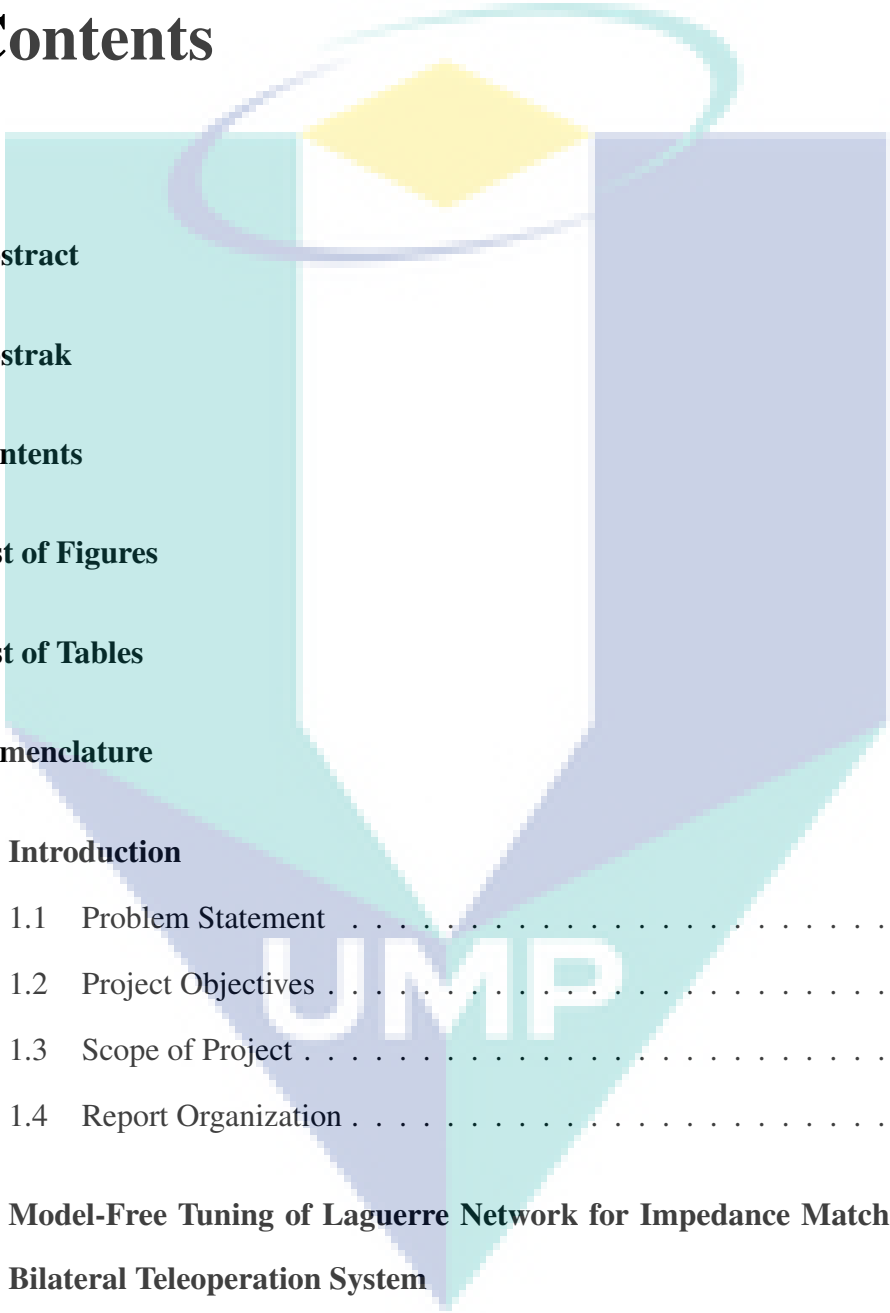
Terdapat beberapa kemungkinan aplikasi yang dapat menggunakan algoritma kawalan yang berasal dari projek ini. Secara nyata, telerobotik bawah laut mungkin mendapati teknik yang dicadangkan itu bermanfaat kerana pendekatan bebas model yang menangani terutamanya kepada data input-output yang diukur dalam prosedur penalaan, dapat membantu mengatasi ketidakpastian yang wujud di lingkungan bawah air. Selain itu, kami juga telah menyelidiki dan menganalisis kemungkinan teknik ini ketika bekerja dengan konfigurasi manipulator multi-hamba. Oleh itu, ini membuka peluang untuk aplikasi yang menggunakan konfigurasi multi-robot seperti dalam industri automotif atau pembuatan.

Secara umum, didapati bahawa impedans simetri antara manipulator master dan slave dapat dicapai dengan penggunaan penyama dalam bentuk jaringan Laguerre yang dihubungkan dalam suap-gelung ke manipulator induk. Ini juga berlaku

untuk sistem satu-induk-multi-hamba, tetapi algoritma penguraian pasif tambahan juga mesti digunakan untuk merawat manipulator multi-hamba ke dalam subsistem *Locked dan Shape*.



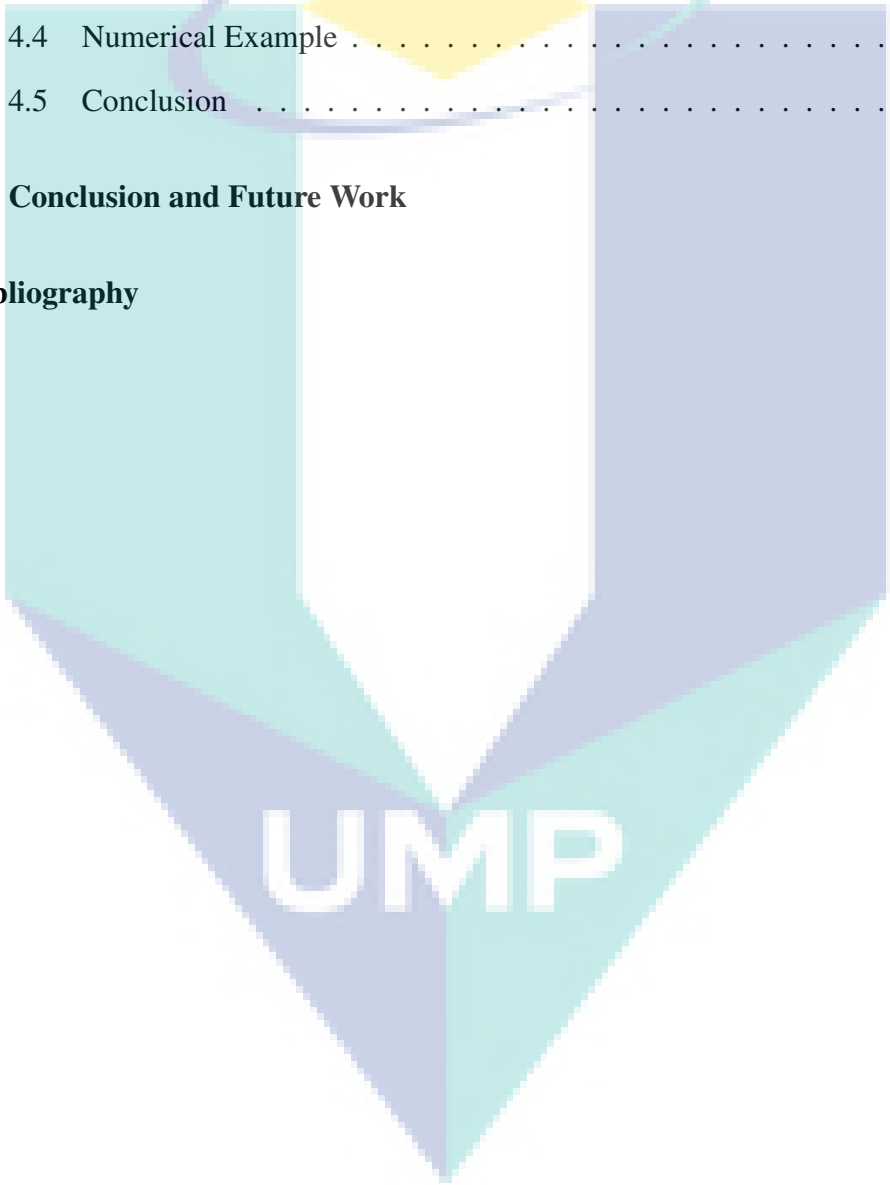
Contents

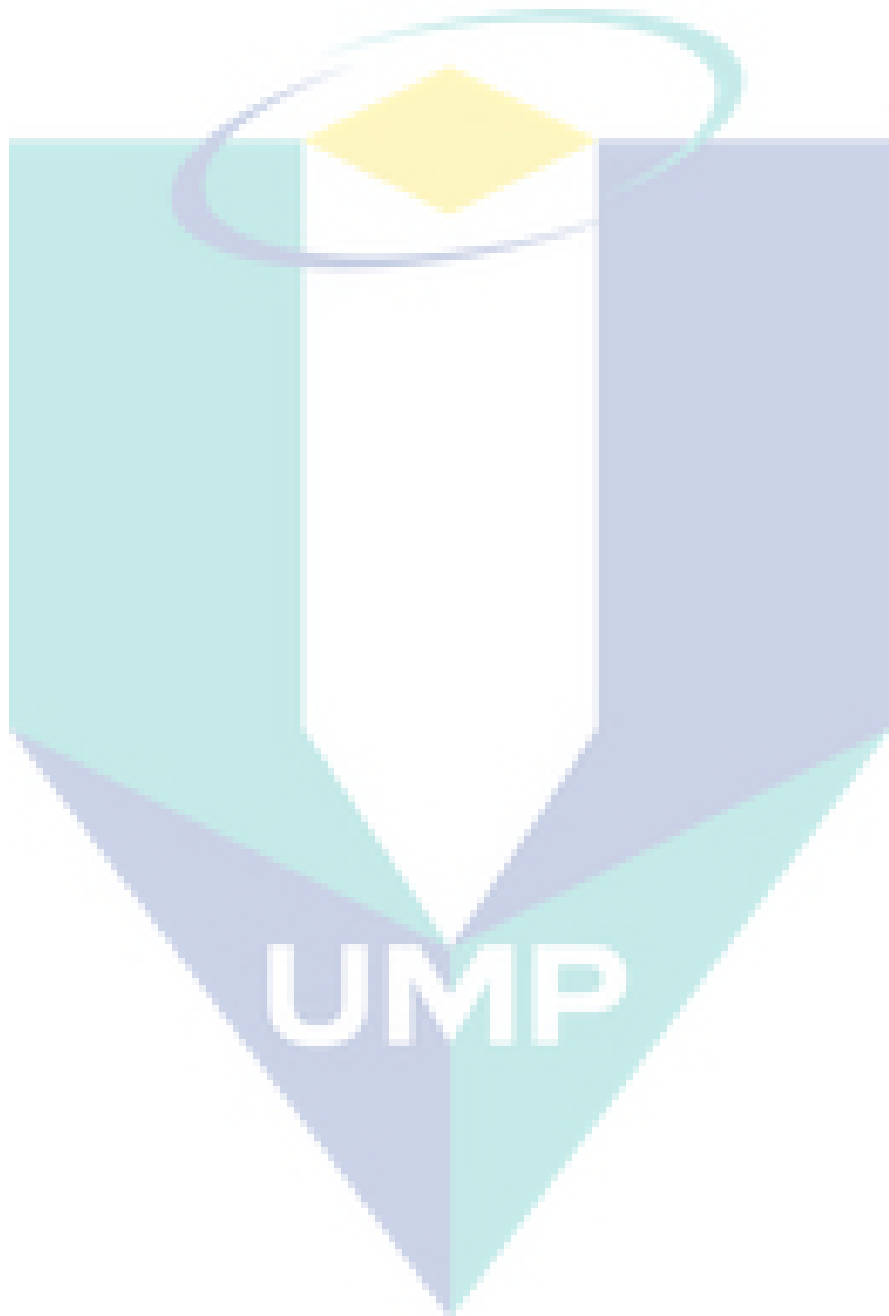


Abstract	i
Abstrak	iii
Contents	vii
List of Figures	x
List of Tables	xi
Nomenclature	xi
1 Introduction	1
1.1 Problem Statement	2
1.2 Project Objectives	4
1.3 Scope of Project	5
1.4 Report Organization	5
2 Model-Free Tuning of Laguerre Network for Impedance Matching in Bilateral Teleoperation System	7
2.1 Introduction	7
2.2 Problem Formulation	9
2.2.1 Overview of the two-ports network	9
2.2.2 Basic Structure of a Teleoperation System	11

2.2.3	Improvement to The Existing Structure	12
2.3	Algorithm for Impedance Matching	14
2.3.1	Particle Swarm Optimization	14
2.3.2	Equalizer $F(z)$ in the form of a Laguerre Network	15
2.3.3	Fictitious-Reference-Iterative Tuning	16
2.3.4	Attaining a matched impedance via PSO and FRIT	17
2.4	Numerical Results and Analysis	19
2.5	Conclusion	22
3	Data-driven Impedance Matching in Multilateral Teleoperation Systems	25
3.1	Introduction	25
3.2	Problem formulation	28
3.2.1	Notations and graph theory	28
3.2.2	Overview of the two-ports network	29
3.2.3	Teleoperation architecture	30
3.3	Multilateral to bilateral teleoperation	32
3.3.1	Total dynamics of the slave agents	32
3.3.2	Passive decomposition[1] in handling	34
3.3.3	Tele-operation time T_{tele}	38
3.4	Impedance matching by FRIT	39
3.4.1	FRIT	41
3.4.2	Laguerre network	43
3.4.3	Selection of dynamics C_1, C_2, C_3 and C_4	48
3.5	Numerical example	49
3.6	Conclusion	52
4	A Fictitious Reference Iterative Tuning Method for Buck Converter-Powered Motor Control System	55

4.1	Introduction	55
4.2	Problem Statements	58
4.2.1	Buck-converter powered dc motor model	59
4.3	Algorithm for Controller Tuning	60
4.3.1	A brief review of SKF algorithm	60
4.3.2	Fictitious Reference Iterative Tuning	62
4.4	Numerical Example	64
4.5	Conclusion	68
5	Conclusion and Future Work	69
	Bibliography	71





List of Figures

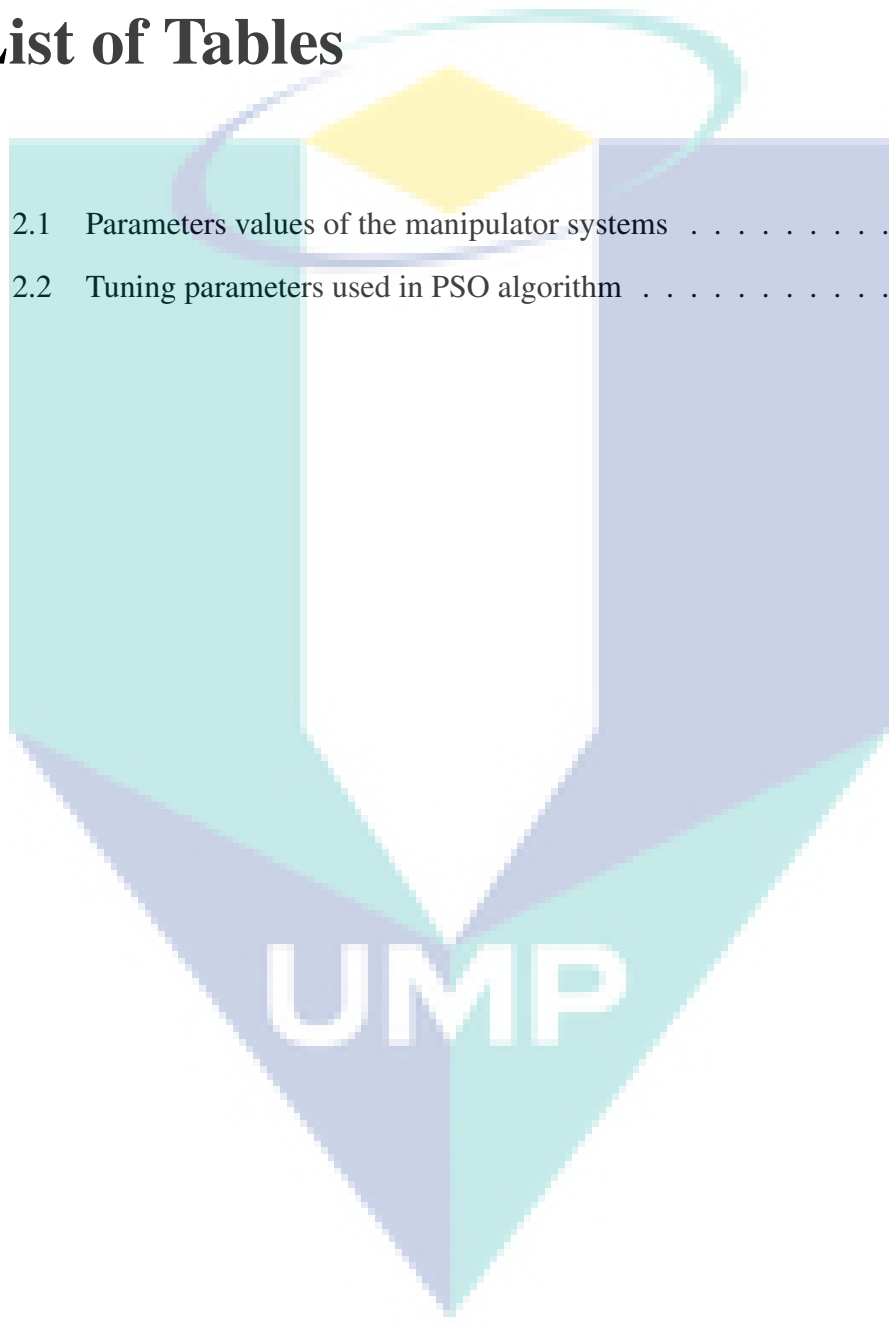
1.1	General two-port model of a bilateral teleoperation system	3
2.1	General two-ports model of a bilateral teleoperation system [2] . . .	10
2.2	Four-channels structure proposed by Zhu & Salcudean [2]	12
2.3	Four-channels structure illustrating the additional equalizer F	13
2.4	Structure of the Laguerre network	15
2.5	Two-steps of tuning:(a) to attain H^* , (b) to attain F^*	17
2.6	Velocity matching through equalizer $H(z)$	20
2.7	Convergence of the cost function J_H	21
2.8	Location of poles and zeros of $H(z)$	22
2.9	Performance comparison before and after tuning.	23
2.10	Convergence of the cost function J_F	24
3.1	General two-ports model of a bilateral teleoperation system[3]. . . .	29
3.2	General structure of teleoperation indicating the equalizer F and intervenient impedances, C_{mc} & C_{sc}	40
3.3	Concept of impedance matching by FRIT.	42
3.4	Two-steps of tuning[4] to obtain optimum F	44
3.5	Structure of the Laguerre Network.	46
3.6	Communication topology between agents (No. 6 is the virtual agent representing the target object).	49

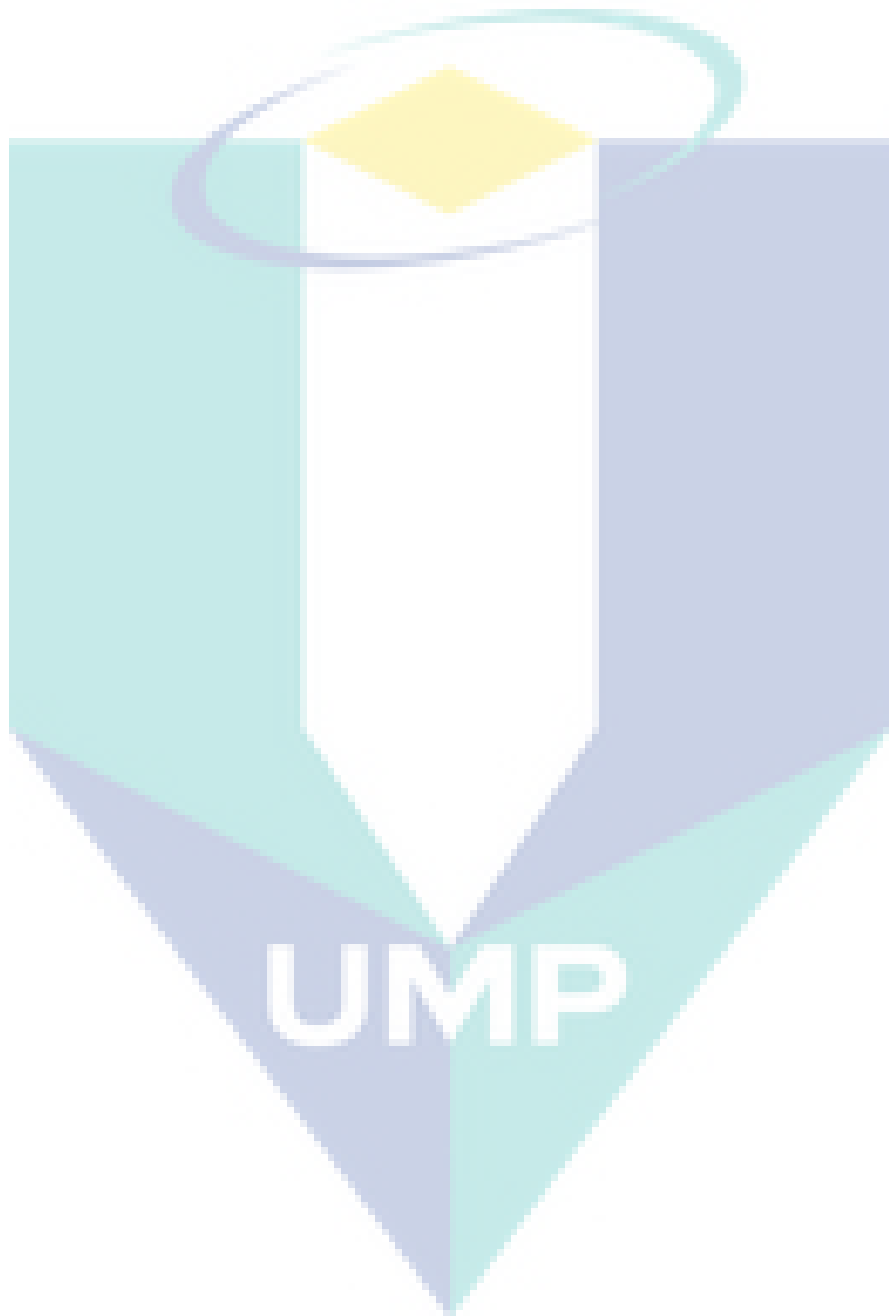
3.7	Asymptotic convergence of the agents onto their intended final positions on the target object as $t < T_{tele}$, with $\varphi(0) = 0$	51
3.8	Velocity matching through gain $\mathcal{H}(z)$	52
3.9	Comparison of optimized fictitious signal (3.52) with the initial f_{Lc}	53
3.10	Signals comparison for positions, velocities and forces.	54
4.1	Block diagram of the closed system	58
4.2	Schematic of the buck converter powered DC motor system	60
4.3	Fictitious signal $\tilde{r}(k)$ derivation	63
4.4	Angular velocity and duty responses for $\rho^0 = [0.5, 1, 0.25, 0.5]$ captured in a time interval $t_0 = 0$ s and $t_f = 0.3$ s.	66
4.5	The convergence of the cost function J_2	66
4.6	Performance comparison between the model-free design (PID controller tuned with FRIT and SKF) and model-based design (SFCI controller designed by pole-placement method).	67
4.7	Performance comparison in terms of duty ratio between the two controllers.	68



List of Tables

2.1	Parameters values of the manipulator systems	19
2.2	Tuning parameters used in PSO algorithm	20





Chapter 1

Introduction

Teleoperation system extend the human operator's capability to perform task at the remote site. In general, the teleoperation system can be categorized into bilateral teleoperation[5, 6] and multilateral teleoperation[7]. The bilateral teleoperation system commonly consists of only a single master and single slave manipulators as part of its basic structure. Meanwhile, the multilateral teleoperation system requires more number of manipulators, either on the master side or slave sides.

Various studies that have been carried out on bilateral teleoperation focused on the utilization of 4-channels structures. In [3, 8], it was emphasized that the proper use of all four channels is of critical importance in achieving high performance of teleoperation in the sense accurate transmission of task impedance to the operator. Some instances of works on 4-channels structures are discussed in [2] where a position and rate control was proposed, and in [9] where the symmetric impedance matched with tracking was designed. In [10], a nonlinear teleoperation system has been considered. Other technique that also utilizes the 4-channels structure is the wave-variable control as surveyed in [15]. The example of applications on wave variable control especially in multilateral framework was discussed in [16].

Two main issues normally addressed in the research field of teleoperation: (1) stability, and (2) transparency. Considering the latter case, the transparency between

the master-slave manipulators in a bilateral teleoperation system can be achieved by having a matched impedance between both sides of the structures. In next section, we elaborate further our problem formulation in improving the transparency by considering both cases of bilateral and multilateral teleoperation .

1.1 Problem Statement

To establish a clear argument on the problem statement of our work, we provide the general background of the overall teleoperation hereupon. The relation between the master and slave in a bilateral teleoperation environment can be represented by a two-ports network as shown in Fig. 1.1. It is desirable to obtain the transmitted impedance Z_t to be equal to the task impedance Z_e , i.e.,

$$Z_t = Z_e. \quad (1.1)$$

The two-ports network in Fig.1.1 can be further described by the general hybrid matrix formulation given by

$$\begin{bmatrix} F_h \\ \dot{p}_m \end{bmatrix} = \underbrace{\begin{bmatrix} H_{11}(s) & H_{12}(s) \\ H_{21}(s) & H_{22}(s) \end{bmatrix}}_{\mathbf{H}(s)} \begin{bmatrix} \dot{p}_s \\ -F_e \end{bmatrix} \quad (1.2)$$

where F_h, F_e are the exerted human force and reflected environment force, respectively. Meanwhile, \dot{p}_m, \dot{p}_s are the velocities of the master and slave manipulators. The transfer function $H_{ij}(s)$, $i, j = 1, 2$ is the component of hybrid matrix $\mathbf{H}(s)$ in (1.2) to describe the relationship between F_h, \dot{p}_m with \dot{p}_s, F_e .

Further solving equation (1.2), the transmitted impedance in equation (1.1) can

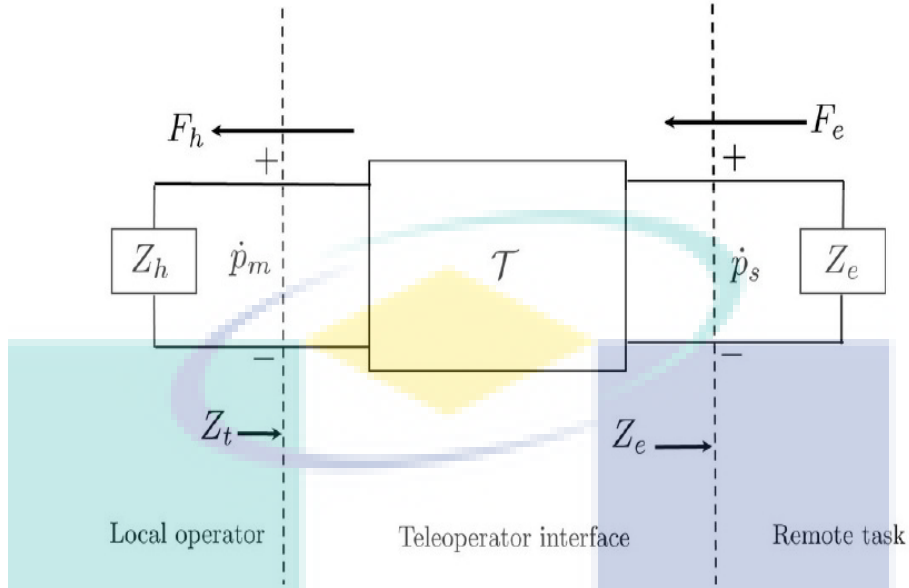


Figure 1.1: General two-port model of a bilateral teleoperation system

be defined by

$$F_h = \underbrace{(H_{11} - H_{12}Z_e)(H_{21} - H_{22}Z_e)^{-1}}_{Z_t} \dot{p}_m \quad (1.3)$$

Here, the fundamental insights that can be observed from equation (1.3) are as follows[8]:

- (a) Perfect transparency $Z_t \equiv Z_e$ requires that $H_{22} = 0$, $H_{21}Z_e = Z_e(-H_{12})$, and $H_{11} = 0$.
- (b) As $Z_e \rightarrow 0$, the transmitted impedance is insensitive to Z_e if $H_{11} \neq 0$, since Z_t depends only on the ratio $H_{11}H_{21}^{-1}$.
- (c) As $Z_e \rightarrow \infty$, the transmitted impedance becomes $H_{12}H_{22}^{-1}$, which insensitive to Z_e if $H_{22} \neq 0$.

From the given insights, it can be seen that each H_{ij} parameters in equation (1.2) is potentially affected by the mechanical dynamics of the master and slave, as well as by the control architecture. Here, the condition (a) can be achieved if there

exists symmetric in the master and slave. This implies that by choosing identical mechanical dynamics and control for both master and slave, we might obtain ideal hybrid matrix in the form of

$$\mathbf{H} = \begin{bmatrix} 0 & \mathbf{I} \\ \mathbf{I} & 0 \end{bmatrix} \quad (1.4)$$

where \mathbf{I} is the identity matrix. Here, we call this condition as a **matched impedance** (impedance matching between the transmitted impedance and the task impedance).

However, in term of actual system implementation, to satisfy the condition in equation (1.4) is practically challenging. In practical sense, the dynamic of the master and slave differs from one to the other (i.e.; a joystick as the master, and robotic hand gripper as slave). Hence, it opens for the possibility that the symmetric condition to be achieved by introducing an additional controller on the master side, so that (1.4) is feasible.

1.2 Project Objectives

The objectives of this project are stated as follows

- I) To design a controller/equalizer on the master manipulator utilizing the Laguerre function in achieving a matched impedance between the master and slave sides of the four-channels teleoperation system
- II) To improve the existing Fictitious-Reference-Iterative-Tuning (FRIT) algorithm for basis tuning of the Laguerre network implemented as the designed controller structure.

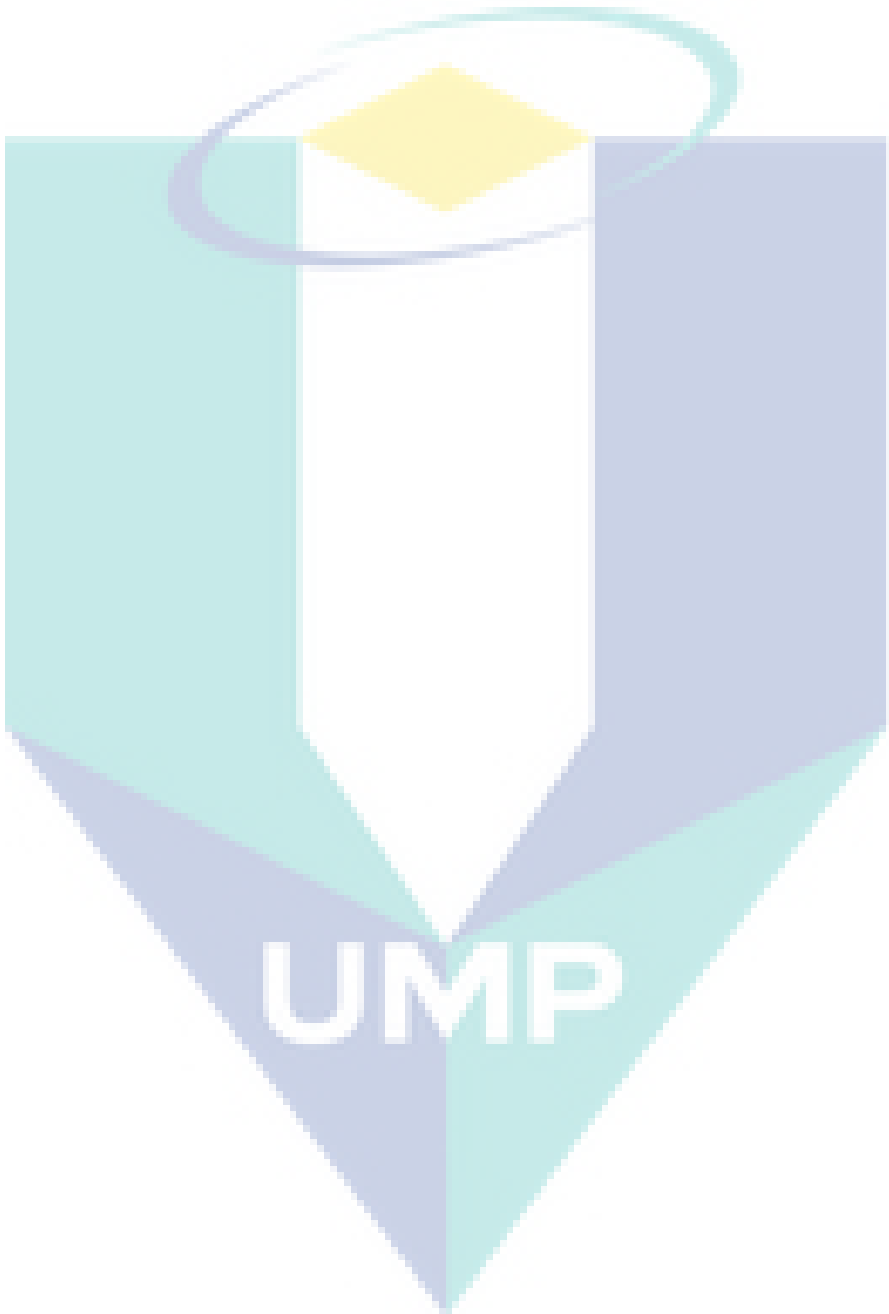
1.3 Scope of Project

In this project, the focal point of the research work will be on formulating the algorithms to attain symmetrical impedance in terms of mechanical dynamics between the master and slave sides of the teleoperation system. Hence, the numerical analyses utilizing the Matlab Computation Tools were employed to investigate the effectiveness of the proposed methods.

In designing the manipulators, we modeled our systems as comprising of a simple-mass-damper structure. Two different cases had been considered in this study namely: **Case 1)** single master - single slave systems, **Case 2)** single master - multiple slaves systems. By limiting our analyses for the systems without time delay, we assume that the information of forces and velocities were instantaneously transferred between the manipulators.

1.4 Report Organization

This report is organized as follows. In chapter 1, we stated our problem formulation, research objectives, and the scope of works in commencing this project. In chapter 2, we presented the results extracted from our paper published in *The 11th National Seminar of Unmanned System (NUSYS2019)* (DOI:10.1007/978-981-15-5281-6_23). Meanwhile in chapter 3, we presented the results published in *Indonesian Journal of Electrical Engineering 2018* (DOI:10.11591/ijeecs.v10.i2.pp713-724). Chapter 4 contains the results that was published in *Proceedings of the 5th International Conference on Electrical, Control & Computer Engineering (In-ECCE2019)* (DOI:10.1007/978-981-15-2317-5_5). Finally in chapter 5, we state our general conclusion and suggestion for the future work.



Chapter 2

Model-Free Tuning of Laguerre Network for Impedance Matching in Bilateral Teleoperation System

2.1 Introduction

A teleoperator system comprised of dual robots namely the master robot controlled by the human operators, and a remote slave robot which tracks the motion of the master, where it concurrently transmits the environment's force back to the human operator. The teleoperation system extends the human operator's capability to conduct tasks remotely from a base station. Vast applications of teleoperation systems can be found in the underwater explorations[11, 12], telesurgery[13], and military[14].

Various studies had been carried out by researchers in the past focusing on the four-channels architecture of bilateral teleoperation systems. The work in [3, 8] discussed some of the earlier ideas of the four-channels structure, and emphasized that the proper utilization of all channels is crucial in achieving accurate transmission of the task impedance to the operator. In [9], their work focused on designing symmet-

ric impedance matched with position tracking. Meanwhile in [15], the authors provide surveys on the implementation of the wave variable control in the four-channel structure in bilateral teleoperation system. On the other hand, the work in [16] considered the implementation of the wave variable control for four-channels architecture in the multilateral framework. To add further to the lists, our recent work in [17] investigated the potential of introducing a controller connected in-feedback to a single master manipulator, to attain a matched impedance with the Locked-system derived from the multiple slave manipulators formed by multi-agents system.

In this chapter, we focus on obtaining a matched impedance between the master and slave sides of a bilateral teleoperator system by using a model-free approach. Assuming the human and the remote task at the environment to form two sides of the divide, then by introducing a feedback controller to the master system, a symmetry between both sides can be established. For this purpose, a Laguerre network structure is selected as the controller due to orthonormal properties filter, which simplifies the tuning process to only finding the optimal values of the basis of the filters. Here, the task of tuning the basis of the Laguerre network can be performed by employing the Fictitious-Reference-Iterative-Tuning (FRIT) and Particle Swarm Optimization (PSO) algorithms. The FRIT only requires a set of input-output data acquired from a single-shot experiment to be used in tuning process[18]. Hence, the mathematical modeling of the complex system which normally needed in the conventional controller design can partly be eliminated through the employment of FRIT.

The PSO, on the other hand, is a metaheuristic optimization technique of finding the optimal solution from a predefined search space. First introduced by Kennedy and Eberhart [19] in 1995, the algorithm mimics the behavior of swarm or flock of fishes in minimizing or maximizing the specified fitness function. Our work focus on implementing the algorithm in minimizing the cost function, formulated based on the fictitious signals utilizing the recorded data.

The organization of this chapter is as follows. In section 2.2, we provide the problem formulation where the overview of the two-ports and basic teleoperation structures are presented. In section 2.3, we discuss our proposed algorithm to achieve impedance matching. Next in section 2.4, a numerical example to illustrate the effectiveness of proposed method is discussed. Finally, we conclude the findings in section 2.5.

Mathematical Preliminaries: We denote \mathbb{R} and \mathbb{R}^n as the set of real numbers and vectors with dimension respectively. Suppose $v \in \mathbb{R}^n$, then the vector norm is defined by $\|v\| := \sqrt{v^T v}$ where T is the transposition. Meanwhile, the notation of $\|v(k)\| = K^2$ implies

$$\|v(k)\|_K^2 := \sum_{k=1}^K \|v(k)\|^2 = \|v(1)\|^2 + \|v(2)\|^2 + \cdots + \|v(K)\|^2. \quad (2.1)$$

Finally, we define $\mathbf{1}^m = [1, \dots, 1] \in \mathbb{R}^{1 \times m}$ as the m -dimensional row vector with all elements equal to 1.

2.2 Problem Formulation

2.2.1 Overview of the two-ports network

The general model of two-ports network in bilateral teleoperation is depicted in Fig. 2.1. In the bilateral teleoperation mechanism, the operator's force on the master f_h is transmitted to the remote task through the teleoperation system \mathcal{T} , and at the same time the environment force f_e is transmitted back to the operator. Considering the master velocity \dot{x}_m and the slave velocity \dot{x}_s , the perfect trans-parency is achieved if $f_h \equiv f_e$ for $\dot{x}_m = \dot{x}_s$. The relation between the forces and motions in bilateral

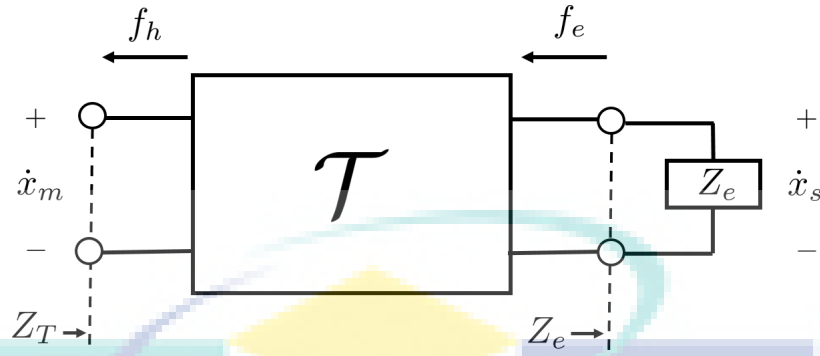


Figure 2.1: General two-ports model of a bilateral teleoperation system [2]

teleoperation system can be generalized in the hybrid matrix [2] of

$$\begin{bmatrix} f_h(s) \\ \dot{x}_m(s) \end{bmatrix} = \begin{bmatrix} h_{11}(s) & h_{12}(s) \\ h_{21}(s) & h_{22}(s) \end{bmatrix} \begin{bmatrix} \dot{x}_s(s) \\ -f_e(s) \end{bmatrix} \quad (2.2)$$

where $h_{ij}(s)$ is a SISO transfer function. From Eq. 3.4, it can be shown that

$$f_h = \underbrace{(h_{11} - h_{12}Z_e)(h_{21} - h_{22}Z_e)^{-1}}_{Z_T} \dot{x}_m. \quad (2.3)$$

To achieve a perfect transparency such that transmitted impedance Z_T equals to the environment impedance Z_e , the necessary and sufficient conditions are $h_{22} = 0$, $h_{21}Z_e = Z_e(-h_{12})$, and $h_{11} = 0$. Hence, for an ideal case, a perfect transparency for all frequencies implies

$$\begin{bmatrix} h_{11} & h_{12} \\ h_{21} & h_{22} \end{bmatrix} = \begin{bmatrix} 0 & -1 \\ 1 & 0 \end{bmatrix}. \quad (2.4)$$

2.2.2 Basic Structure of a Teleoperation System

We modelled the motion of the master manipulator by a simple mass-damper-spring system given by

$$m_m \ddot{x}_m + d_m \dot{x}_m + k_m x_m = f_m + f_h \quad (2.5)$$

where m_m, d_m, k_m are the mass, damping factor, and spring constants, respectively. Meanwhile, f_m , and x_m are the master's exerted force and total displacement, respectively. In the similar form, the slave manipulator is governed by the equation of motion of

$$m_s \ddot{x}_s + d_s \dot{x}_s + k_s x_s = f_s - f_e \quad (2.6)$$

where m_s, d_s, k_s are the mass, damping factor, and spring constants. The signals f_s and x_s are the slave's exerted force and the total displacement of the manipulator.

Figure 2.2 illustrates the general structure of a four-channels bilateral teleoperation system. The total impedances of the human and environment are denoted by Z_h and Z_e respectively. Meanwhile, Z_m and Z_s are the impedances of the master and slave manipulators. The local controllers for both master and slave manipulators are denoted by C_m and C_s . On the other hand, the controllers C_1 to C_4 are to dictate the communication link between the master and the slave sides. Zhu and Salcudean [2] reported that the perfect transparency can be achieved by properly designing C_1 to C_4 . For transparency under position control, a fully transparent teleoperator system satisfies the condition given in equation (2.4) by the selection of $C_1 = Z_s + C_s$, $C_2 = C_3 = 1$, and $C_4 = -(Z_m + C_m)$. However, this control strategy requires for acceleration measurement to implement C_1 and C_4 . As to overcome this issue, the "intervient impedance" was introduced to eliminate the need for acceleration measurement[2]. With low-gain PD control of C_m and C_s , and with the selection

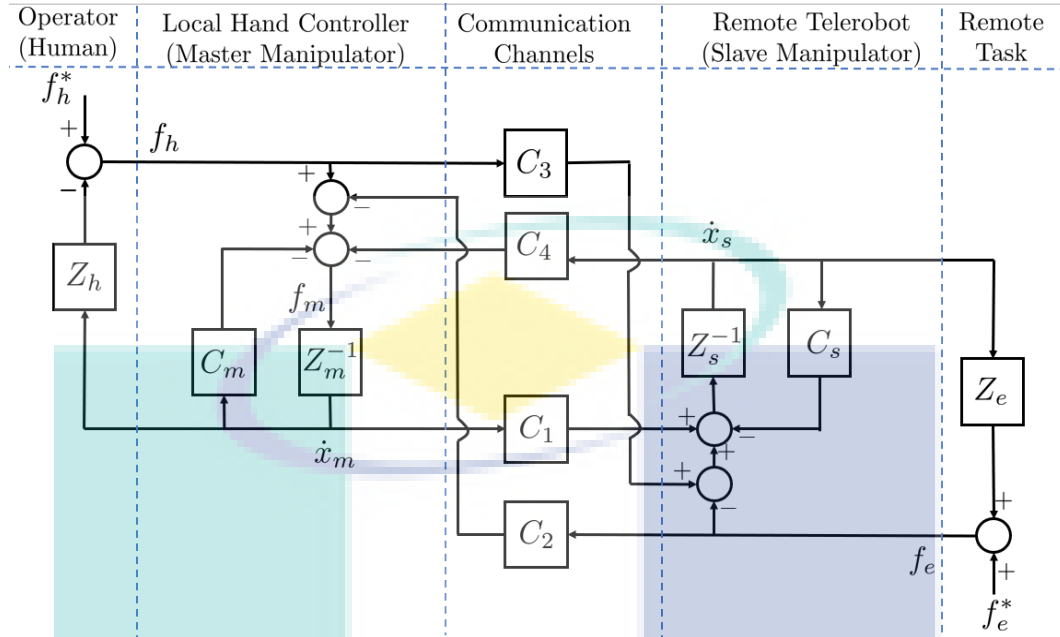


Figure 2.2: Four-channels structure proposed by Zhu & Salcudean [2]

of $C_1 = C_s$, $C_2 = C_3 = 1$, $C_4 = -C_m$, a nearly perfect transparency is achievable when we have the master impedance identical to the slave impedance such that $Z_m \equiv Z_s$. However, in most cases $Z_m \neq Z_s$. Hence, this chapter will discuss our proposed method to reach to the similar behavior of $Z_m \equiv Z_s$.

2.2.3 Improvement to The Existing Structure

To improve the existing structure of the four-channel teleoperation system, Tsuji et al.[4] introduced an additional equalizer or controller connected in-feedback to the master manipulator. By using the same local controller C_m for both the master and slave manipulators, the equalizer F can be properly tuned so that there exists symmetry between the impedance of the master and slave system. The new structure of the four-channels teleoperation system is depicted in Fig. 2.3. With this implementation, the controllers C_1 to C_4 can be chosen as $C_1 = C_m$, $C_2 = C_3$, and $C_4 = -C_m$. Now, the aim is to design an optimal controller F to achieve $Z_F := Z_m + F \equiv Z_s$. In the next section, we present the structure of the Laguerre network as to form the basic structure of F . Further more, the method of tuning where the metaheuristic-

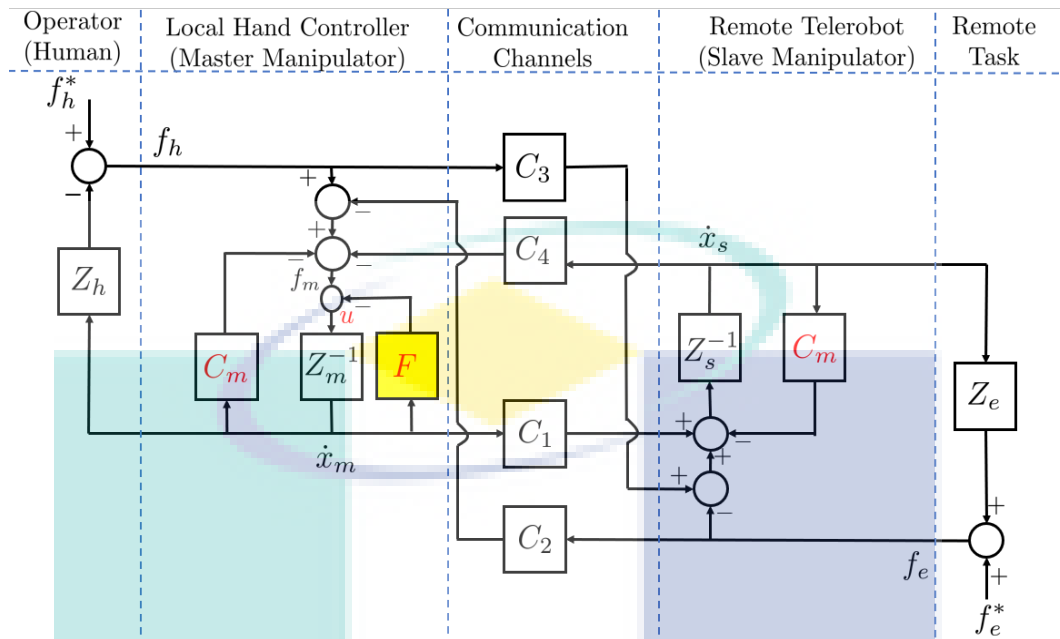


Figure 2.3: Four-channels structure illustrating the additional equalizer F

tic optimization algorithm and fictitious-reference signal generation are also briefly discussed.

Remark: Even though the modeling of manipulators is presented in this chapter, it is not a necessity in implementing our proposed algorithm. It will be discussed further in the next section to illustrate that only the recorded input-output data are required in the process of tuning the controllers. Hence, this technique is totally a model-free approach.

2.3 Algorithm for Impedance Matching

2.3.1 Particle Swarm Optimization

The PSO is an optimization method based on the metaphor of social behavior of flocks of birds or school of fish. First introduced by Kennedy and Eberhart[19], the algorithm started with the initialization of the pools particles/agents with random positions and velocities in multi-dimensional space. Let $p_i(k) \in \mathbb{R}^{1 \times D}$ and $q_i(k) \in \mathbb{R}^{1 \times D}$, $i = 1, 2, \dots, N$, denote the position and velocity of each agent i in D dimension at iteration k . Let the fitness function's value associated with the position $p_i(k)$ is denoted by $F_{it} \in \mathbb{R}$. Each of the agents is assumed to optimize the fitness function F_{it} , by evaluating the best-value-so-far ($p_{best_i} \in \mathbb{R}^{1 \times D}$) and its current position. The velocity of each agent i will be updated based on the following equation

$$q_i(k+1) = \omega q_i(k) + \eta_1 r_1 (p_{best_i} - p_i(k)) + \eta_2 r_2 (g_{best} - p_i(k)) \quad (2.7)$$

where $\omega \in \mathbb{R}$ is the weighting function, $\eta_1, \eta_2 \in \mathbb{R}$ are the weighting factors, $r_1, r_2 \in \mathbb{R}$ are the cognitive and social learning parameters generated randomly between 0 and 1. Meanwhile p_{best_i} is the p_{best} value of agent i , and $g_{best} \in \mathbb{R}^{1 \times D}$ is the best value so far in the group among the p_{best_s} of all agents. The following function is used to update the weighting function in equation (2.7):

$$\omega = \omega_{max} - \left(\frac{\omega_{max} - \omega_{min}}{iter_{max}} \right) \times iter \quad (2.8)$$

where $\omega_{max}, \omega_{min} \in \mathbb{R}$ are the initial and final weights, $iter_{max} \in \mathbb{R}$ is the maximum number of iteration, and $iter$ is the current iteration number. Thus, based on the updated velocity in (2.7), each agent i will update its position such that

$$p_i(k+1) = p_i(k) + q_i(k+1). \quad (2.9)$$

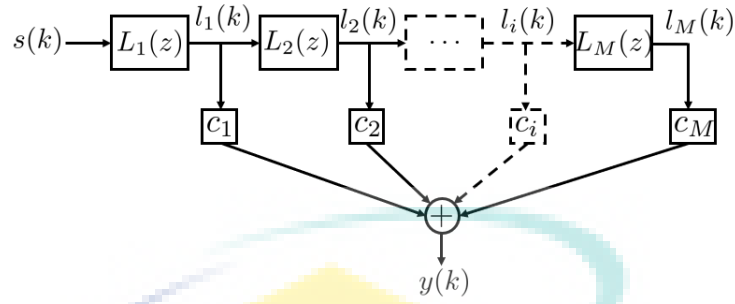


Figure 2.4: Structure of the Laguerre network

At the end of iteration, the agents shall all converge to the optimal position p^* , where

$$p^* := \min_{p_i} F_{it}, \forall i. \quad (2.10)$$

2.3.2 Equalizer $F(z)$ in the form of a Laguerre Network

The discrete time SISO system can be approximated to use a series of Laguerre filters of [20]

$$L_i(z) = \sqrt{(1-a^2)t_s} \frac{(z^{-1}-a)^{i-1}}{(1-az^{-1})^i} \quad (2.11)$$

as to form $y(z) = F(z)s(z) = \sum_{i=1}^M c_i L_i(z)$ as shown in Fig. 2.4. The parameter $a \in \mathbb{R}$ is the pole of the Laguerre network, and $0 \leq a < 1$ for the stability of the network[21], with t_s as the sampling time. The input and output signals of the network are denoted by $s(k) = \mathcal{Z}^{-1}[s(z)]$ and $y(k) = \mathcal{Z}^{-1}[y(z)]$, respectively. Here, we use $\mathcal{Z}[\cdot]$ to denote the inverse z-transform operator. The parameters $c_i \in \mathbb{R}, i = 1, \dots, M$ are the coefficients that form the basis of the Laguerre network. Meanwhile, the signal of $l_i(k) \in \mathbb{R}, i = 1, \dots, M$ is the output of the i -th-order filter in the Laguerre network. By this notation, the SISO state-space model of the overall

network can be represented by

$$F(z) : \begin{cases} l(k+1) = Al(k) + Bu(k) \\ y(k) = Cl(k) \end{cases} \quad (2.12)$$

where $l = [l_1, \dots, l_M]^T \in \mathbb{R}^M$ is the state vector, $A \in \mathbb{R}^{M \times M}$ is the system matrix, $B \in \mathbb{R}^M$ is the input matrix, and $C = [c_1, \dots, c_M] \in \mathbb{R}^{1 \times M}$ is the output matrix. The elements of A and B are given by

$$[A]_{ij} := \begin{cases} a & \text{if } i = j \\ (-1)^{(i-j+1)} a^{(i-j-1)} (1 - a^2) & \text{if } i < j \\ 0 & \text{otherwise} \end{cases} \quad (2.13)$$

$$[B]_i := (-a)^{(i-1)} \sqrt{(1 - a^2) t_s}. \quad (2.14)$$

2.3.3 Fictitious-Reference-Iterative Tuning

The equalizer F needs to be properly designed and tuned to attain $Z_F \equiv Z_s$. Similar procedure of tuning as discussed in [4] was adopted in this work. Figure 2.5 illustrates the two-process of tuning which had been carried out to obtain the optimal controllers. In the first process (see Fig. 2.5(a)), an equalizer H was first to be determined to match the velocities \dot{x}_m and \dot{x}_s . Similar to our previous work in [17], we selected $H(z) := P(z)/Q(z)$ as a bi-proper transfer function in the form of

$$H(z) = \frac{1 + \hat{a}_1 z^{-1} + \dots + \hat{a}_p z^{-p}}{1 + \hat{b}_1 z^{-1} + \dots + \hat{b}_p z^{-p}}. \quad (2.15)$$

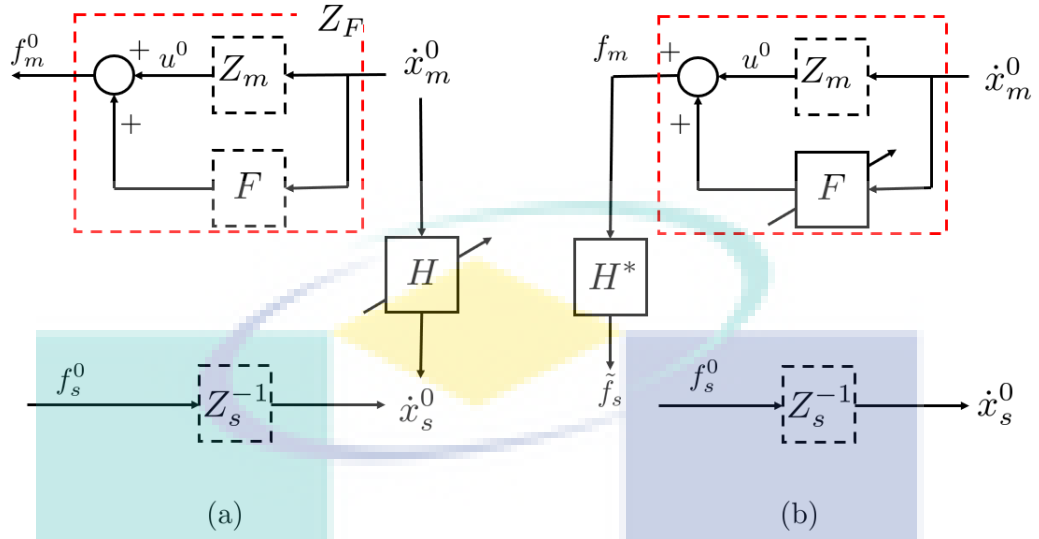


Figure 2.5: Two-steps of tuning:(a) to attain H^* , (b) to attain F^*

In the second process, a fictitious signal was formulated to utilize (2.15) (see Fig. 2.5(b)). The fictitious signal can be defined as

$$\tilde{f}_s(k) = H^*(z) \left(u^0(k) + F(z) \dot{x}_m^0(k) \right) \quad (2.16)$$

where $H^*(z)$ is the transfer function of $H(z)$ with the optimal parameters. Meanwhile, u^0 and \dot{x}_m^0 are the recorded input-output data measured from the master's manipulator.

2.3.4 Attaining a matched impedance via PSO and FRIT

To obtain the optimal transfer function $H^*(z)$, we need to solve the constraint optimization problem defined by

$$\min_{H(z)} J_H, \quad \text{s.t. } |z| \leq 1 \quad (2.17)$$

where for the recorded initial data $\dot{x}_m^0(k)$ and $\dot{x}_s^0(k)$,

$$J_H := \|\dot{x}_s^0(k) - H(z)\dot{x}_m^0(k)\|_K^2. \quad (2.18)$$

Meanwhile, to attain the optimal $F^*(z)$, we solve the second optimization problem given by

$$\min_{F(z)} J_F \quad (2.19)$$

where for recorded initial data $f_m^0(k)$ and $f_s^0(k)$,

$$\begin{aligned} J_F &:= \|f_s^0(k) - \tilde{f}_s(k)\|_K^2 \\ &= \|f_s^0(k) - H^*(z)(u^0(k) + F(z)\dot{x}_m(k))\|_K^2 \\ &= \|(H^{*-1}(z)f_s^0(k) - u^0(k)) - F(z)\dot{x}_m(k)\|, \\ u^0(k) &= f^0(m)(k) - F^0(z)\dot{x}_m(k). \end{aligned} \quad (2.20)$$

The following algorithm has been implemented to obtain the optimal controllers $H^*(z)$ and $F^*(z)$:

- Step 1:** Let the tunable parameters of the controller $F(z)$ be defined as $\rho = [a, c_1, \dots, c_M] \in \mathbb{R}^{1 \times D_1}$. By arbitrarily selecting the initial value ρ^0 , the set of data $\dot{x}_m^0, \dot{x}_s^0, f_s^0$ and u^0 are then generated.
- Step 2:** First, we tune the equalizer H by employing the PSO algorithm. Let $p_i := [\hat{a}_1, \dots, \hat{a}_P, \hat{b}_1, \dots, \hat{b}_P] \in \mathbb{R}^{1 \times D_2} \mid p_i \in [p_{H_{\min}}, p_{H_{\max}}], \forall i$. Initialize the positions of PSO agents in the specified search space. Define the fitness function F_{it} for each agent according to equation (2.18), such that $F_{it} = J_H$.
- Step 3:** Update the agents' velocities based on equation (2.7) and agents' positions based on equation (2.9) at each iteration. At the final iteration time, all agents

Table 2.1: Parameters values of the manipulator systems

Manipulator	Mass (kg)	Damper (Ns/m)	Spring (N/m)
Master	$m_m = 1.5$	$d_m = 0.4952$	$k_m = 0$
Slave	$m_s = 3$	$d_s = 2.4762$	$k_s = 1.4621$

shall converge to the optimal position of p^* corresponds to optimization problem defined in equation (2.17). Assign the coefficients of transfer function in (2.15) with p^* . Repeat from **Step 2** if results are not satisfactory.

Step 4: Next, we tune the controller F by also employing the PSO algorithm. Let $p_i := \rho \in \mathbb{R}^{1 \times D_1} \mid p_i \in [p_{F_{\min}}, p_{F_{\max}}], \forall i$. Initialize the positions of PSO agents in the specified search space. Define the fitness function F_{it} for each agent according to equation (3.51), such that $F_{it} = J_F$.

Step 5: Update the agents' velocities based on equation (2.7)) and agents' positions based on equation (2.9) at each iteration. At the final iteration time, all agents shall converge to the optimal position of corresponds to optimization problem defined in equation (2.19). Assign $\rho = p^*$. Repeat from **Step 4** if results are not satisfactory.

2.4 Numerical Results and Analysis

To illustrate the effectiveness of our proposed method, we present an example in this section. We conducted a numerical analysis employing the Matlab simulation package to execute the developed theoretical models. The parameters used in the teleoperation system are summarized in Table 2.1. The impedance of the human operator was defined as $Z_h = s^2 + 5s + 10$. Meanwhile, the number of basis of the truncated Laguerre filters was chosen as $M = 10$, and the sample time $t_s = 0.01$ s. We assume there was no time delay in the communication link, and the environment's impedance was set to zero to imply that the slave manipulator moves

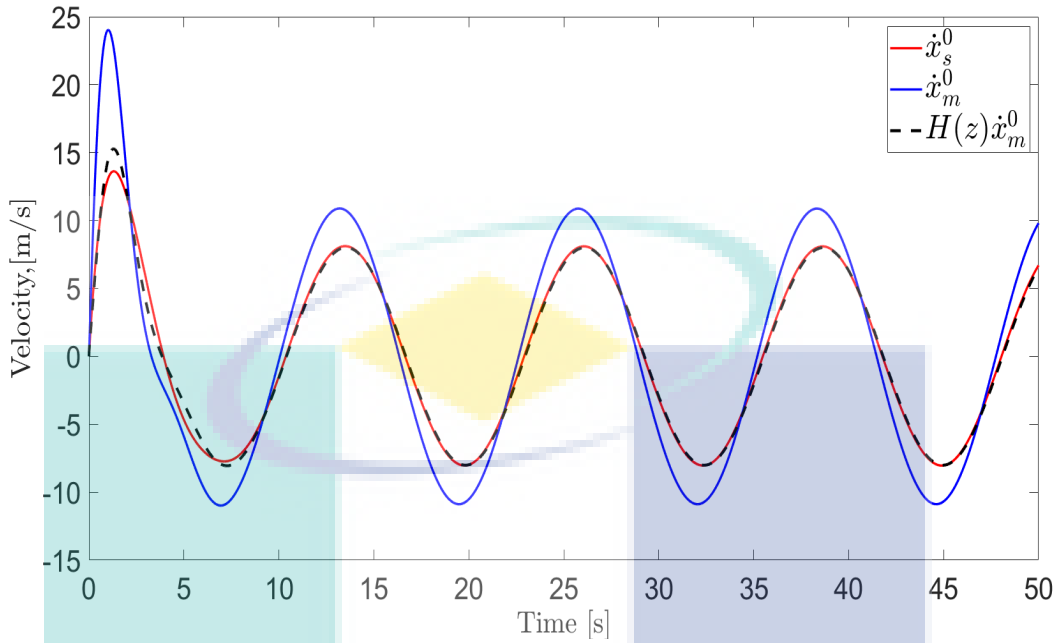


Figure 2.6: Velocity matching through equalizer $H(z)$

freely without any attached load. The transfer function of the local controllers for both master and slave were chosen as $C_m = 2 \left(1 + \frac{1}{100s} + 0.2s \right)$. Meanwhile, the controllers C_1 to C_4 were selected based on the description provided in Section 2.2.3.

In Table 2.2, we provide the parameters of the PSO algorithm that were used in the tuning process. For both procedures, we used the weighting factor $\eta_1 = \eta_2 = 1.4$. Meanwhile, $\omega_{\min} = 0.4$ and $\omega_{\max} = 0.9$, respectively.

Figure 2.6 illustrates the performance of the equalizer $H(z)$ with $p = 6$ in equalizing the velocities between the manipulators. As presented in the figure, the initial recorded velocity signals of the master and slave manipulator are indicated

Table 2.2: Tuning parameters used in PSO algorithm

	# of parameters D	# of agents N	Max iteration $iter_{max}$	Min Range p_{min}	Max Range p_{max}
Tuning H	$D_2 = 12$	200	150	-1	1
Tuning F	$D_1 = 11$	100	400	$[0, -200 \times \mathbf{1}^M]$	$[1, 50 \times \mathbf{1}^M]$

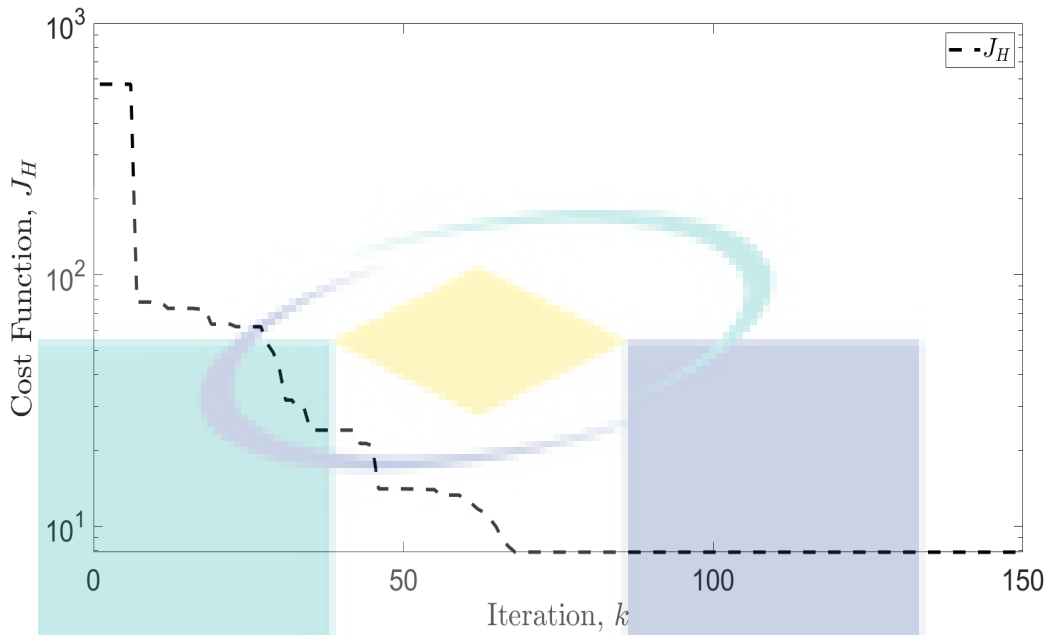


Figure 2.7: Convergence of the cost function J_H

in the blue and red lines, respectively. It can clearly be seen that the velocity \dot{x}_m^0 was matched with \dot{x}_s^0 through the equalizer $H(z)$ (as indicated by the dashed-black line). The convergence of the cost function (2.18) is exhibited in Fig. 2.7 where $J_H = 7.8817$ at the final iteration $k = 150$. Meanwhile, Fig. 2.8 indicates the location of the poles and zeros of $H(z)$ which all lie inside the unit circle to signify $H(z)$ and $H(z)^{-1}$ are always stable.

The comparison of the positions, velocities and exerted forces of the master and slave manipulators, before and after tuning are depicted in Figs.2.9(a) and 2.9(b) respectively. From Fig.2.9(b), it can be observed that the trends of velocities of both manipulators are almost identical for all time t . Except for the position of the master manipulator where it was slightly lagging than the position of the slave. Similar observation can be obtained from the exerted forces response of the manipulators. Here, it could be seen that they have almost identical patterns. Additional result to illustrate the convergence of the cost function (2.18) is provided in Fig.2.10. The cost function value was obtained as $J_F = 30294.2498$ at the final iteration time of $k = 400$.

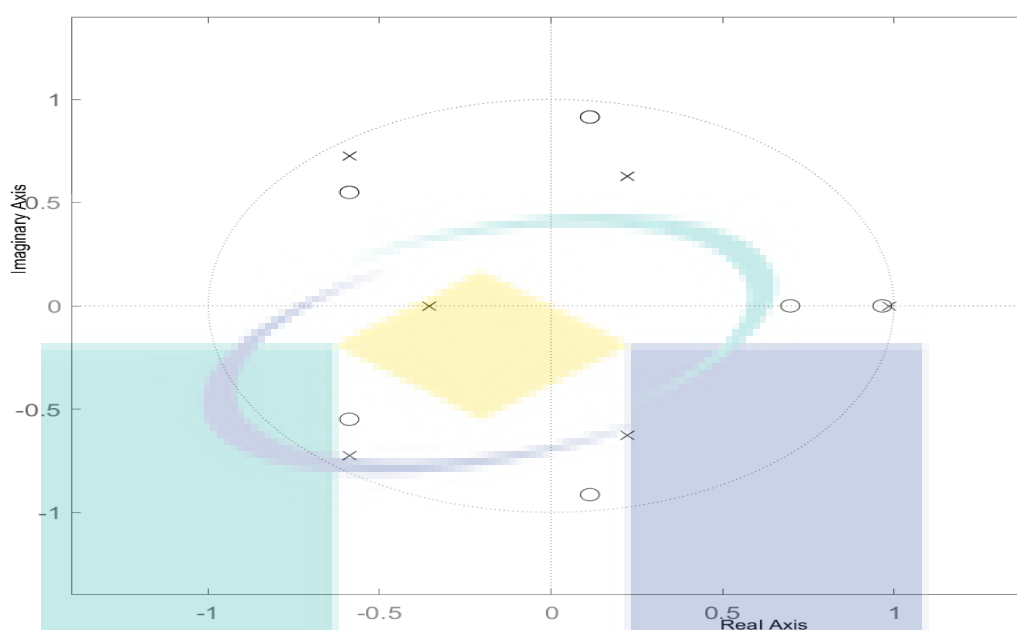


Figure 2.8: Location of poles and zeros of $H(z)$

2.5 Conclusion

In this chapter, the tuning algorithm based on a model-free approach to improve transparency through impedance matching between the master and slave manipulators of a bilateral teleoperation system has been demonstrated. By introducing a controller connected in-feedback to the master manipulator, it provides the possibility of obtaining a symmetric impedance between both sides of the teleoperation system. Furthermore, the utilization of FRIT has eliminated the necessity of obtaining the plant model through mathematical modeling in designing the controllers. Hence, it is truly a model-free approach. Meanwhile, the implementation of the PSO algorithm further simplified the process of obtaining the optimal controller parameters. From the presented numerical results, it can be concluded that the proposed algorithm exhibits promising results to achieve a matched impedance between the master and slave manipulators. However, the formulation of the cost function warrants for further investigation to ensure ultimate convergence of its value towards zero.

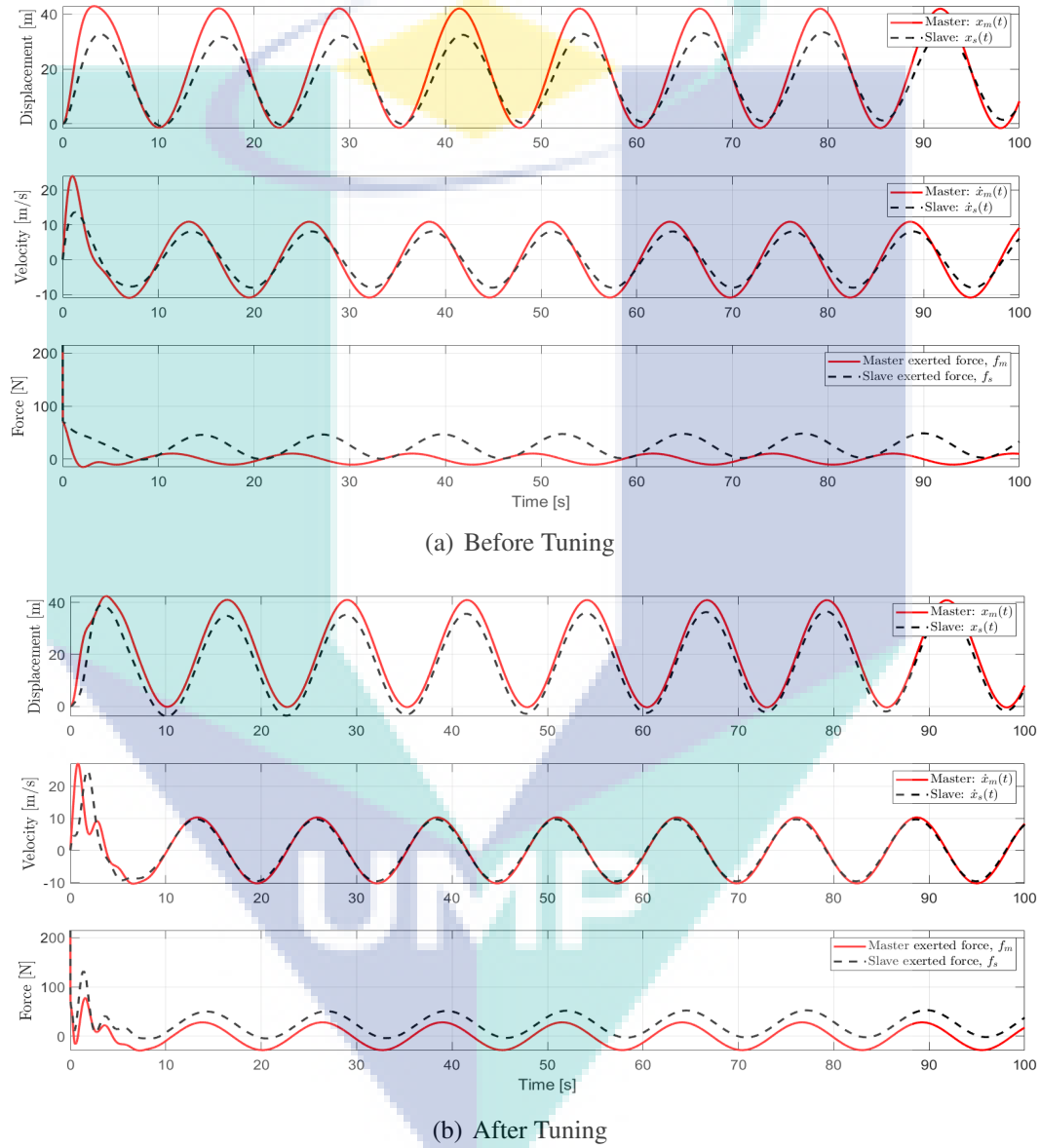


Figure 2.9: Performance comparison before and after tuning.

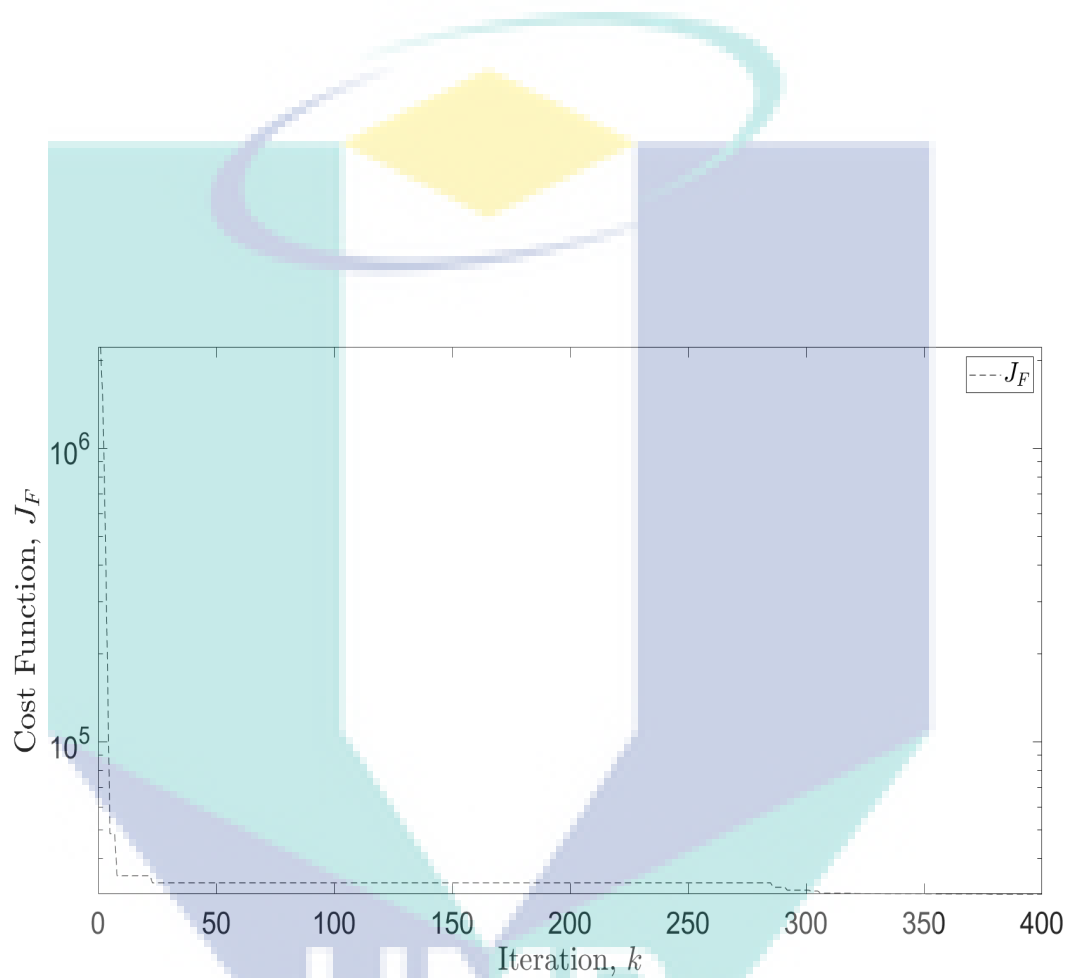


Figure 2.10: Convergence of the cost function J_F

Chapter 3

Data-driven Impedance Matching in Multilateral Teleoperation Systems

3.1 Introduction

Teleoperation systems extend the human operators' capability to perform task at the remote site. In general, the teleoperation systems can be categorized into bilateral teleoperation[5, 22, 23] and multilateral teleoperation[16, 24]. The bilateral teleoperation system commonly consists of only a single master and single slave manipulators as part of its basic structure. Meanwhile, the multilateral teleoperation system requires more number of manipulators, either on the master side or the slave side.

To properly control the multilateral teleoperation system pose some challenge especially when we consider a single master with multi-slaves configuration. Generally, there is inadequate degree-of-control on the master side to effectively manipulate the slave side, hence requires that the slaves to have a certain degree of self-control. To address the issues related to the multilateral teleoperation, we focus on two main questions:

- How can we treat a multilateral system as a bilateral system?

- Is there any mechanism that can be implemented to improve the transparency (i.e., a faithful transmission of force and velocity) between master and the multiple-slave in a 4-channels structure?

The fact that many works have been done in the past focusing on the bilateral teleoperations[25], then converting the multilateral teleoperation system to suit the existing bilateral structure gives some advantages in terms of the controller design. Furthermore, as the total dynamics of slave manipulators can be changed (i.e., adding (subtracting) slave manipulators, or establish new configuration on the communication topology between agents), it is certainly cost inefficient if the dynamics of the master manipulator has also to be redesigned whenever the dynamics of slave manipulators has changed. Therefore, by introducing a single tunable equalizer to the master renders flexibility to adjust the overall dynamics of the master to achieve symmetry between both sides of teleoperation. Moreover, by this approach the system designer does not need to have exact knowledge on the dynamics of the newly-changed slave manipulators.

Various studies that have been carried out on bilateral teleoperation were focusing on the utilization of 4-channels architecture. Lawrence[3, 8] emphasized that the proper use of all four channels is of critical importance in achieving high performance telepresence in the sense of accurate transmission of task impedance to the operator. Some instances of works on 4-channels structure discussed in Zhu & Salcudean[2] where they proposed a position and rate control, and Namerikawa & Kawada[9] where they designed the symmetric impedance matched with position tracking. Other technique that also utilizes the 4-channels structure is the wave-variable control as surveyed in Sun *et al.*[15] The example of application on wave variable control in the multilateral framework was discussed in Kanno & Yokokohji[16].

In this chapter, we focus on the passive decomposition technique[1] to convert from multilateral teleoperation into a bilateral teleoperation. Since the whole tele-

operation process can be separated into two operations, namely grasping and handling, we use the sub-dynamics from the result of decomposition to determine the time (or in our case, T_{tele}), that differentiate between them. In addition, we investigate the potential of implementing an equalizer connected to the master manipulator in order to achieve impedance matching between both sides of teleoperation. Due to the orthonormal properties of the Laguerre function[26], the equalizer can be realized by a Laguerre network of high order of moderately damped system [27]. In most applications, the optimum structure of this network can be obtained by simply selecting the optimal values for the basis of the Laguerre filters[28].

The equalizer should be properly tuned to improve the overall performance. Hence, we adopted the so-called Fictitious-Reference-Iterative Tuning (FRIT) in our problem formulation. Unlike other tuning algorithms which requires the mathematical model of the plant prior tuning, FRIT utilizes the recorded input-and-output data to simultaneously attain the plant model and the optimum controller parameters[18, 29]. Interestingly, it requires only a single-shot of measurement data for this purpose[30, 31].

The motivation of this work is to extend the results of Tsuji *et al.*[4] to improve transparency through impedance matching. To mention some of the key differences, in Tsuji *et al.*[4] they considered a scalar case of a bilateral system and chose a simple dynamics to form the equalizer. In our work, we considered a multilateral teleoperation system and formed the equalizer by selecting a truncated Laguerre network. Also, we utilized the data tuning in two-dimensional space.

The following sections are organized as follows. In Sect. 3.2, we provide basic notations and brief theory on bilateral teleoperation. Section 3.3 presents the passive decomposition technique and the estimation of teleoperation time. In Sect. 3.4 we discuss our tuning algorithm. A numerical example is given in Sect. 3.5. Finally, we conclude our finding in Sect. 3.6.

3.2 Problem formulation

In this section, we present the notations and basic structure of a teleoperation system.

3.2.1 Notations and graph theory

Let \mathbb{R} and \mathbb{R}^m denote the sets of real numbers and vectors of dimension m , respectively. Let $\mathbf{1} = [1, \dots, 1]^T$ be a vector with all elements of 1 and T is the transposition. We use $\mathbf{I}_n \in \mathbb{R}^{n \times n}$ to denote the identity matrix. To denote the inner and cross products for $v, w \in \mathbb{R}^p$, we use $\langle v, w \rangle = v^T w$ and $v \times w$, respectively. The vector norm is defined by $\|v\| := \sqrt{v^T v}$, and $\|v(k)\|_K^2$ implies

$$\|v(k)\|_K^2 := \sum_{k=1}^K \|v(k)\|^2. \quad (3.1)$$

For $A = (a_{ij}) \in \mathbb{R}^{n \times m}$ and $B \in \mathbb{R}^{l \times k}$, the Kronecker product $A \otimes B \in \mathbb{R}^{nl \times mk}$ is defined by

$$A \otimes B = \begin{bmatrix} a_{11}B & \dots & a_{1m}B \\ \vdots & \ddots & \vdots \\ a_{n1}B & \dots & a_{nm}B \end{bmatrix}.$$

We call $A = A^T \in \mathbb{R}^{n \times n}$ *positive definite* if $\forall x \neq 0, x^T A x > 0$. To indicate strict non-negativity, $A > 0$ implies $A > 0$ iff $\lambda_{\min}(A) > 0$. Also, $A \geq 0, \lambda_{\min} = 0$ implies its positive semi-definiteness. On the other hand, if $A \neq A^T \in \mathbb{R}^{n \times n}$, then $A = A_{sym} + A_{skew}$ where $A_{sym} = \frac{1}{2}(A + A^T)$ and $A_{skew} = \frac{1}{2}(A - A^T)$, respectively.

For N number of agents, a graph \mathbb{G} is built upon a finite set called a *vertex set* mapped by $\mathcal{V} = \{v_1, v_2, \dots, v_N\}$ and the *edge set* of \mathcal{E} . We say $v_i, v_j \in \mathcal{E}$ if there is a communication link between them. Additionally, $\mathcal{N}_i = \{v_j \mid v_i, v_j \in \mathcal{E}, \forall j\}$ is the neighborhood set of v_i . The relationship between $v_i, v_j \in \mathcal{V}$ for an undirected \mathbb{G} is

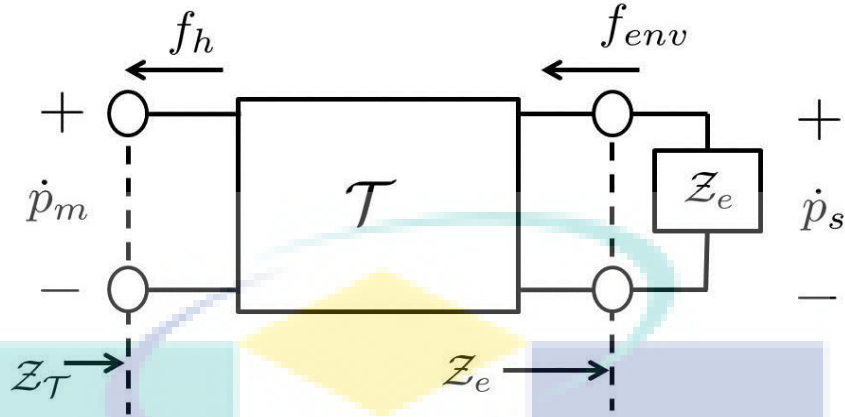


Figure 3.1: General two-ports model of a bilateral teleoperation system[3].

encoded by the *adjacency matrix* $\mathcal{A}(\mathbb{G}) = [a_{ij}] \in \mathbb{R}^{N \times N}$, where

$$a_{ij} := \begin{cases} 1 & \text{if } v_j \in \mathcal{N}_i \\ 0 & \text{otherwise} \end{cases} \quad (3.2)$$

The *degree matrix* $\mathcal{D}(\mathbb{G}) \in \mathbb{R}^{N \times N}$ is a diagonal matrix that is $\mathcal{D}(\mathbb{G}) = \mathbf{diag}\{d_1, \dots, d_N\} = \mathbf{diag}(\mathcal{A}(\mathbb{G})\mathbf{1})$ with $d_i := |\mathcal{N}_i| = \sum_{j=1}^N a_{ij}$, and $|\mathcal{N}_i|$ is the cardinality of \mathcal{N}_i . The Laplacian matrix associated with \mathbb{G} is defined by[32]

$$\mathcal{L}(\mathbb{G}) := \mathcal{D}(\mathbb{G}) - \mathcal{A}(\mathbb{G}) \geq 0. \quad (3.3)$$

Definition 3.2.1. A graph \mathbb{G} is said to be *strongly connected* if there always exists path from vertex v_i to v_j , $\forall (i, j) \in \mathcal{V}$.

Definition 3.2.2. A graph \mathbb{G} is said to be *balanced* if $deg_{in}^i = deg_{out}^i$, where deg_{in}^i is the number of incoming links into the node v_i , and deg_{out}^i is the number of outgoing link from the node v_i , $\forall i$.

3.2.2 Overview of the two-ports network

The general model of a two-ports network in bilateral teleoperation is depicted in Fig. 3.1. In the bilateratel teleoperation mechanism, the operator's force on the

master f_h is transmitted to the remote task through the teleoperation system \mathcal{T} , and at the same time the environment force f_{env} is transmitted back to the operator. Considering the master velocity $q_m = \dot{p}_m$, and the slave velocity $q_s = \dot{p}_s$, then a perfect transparency is achieved if $f_h = f_{env}$ for $q_m = q_s$. The relation between the force and motions in a bilateral teleoperation system can be generalized in the hybrid matrix[3, 8] of

$$\begin{bmatrix} f_h(s) \\ q_m(s) \end{bmatrix} = \begin{bmatrix} h_{11}(s) & h_{12}(s) \\ h_{21}(s) & h_{22}(s) \end{bmatrix} \begin{bmatrix} q_s(s) \\ -f_{env}(s) \end{bmatrix}. \quad (3.4)$$

It can be derived that[3, 8] (dropping s for clarity)

$$f_h = \underbrace{(h_{11} - h_{12}\mathcal{Z}_e)(h_{21} - h_{22}\mathcal{Z}_e)^{-1}}_{\mathcal{Z}_T} q_m. \quad (3.5)$$

To achieve perfect transparency such that the transmitted impedance \mathcal{Z}_T equals to the environment impedance \mathcal{Z}_e , it requires that $h_{22} = 0$, $h_{21}\mathcal{Z}_e = \mathcal{Z}_e(-h_{12})$, and $h_{11} = 0$. Hence, in an ideal case, a perfect transparency for all frequencies implies

$$\begin{bmatrix} h_{11} & h_{12} \\ h_{21} & h_{22} \end{bmatrix} = \begin{bmatrix} 0 & -\mathbf{I} \\ \mathbf{I} & 0 \end{bmatrix}. \quad (3.6)$$

In this chapter, we assume that the effect of the time delay can be neglected.

3.2.3 Teleoperation architecture

We consider a simple agent governed by the equation of motion

$$m_m \ddot{p}_m = f_m + f_h. \quad (3.7)$$

as the master manipulator. Conversely, the slave manipulators depicted by a network of agents such that each agent i moves dynamically through

$$m_i \ddot{p}_i = f_i - f_{e_i}, \forall i \in \mathbb{G}. \quad (3.8)$$

The variables $m_l \in \mathbb{R}$, and $p_l \in \mathbb{R}^2$ are the agent's mass and position. The subscripts $l = m, i$ stand for the *master* and *slave* i manipulators, respectively. The signals $f_m \in \mathbb{R}^2$ and $f_h \in \mathbb{R}^2$ are the exerted force of the master manipulator and the corresponding applied force of the human operator. Similarly, the signal $f_i \in \mathbb{R}^2$ is the exerted force of each agent i . The force $f_{e_i} \in \mathbb{R}^2$ is the *estimated* environment's force *felt* by each agent i at its position relative to the center-of-mass (CoM) of the environment.

The object in the environment is considered to be a solid disk of radius R that moves on a sliding flat surface. Assuming that all agents are friction-less (i.e., they move on friction-less wheels), the friction force only exists between the contact of the disk and the sliding surface. The desired final position of each agent i on the environment is defined as

$$\tilde{p}_i := R \begin{bmatrix} \cos \alpha_i(t) \\ \sin \alpha_i(t) \end{bmatrix}, \quad (3.9)$$

where $\alpha_i(t) = \alpha_i^0 + \varphi(t)$ is the desired angular position of i , and $\alpha_i^0 = 2\pi(i-1)/N \in \mathbb{R}$, $\forall i$. Meanwhile, $\varphi(t)$ is the environment's nominal angular displacement used in (3.10). For brevity, we drop the time notation (t) in most equations, but use so whenever to emphasize its time-varying property. Defining F_f as the friction force, the dynamical equation of the object is denoted by

$$\begin{cases} m_e \ddot{p}_e = \sum_{i=1}^N \tilde{f}_i - F_f \\ \frac{1}{2} m_e R^2 \ddot{\varphi} = \sum_{i=1}^N \tilde{\tau}_i. \end{cases} \quad (3.10)$$

where $m_e \in \mathbb{R}$ and $p_e \in \mathbb{R}^2$ are the mass and CoM's position of the target/object, respectively. The force $\tilde{f}_i \in \mathbb{R}^2$ and torque $\tilde{\tau}_i \in \mathbb{R}$ in (3.10) are defined by

$$\tilde{f}_i = \begin{cases} \frac{\langle f_i, -\tilde{p}_i \rangle}{\langle -\tilde{p}_i, -\tilde{p}_i \rangle} (-\tilde{p}_i) & \text{if } \|p_{ie}\| \leq R \\ 0 & \text{otherwise} \end{cases} \quad (3.11)$$

$$\begin{bmatrix} 0 \\ 0 \\ \tilde{\tau}_i \end{bmatrix} = \begin{cases} \begin{bmatrix} \tilde{p}_i \\ 0 \end{bmatrix} \times \begin{bmatrix} f_i - F_f \\ 0 \end{bmatrix} & \text{if } \|p_{ie}\| \leq R \\ \mathbf{0} & \text{otherwise.} \end{cases} \quad (3.12)$$

where $\|p_{ie}\| := \|p_i - p_e\|$.

Remark 3.2.1. The vector projection (3.11) can be regarded as the effective force f_i acting on the CoM of the environment while (3.12) is the tendency of f_i to rotate the object around its CoM.

3.3 Multilateral to bilateral teleoperation

The total dynamics of the slave agents and the passive decomposition technique[1] to transform the multilateral teleoperation into a bilateral teleoperation are described in this section. We assume that a specified time T_{tele} separates two main operations: *grasping*, and *handling*.

3.3.1 Total dynamics of the slave agents

Following Kawakami & Namerikawa[33] and to use (3.9), we introduce a change of variables as

$$\hat{p}_i = p_i - \tilde{p}_i. \quad (3.13)$$

The force f_i in (3.8) can be separated into two control components depending on the time interval, i.e., grasping and handling. We express

$$f_i = \begin{cases} f_i^{fc}, & t < T_{tele} : (\text{grasp}) \\ f_i^{fc} + f_i^{tc}, & t \geq T_{tele} : (\text{grasp + handle}) \end{cases} \quad (3.14)$$

where f_i^f and f_i^{tc} are the formation and teleoperation control laws, respectively.

The consensus control law

$$f_i^{fc} = \gamma_i \left[a_{ie} \left\{ -k(\hat{p}_i - p_e) - b(\dot{\hat{p}}_i - \dot{p}_e) \right\} + \sum_{j=1}^N a_{ij} \left\{ -k(\hat{p}_i - \hat{p}_j) - b(\dot{\hat{p}}_i - \dot{\hat{p}}_j) \right\} \right] \quad (3.15)$$

is used to achieve simultaneous grasping. Here $a_{ie} = 1$ if i can measure its relative positions and velocity with respect to object's CoM, and $a_{ie} = 0$ otherwise. The gain a_{ij} corresponds to the communication topology defined in (3.2). Meanwhile, the variables $k, b \in \mathbb{R}$ are the control gains. The gain $\gamma_i \in \mathbb{R}$ is defined by

$$\gamma_i = \frac{1}{a_{ie} + \sum_{i=1}^N a_{ij}}. \quad (3.16)$$

Substituting (3.13) and (3.15) into (3.8) and since $f_{e_i} = 0$ for $t < T_{tele}$, we now rewrite the dynamics of agent i as

$$m_i \ddot{\hat{p}}_i = \gamma_i \left[a_{ie} \left\{ -k(\hat{p}_i - p_e) - b(\dot{\hat{p}}_i - \dot{p}_e) \right\} + \sum_{j=1}^N a_{ij} \left\{ -k(\hat{p}_i - \hat{p}_j) - b(\dot{\hat{p}}_i - \dot{\hat{p}}_j) \right\} \right] \quad (3.17)$$

Assuming that the environment/object acts as the virtual $(N + 1)$ th agents, then we have $p_e = \hat{p}_{N+1} = p_{N+1} - \tilde{p}_{N+1}$, with $\tilde{p}_{N+1} = 0$ and $a_{ie} = a_{i(N+1)}$. In addition, the mass of the virtual agent is to take the average mass of all agents given by $m_{N+1} = \frac{1}{N} \sum_{i=1}^N m_i$. By this, (3.17) can be written as

$$\frac{m_i}{\gamma_i} \ddot{\hat{p}}_i = -k \sum_{j=1}^{N+1} a_{ij} (\hat{p}_i - \hat{p}_j) - b \sum_{j=1}^{N+1} a_{ij} (\dot{\hat{p}}_i - \dot{\hat{p}}_j). \quad (3.18)$$

The total dynamics consisting of $N + 1$ agents is given by

$$\mathbf{M}\ddot{\mathbf{p}} + b(\hat{\mathcal{L}} \otimes \mathbf{I}_2)\dot{\mathbf{p}} + k(\hat{\mathcal{L}} \otimes \mathbf{I}_2)\mathbf{p} = \begin{cases} \mathbf{0}, & t < T_{tele} \\ \mathbf{f} - \mathbf{f}_e, & t \geq T_{tele} \end{cases} \quad (3.19)$$

where $\mathbf{p} = [\hat{p}_1^T, \dots, \hat{p}_{N+1}^T]^T \in \mathbb{R}^{2(N+1)}$, $\mathbf{f} = [f_1^{tcT}, \dots, f_{N+1}^{tcT}]^T$, $\mathbf{f}_e = [f_{e_1}^T, \dots, f_{e_{N+1}}^T]^T$, and

$$\mathbf{M} := \mathbf{diag}\left(\frac{m_1}{\gamma_1}, \dots, \frac{m_{(N+1)}}{\gamma_{N+1}}\right) \otimes \mathbf{I}_2. \quad (3.20)$$

Furthermore, the Laplacian matrix defined by

$$\hat{\mathcal{L}} = \begin{bmatrix} \sum_{j=1}^{N+1} a_{1j} & -a_{12} & \dots & -a_{1(N+1)} \\ -a_{21} & \sum_{j=1}^{N+1} a_{2j} & -a_{23} & -a_{2(N+1)} \\ \vdots & & \ddots & \vdots \\ -a_{(N+1)1} & -a_{(N+1)2} & \dots & \sum_{j=1}^{N+1} a_{(N+1)j} \end{bmatrix} \in \mathbb{R}^{(N+1) \times (N+1)} \quad (3.21)$$

is composed of the assorted actual and virtual slave agents.

3.3.2 Passive decomposition[1] in handling

Introduce a new coordinate system in the form of

$$\mathbf{z} = [z_1^T, z_2^T, \dots, z_{N+1}^T]^T := \mathbf{S}\mathbf{p} \quad (3.22)$$

where S is the transformation matrix defined by

$$S := \begin{bmatrix} \hat{\mathbf{M}}_1 & \hat{\mathbf{M}}_2 & \dots & \hat{\mathbf{M}}_N & \hat{\mathbf{M}}_{N+1} \\ \mathbf{I} & \mathbf{0} & \dots & \mathbf{0} & -\mathbf{I} \\ \mathbf{0} & \mathbf{I} & \ddots & \mathbf{0} & -\mathbf{I} \\ \vdots & \ddots & \ddots & \vdots & \vdots \\ \mathbf{0} & \mathbf{0} & \dots & \mathbf{I} & -\mathbf{I} \end{bmatrix} \in \mathbb{R}^{n(N+1) \times n(N+1)}, \quad (3.23)$$

$$\hat{\mathbf{M}}_i = \frac{m_i}{m_L \gamma_i} \mathbf{I}_2, \quad i = 1, \dots, N+1, \quad (3.24)$$

$$m_L = \sum_{i=1}^{N+1} \frac{m_i}{\gamma_i}. \quad (3.25)$$

The sub-coordinate $z_1 \in \mathbb{R}^2$ corresponds to the Locked system's coordinate. Accordingly, $\mathbf{z}_e = [z_2^T, \dots, z_{N+1}^T]^T \in \mathbb{R}^{2N}$ represents the Shape system's coordinate[1].

Remark 3.3.1. The first row of S describes the weighted center average of the agents' formation. Meanwhile, the rest of the rows provide the relative position error between i and the environment's CoM. The Locked system can be regarded as a single slave manipulator in contact with the master manipulator to form the bilateral teleoperation mode. Simultaneously, appropriate decentralized control strategies are designed on the Shape system to maintain the desired formation between the slave agents.

Substituting (3.22) into (3.19), we obtain the total dynamics in the new coordinate system as

$$S^{-T} \mathbf{M} S^{-1} \ddot{\mathbf{z}} + b S^{-T} (\hat{\mathcal{L}} \otimes \mathbf{I}_2) S^{-1} \dot{\mathbf{z}} + k S^{-T} (\hat{\mathcal{L}} \otimes \mathbf{I}_2) S^{-1} \mathbf{z} = S^{-T} (\mathbf{f} - \mathbf{f}_e). \quad (3.26)$$

In contrast to Lee & Spong[1], the S^{-1} in (3.26) is obtained as

$$S^{-1} = \begin{bmatrix} \mathbf{I} & \Phi_2 & \Phi_3 - \mathbf{I} & \dots & \Phi_{N+1} - \mathbf{I} \\ \mathbf{I} & \Phi_2 - \mathbf{I} & \Phi_3 & \dots & \Phi_{N+1} - \mathbf{I} \\ \vdots & \vdots & \vdots & \ddots & \vdots \\ \mathbf{I} & \Phi_2 - \mathbf{I} & \Phi_3 - \mathbf{I} & \dots & \Phi_{N+1} \\ \mathbf{I} & \Phi_2 - \mathbf{I} & \Phi_3 - \mathbf{I} & \dots & \Phi_{N+1} - \mathbf{I} \end{bmatrix} \quad (3.27)$$

with $\Phi_i := \left(1 - \frac{m_{i-1}}{\gamma_{i-1}m_L}\right)\mathbf{I}_2$. However, similar results are observed in which the mass matrix (3.20) is block-diagonalized such that

$$S^{-T}\mathbf{M}S^{-1} =: \begin{bmatrix} m_L\mathbf{I}_2 & \mathbf{0} \\ \mathbf{0} & \bar{\mathbf{M}} \end{bmatrix} \quad (3.28)$$

where $\bar{\mathbf{M}} = \bar{\mathbf{M}}^T > 0 \in \mathbb{R}^{2N \times 2N}$. Similarly, the information graph (3.21) is decomposed to attain

$$S^{-T}(\hat{\mathcal{L}} \otimes \mathbf{I}_2)S^{-1} = \begin{bmatrix} \mathbf{0}_{2 \times 2} & \mathbf{D}^T \\ \mathbf{0}_{N \times 2} & \bar{\mathbf{L}} \end{bmatrix}. \quad (3.29)$$

where the structures of $\mathbf{D} \in \mathbb{R}^{2N \times 2}$ and $\bar{\mathbf{L}} \in \mathbb{R}^{2N \times 2N}$ are identical to the one defined by Lee & Spong[1].

The Locked and Shape systems of the total dynamics (3.19) as $t \geq T_{tele}$ are obtained as

$$m_L\ddot{\mathbf{z}}_1 + b\mathbf{D}^T\dot{\mathbf{z}}_e + k\mathbf{D}^T\mathbf{z}_e = f_{Lc} - f_{Lc}^{env} \quad (3.30)$$

$$\bar{\mathbf{M}}\ddot{\mathbf{z}}_e + b\bar{\mathbf{L}}\dot{\mathbf{z}}_e + k\bar{\mathbf{L}}\mathbf{z}_e = f_{Sh} - f_{Sh}^{env} \quad (3.31)$$

where $[f_{Lc}^T, f_{Sh}^T]^T = S^{-T}\mathbf{f}$, and $[f_{Lc}^{envT}, f_{Sh}^{envT}]^T = S^{-T}\mathbf{f}_e$. Notice that the Locked system (3.30) is coupled with the Shape system (3.31) through \mathbf{D} . In one ap-

proach, Nam & Namerikawa[24] introduced a decoupling control input into the system to eliminate the coupled term. However, Lee & Spong[1] emphasized that \mathbf{D} can be eliminated through proper selection of graph topology (3.3) to satisfy Defs. 3.2.1 & 3.2.2. Hence, following this result the newly decoupled Locked system is redefined as

$$m_L \ddot{z}_1 = f_{Lc} - f_{Lc}^{env}. \quad (3.32)$$

The following lemma provides the sufficient conditions for selecting gains k, b to ensure that all slave agents simultaneously arrive to the intended final targets by the consensus control law (3.15).

Lemma 3.3.1. Suppose for the total dynamics of the slave agents in (3.19) and $t < T_{tele}$, there exist gains $k, b > 0$ to guarantee simultaneous asymptotic convergence of all slave agents to their intended final positions on the environment/target iff the following conditions are met

$$2b^2 \bar{\mathbf{L}}_{sym} - k \bar{\mathbf{M}} > 0 \text{ and } \bar{\mathbf{L}}_{sym} > 0, \quad (3.33)$$

where $\bar{\mathbf{L}}_{sym}$ is the symmetric component of $\bar{\mathbf{L}}$.

Proof. We use a similar proof to Lee & Spong[1, Th.1]. As for $t < T_{tele}$, we have $f_{Sh} - f_{Sh}^{env} = 0$. Hence, the sub-system (3.31) can be regarded as an autonomous LTI system of $\dot{x}(t) = Ax(t)$ where $x = [\mathbf{z}_e^T, \mathbf{z}_e^T]^T \in \mathbb{R}^{2N}$, and

$$A = \begin{bmatrix} -b \bar{\mathbf{M}}^{-1} \bar{\mathbf{L}} & -k \bar{\mathbf{M}}^{-1} \bar{\mathbf{L}} \\ \mathbf{I} & \mathbf{0} \end{bmatrix}. \quad (3.34)$$

Next, a Lyapunov function $V : \mathbb{R}^{2N} \rightarrow \mathbb{R}$ is chosen as

$$V(x) := \frac{1}{2} x^T \bar{\mathbf{P}} x > 0, \quad (3.35)$$

where

$$\bar{P} := \begin{bmatrix} \bar{\mathbf{M}} & \frac{k}{b}\bar{\mathbf{M}} \\ \frac{k}{b}\bar{\mathbf{M}} & 2k\bar{\mathbf{L}}_{sym} \end{bmatrix} =: \bar{P}^T > 0 \iff (3.33). \quad (3.36)$$

Using the dynamic of $\dot{x} = Ax$, we can show the time derivative of the Lyapunov function (3.35) as

$$\begin{aligned} \dot{V}(x) &= \frac{1}{2}\dot{x}^T \bar{P}x + \frac{1}{2}x^T \bar{P}\dot{x} \\ &= \frac{1}{2}x^T (A^T \bar{P} + \bar{P}A)x. \end{aligned} \quad (3.37)$$

Here, we choose a matrix \bar{Q} such that

$$\bar{Q} = \begin{bmatrix} \bar{Q}_{11} & \bar{Q}_{12} \\ \bar{Q}_{21} & \bar{Q}_{22} \end{bmatrix} = -\frac{1}{2}(A^T \bar{P} + \bar{P}A), \quad (3.38)$$

where

$$\bar{Q}_{11} = \frac{1}{2}b(\bar{\mathbf{L}} + \bar{\mathbf{L}}^T) - \frac{k}{b}\bar{\mathbf{M}} = b\bar{\mathbf{L}}_{sym} - \frac{k}{b}\bar{\mathbf{M}} \quad (3.39)$$

$$\bar{Q}_{12} = \frac{1}{2}k\bar{\mathbf{L}}^T - \frac{1}{2}(2k)\bar{\mathbf{L}}_{sym} + \frac{1}{2}k\bar{\mathbf{L}} = 0 \quad (3.40)$$

$$\bar{Q}_{21} = \bar{Q}_{12}^T = 0 \quad (3.41)$$

$$\bar{Q}_{22} = \frac{1}{2}\frac{k^2}{b}(\bar{\mathbf{L}} + \bar{\mathbf{L}}^T) = \frac{k^2}{b}\bar{\mathbf{L}}_{sym}. \quad (3.42)$$

Therefore, we have $\dot{V}(x) < 0, \forall x \neq 0$, because $\bar{Q} = \bar{Q}^T > 0$ by (3.33). \square

3.3.3 Tele-operation time T_{tele}

The estimation of T_{tele} is crucial since it is considered as the *waiting time* by the master manipulator before a teleoperation session begins. This parameter is non-unique since it depends on the positions and velocities of all slave agents at $t = 0$.

Theorem 3.3.1. Suppose for any k and b satisfying Lem. 3.3.1, with any arbitrary initial positions $\mathbf{p}(0) \in \mathbb{R}^{2N}$ and velocities $\dot{\mathbf{p}}(0) \in \mathbb{R}^{2N}$ of the agents, then the approximate “maximum” time T_{tele} taken by the agents to reach to the intended final positions on the environment such that for a small scalar $\tilde{\epsilon} > 0$, $\|x\| < \tilde{\epsilon}$ for $t > T_{tele}$.

Proof. Suppose the matrix A defined in (3.34) is a stable matrix. Hence, there exist $\bar{a} > 0$ and $\bar{k} > 0$ such that $\|e^{At}\| \leq \bar{k}e^{-\bar{a}t}$. Then,

$$\|x(t)\| = \|e^{At}x(0)\| \leq \|e^{At}\| \|x(0)\| \leq \bar{k}e^{-\bar{a}t}\|x(0)\|. \quad (3.43)$$

Hence, when $t > \frac{1}{\bar{a}} \ln \bar{k}\|x(0)\|/\tilde{\epsilon}$, $\|x(t)\| \leq \tilde{\epsilon}$. Therefore, $T_{tele} = \frac{1}{\bar{a}} \ln \bar{k}\|x(0)\|/\tilde{\epsilon}$. \square

In the next section, we present our approach to achieve impedance matching between master and multi-slave manipulators. Consider the time interval $t > T_{tele}$, and based on the block diagram in Fig. 3.2, the following control laws for the sub-dynamics of (3.32) and (3.31) are used:

$$f_{Lc} = C_1\dot{p}_m - C_m\dot{z}_1 + C_3f_h, \quad (3.44)$$

$$f_{Sh} = f_{Sh}^{env}. \quad (3.45)$$

3.4 Impedance matching by FRIT

In this chapter, we extend the work of Tsuji *et al.*[4] to improve transparency between the master and slave manipulators in the framework of multi-agents system. Rewriting the dynamics of the master and slave (Locked) manipulators in terms of their impedance yields us to

$$\dot{p}_m = \mathcal{Z}_m^{-1}f_m \quad \text{and} \quad \dot{z}_1 = \mathcal{Z}_{Lc}^{-1}f_{Lc} \quad (3.46)$$

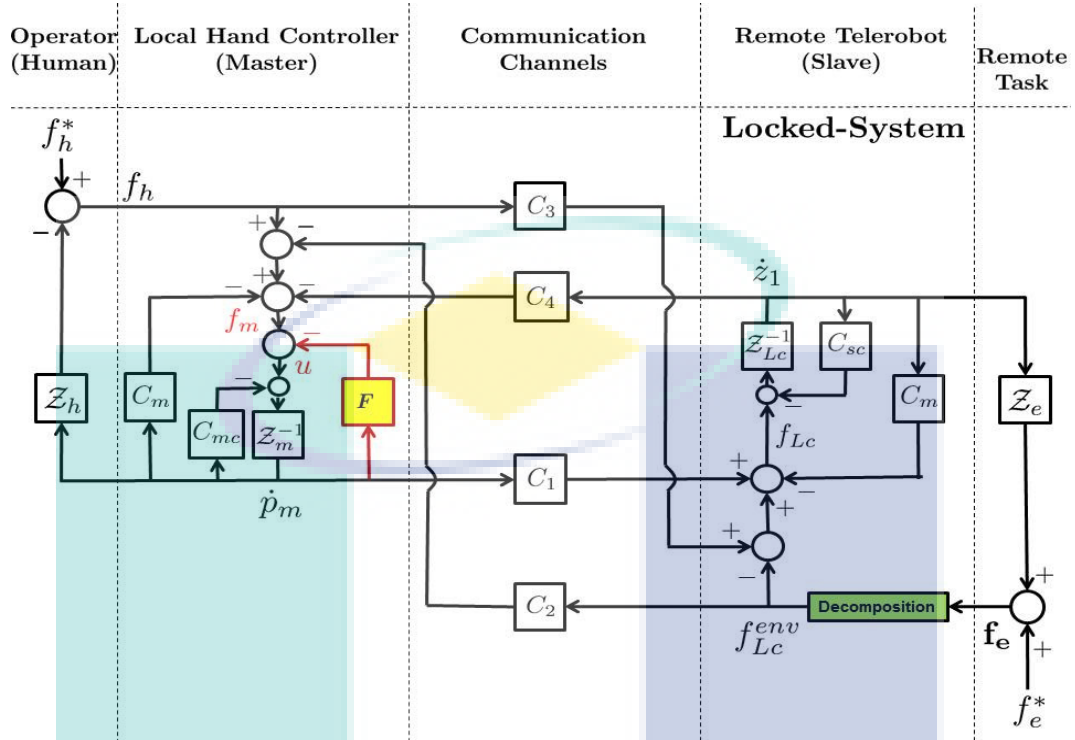


Figure 3.2: General structure of teleoperation indicating the equalizer F and inter-venient impedances, C_{mc} & C_{sc} .

where $Z_m = M_m s$ and $Z_{Lc} = M_{Lc} s$, respectively. An equalizer is placed in the feedback loop of the master manipulator. By optimally tuning this equalizer symmetrize the impedance in both sides of teleoperation. Contrary to Tsuji *et al.*[4], we consider a special structure of F and the tuning procedure is carried-out using the 2-dimensional space data. Figure 3.2 illustrates the placement of the equalizer F in the general structure of our teleoperation system. The control gains C_1, C_2, C_3 and C_4 can be designed accordingly to form either “position-position”, “position-force” or “optimized” teleoperation architectures[2, 3, 8]. To avoid acceleration measurement, additional controllers C_{mc} and C_{sc} (low-gain PD Control) are employed as the inter-venient impedance to the original systems[2]. Hence, (3.46) is rewritten as

$$\dot{p}_m = \hat{Z}_m^{-1} f_m \quad \text{and} \quad \dot{z}_1 = \hat{Z}_{Lc}^{-1} f_{Lc} \quad (3.47)$$

where $\hat{Z}_m = Z_m + C_{mc}$ and $\hat{Z}_{Lc} = Z_{Lc} + C_{sc}$.

3.4.1 FRIT

FRIT is a simple yet powerful tuning algorithm in the sense that we require only a single-shot of experimental data of the closed-loop system to obtain the optimum controller parameters[18]. Figure 3.3 depicts the main concepts of impedance matching using FRIT in Tsuji *et al*[4]. As illustrated in Fig. 3.3(a), the ultimate aim of introducing the equalizer F is to achieve $\hat{Z}_F \rightarrow \hat{Z}_{Lc}$. However, before F can be tuned, it is necessary to match the velocities of the master and the Locked system through \mathcal{H} as depicted in Fig. 3.3(b). Hence, we solve the optimization problem:

$$\min_{\mathcal{H}} J_H, \quad (3.48)$$

where for the recorded initial data $\dot{p}_m^0(k)$ and $\dot{z}_1^0(k)$,

$$J_H := \|\dot{z}_1^0(k) - \mathcal{H}(z)\dot{p}_m^0(k)\|_K^2. \quad (3.49)$$

Based on the optimal $\mathcal{H}(z)$, we solve the second optimization problem:

$$\min_F J_F, \quad (3.50)$$

where for the recorded initial data $f_m^0(k)$ and $f_{Lc}^0(k)$ when the initial equalizer $F_0(z)$ is used,

$$J_F := \|f_{Lc}^0(k) - \tilde{f}_{Lc}(k)\|_K^2, \quad (3.51)$$

and the fictitious reference signal is

$$\tilde{f}_{Lc}(k) := \mathcal{H}(z)(u^0(k) + F(z)\dot{p}_m^0(k)), \quad (3.52)$$

$$u^0(k) = f_m^0(k) - F_0(z)\dot{p}_m^0(k). \quad (3.53)$$

Figure 3.4 delineates the main tuning-steps to obtain the optimal equalizer F .

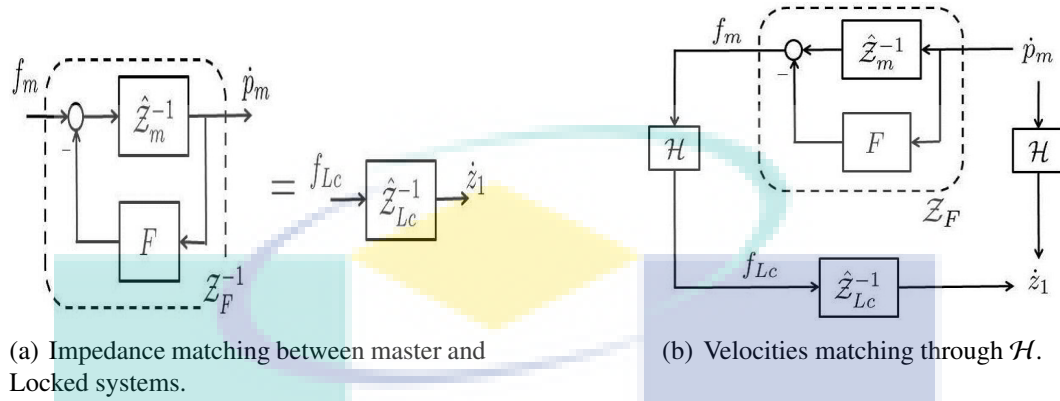


Figure 3.3: Concept of impedance matching by FRIT.

Theorem 3.4.1. Suppose that $\mathcal{H}^* := \arg \min_{\mathcal{H}} J_H$ and $F^* := \arg \min_F J_F$ attain $J_H = 0$ and $J_F = 0$, respectively. Then, if the signal $\dot{z}_1^0(k)$ is rich,

$$\hat{Z}_F = \hat{Z}_m + F^* = \hat{Z}_{Lc}. \quad (3.54)$$

Proof. Since $u^0(k) = \hat{Z}_m \dot{p}_m^0(k)$, when $f_{Lc}^0(k) = \tilde{f}_{Lc}(k)$,

$$\begin{aligned} \dot{z}_1^0(k) &= \hat{Z}_{Lc}^{-1} f_{Lc}^0(k) \\ &= \hat{Z}_{Lc}^{-1} \tilde{f}_{Lc}(k) \\ &= \hat{Z}_{Lc}^{-1} \mathcal{H}^*(z) (u^0(k) + F^*(z) \dot{p}_m^0(k)) \\ &= \hat{Z}_{Lc}^{-1} \mathcal{H}^*(z) (\hat{Z}_m + F^*(z)) \dot{p}_m^0(k) \\ &= \hat{Z}_{Lc}^{-1} (\hat{Z}_m + F^*(z)) \mathcal{H}^*(z) \dot{p}_m^0(k) \end{aligned}$$

If $\dot{z}_1^0(k) = \mathcal{H}^*(z) \dot{p}_m^0(k)$,

$$\dot{z}_1^0(k) = \hat{Z}_{Lc}^{-1} (\hat{Z}_m + F^*(z)) \dot{z}_1^0(k). \quad (3.55)$$

Hence, if (3.54) is satisfied, (3.55) holds. Reversely, if the signal $\dot{z}_1^0(k)$ is rich, (3.54) holds. \square

3.4.2 Laguerre network

We can approximate a discrete time SISO system to use a Laguerre function [34, 20]

$$L_i(z) = \beta \frac{(1 - \alpha z)^{i-1}}{(z - \alpha)^i}, \quad (3.56)$$

as $\hat{y}(z) = g(z)u(z) = \sum_{i=1}^M c_i L_i u(z)$ (Fig. 3.5). Here $\alpha := e^{-pT}$ and $\beta := \sqrt{(1 - \alpha^2)T}$. The parameter p is determined by the system's designer and T is the sample time. Meanwhile $c_i \in \mathbb{R}$, $i = 1, \dots, M$ are the coefficients that form the basis of the Laguerre network. Let $l_i(k) \in \mathbb{R}$, $i = 1, \dots, M$ represents the output of the i th-order filter in the Laguerre network. Then, the SISO state-space model is given by

$$g(z) : \begin{cases} l(k+1) = al(k) + bu(k) \\ \hat{y}(k) = c^T l(k) \end{cases} \quad (3.57)$$

where $l = [l_1, \dots, l_M]^T \in \mathbb{R}^M$, $a \in \mathbb{R}^{M \times M}$, $b \in \mathbb{R}^M$, $c \in \mathbb{R}^M$,

$$\{a\}_{ij} := \begin{cases} \tau_1 & \text{if } i = j \\ \frac{(-1)^{i-j} \tau_2^{i-j-1} (\tau_1 \tau_2 + \tau_3)}{T^{i-j}} & \text{if } i > j \\ 0 & \text{otherwise,} \end{cases} \quad (3.58)$$

$$\{b\}_i := \left(-\frac{\tau_2}{T}\right)^{i-1} \tau_4 \quad (3.59)$$

$$c^T = [c_1 \ \dots \ c_M]. \quad (3.60)$$

$$\tau_1 = e^{-pT}, \quad \tau_2 = T + \frac{2}{p}(e^{-pT} - 1), \quad (3.61)$$

$$\tau_3 = -T e^{-pT} - \frac{2}{p}(e^{-pT} - 1), \quad \tau_4 = \frac{\sqrt{2p}}{p}(1 - \tau_1). \quad (3.62)$$

The MIMO transfer matrix $G(z) = \mathbf{I}_n \otimes g(z)$ has a state-space representation

given as

$$G(z) : \begin{cases} \mathbf{l}(k+1) = \mathbf{A}\mathbf{l}(k) + \mathbf{B}u(k) \\ \hat{\mathbf{y}}(k) = \mathbf{C}^T\mathbf{l}(k), \end{cases} \quad (3.63)$$

where $\mathbf{l} = \mathbf{1}_n \otimes l \in \mathbb{R}^{nM}$, $\mathbf{A} = \mathbf{I}_n \otimes a \in \mathbb{R}^{nM \times nM}$, $\mathbf{B} = \mathbf{I}_n \otimes b \in \mathbb{R}^{nM \times n}$ and $\mathbf{C}^T = \mathbf{I}_n \otimes c^T \in \mathbb{R}^{n \times nM}$.

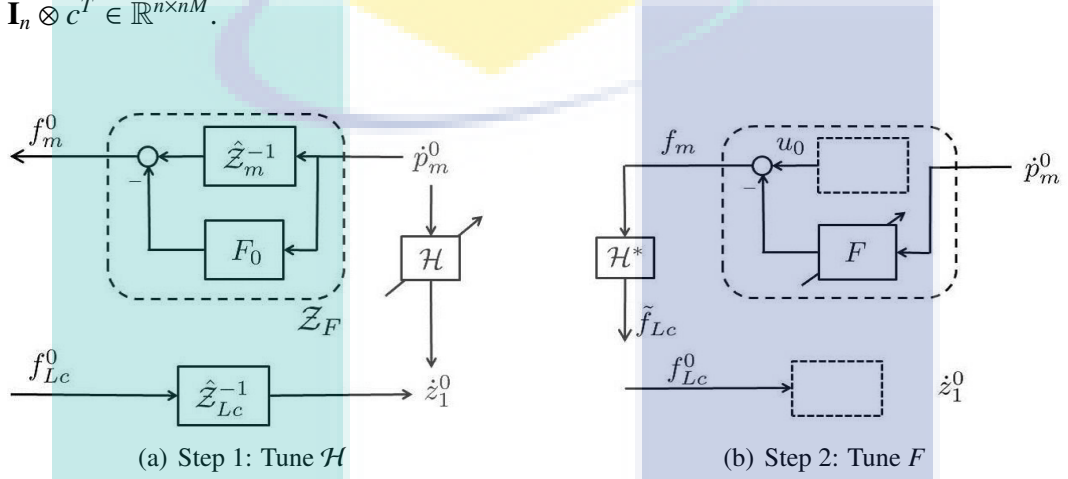


Figure 3.4: Two-steps of tuning[4] to obtain optimum F .

The appropriate design of the equalizer F can be obtained by assigning (3.63) into F . To ensure faster rate convergence of the Laguerre network, Wahlberg[35] suggested that the value of p should be chosen close to the inverse of the system dominant time constant. However for our case, the parameter of p must be chosen so that the designed equalizer will be in-sync with the Shape system (3.31). Hence, the parameter p in (3.56) is to take parameter \bar{a} in (3.43) such that $p = \bar{a}$. Therefore, we are left with the tuneable parameters of c , where the optimum equalizer F can be obtained by simply tuning the basis (3.60).

On the other hand, the selection of the equalizer \mathcal{H} requires \mathcal{H} to be invertible and \mathcal{H}^{-1} is stable. Therefore, we select a biproper transfer function in the form of

$$h(z) = \frac{1 + \bar{a}_1 z^{-1} + \dots + \bar{a}_p z^{-p}}{1 + \bar{b}_1 z^{-1} + \dots + \bar{b}_p z^{-p}} \quad (3.64)$$

to yield us a MIMO transfer matrix of $\mathcal{H} = \mathbf{I}_n \otimes h(z)$. The estimation of the coefficients \bar{a}_i, \bar{b}_i in (3.64) can be obtained by minimizing (3.49) through least-square method (LSM). Re-arranging data such that

$$\Psi_H = \begin{bmatrix} \dot{p}_m^0(P) & \cdots & \dot{p}_m^0(1) & -\dot{z}_1^0(P) & \cdots & -\dot{z}_1^0(1) \\ \vdots & \cdots & \vdots & \vdots & \cdots & \vdots \\ \dot{p}_m^0(K-1) & \cdots & \dot{p}_m^0(K-P) & -\dot{z}_1^0(K-1) & \cdots & -\dot{z}_1^0(K-P) \end{bmatrix},$$

$$\Upsilon_H = \begin{bmatrix} \dot{z}_1^0(P+1) - \dot{p}_m^0(P+1) \\ \vdots \\ \dot{z}_1^0(K) - \dot{p}_m^0(K) \end{bmatrix}, \text{ and } \chi_H = \begin{bmatrix} \bar{a}_1 \\ \vdots \\ \bar{a}_P \\ \bar{b}_1 \\ \vdots \\ \bar{b}_P \end{bmatrix},$$

to give us a linear relation of

$$\Psi_H \chi_H = \Upsilon_H, \quad (3.65)$$

where $\Psi_H \in \mathbb{R}^{n(K-P) \times nP}$, $\chi_H \in \mathbb{R}^{nP}$, and $\Upsilon_H \in \mathbb{R}^{n(K-P)}$. Then, the optimal coefficients are obtained by

$$\chi_H^* = \arg \min_{\chi_H} J_H = \Psi_H^\dagger \Upsilon_H \quad (3.66)$$

where $\Psi_H^\dagger := (\Psi_H^T \Psi_H)^{-1} \Psi_H^T$ is the *Moore-Penrose* pseudoinverse of Ψ_H in (3.65).

Next, we illustrate the tuning procedure to obtain the optimum equalizer F . The cost function (3.51) is simplified to

$$\begin{aligned} J_F &= \left\| f_{Lc}^0 - \mathcal{H}^*(u^0(k) + F(z))\dot{p}_m^0(k) \right\|_K^2 \\ &= \left\| (\mathcal{H}^{*-1} f_{Lc}^0(k) - u^0(k)) - F(z)\dot{p}_m^0(k) \right\|_K^2 \end{aligned} \quad (3.67)$$

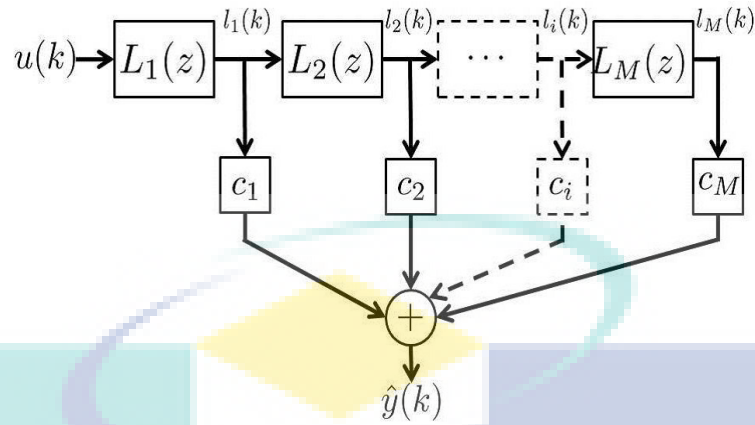


Figure 3.5: Structure of the Laguerre Network.

where \mathcal{H}^* is \mathcal{H} with the optimized parameters obtained by (3.66). The overall algorithm to obtain optimum F is summarized as following:

Step 1 : Set a Laguerre network $F^0(z)$ using (3.63) and $\mathbf{C}_0 = \mathbf{I}_n \otimes c_0 \in \mathbb{R}^{n \times nM}$ with an appropriate initial $c = c_0$ as

$$F^0(z) : \begin{cases} \mathbf{l}(k+1) = \mathbf{A}\mathbf{l}(k) + \mathbf{B}\dot{p}_m(k) \\ \bar{y}_L(k) = \mathbf{C}_0^T \mathbf{l}(k). \end{cases}$$

Step 2 : Perform an experiment to generate the initial data $\dot{p}_m^0, z_1^0, f_{Lc}^0$ and f_m^0 .

Step 3 : Choose a bi-proper transfer function \mathcal{H} , and minimize (3.49) by (3.66) using data obtained in Step 2.

Step 4 : Using the optimally tuned $\mathcal{H}(z)$, find the minimizer $F^*(z)$ to minimize the cost function (3.67).

The sub-algorithm in Step 4 to tune F is as follows:

Step i : Generate the new data $\tilde{y}(k) = \mathcal{H}^{*-1} f_{Lc}^0(k) - u^0(k)$.

Step ii : Using \dot{p}_m^0 in Step 2, generate the state data $\mathbf{l}(k)$.

Step iii : Find the minimizer c^* of the constraint minimization

$$\begin{aligned} \min_c & \left\| \mathbf{C}^T l(k) - \tilde{y}(k) \right\|_K^2 + \eta \|c - c_0\|^2 \\ \text{subject to } & \mathbf{C}^T = \mathbf{I}_n \otimes c^T \in \mathbb{R}^{n \times nM}. \end{aligned} \quad (3.68)$$

This is equivalent to

$$\min_c \sum_{i=1}^n \left\| c^T l(k) - \tilde{y}_i(k) \right\|_K^2 + \eta \|c - c_0\|^2. \quad (3.69)$$

Then, the minimizer is obtained by

$$c^{T*} = \Upsilon_F \Psi_F^T (\Psi_F \Psi_F^T)^{-1} \quad (3.70)$$

where

$$\begin{aligned} \Psi_F &= \begin{bmatrix} l(P+1) \cdots l(K) & l(P+1) \cdots l(K) \cdots \\ l(P+1) \cdots l(K) & \sqrt{\eta} I_M \end{bmatrix} \in \mathbb{R}^{M \times (n(K-P)+M)} \\ \Upsilon_F &= \begin{bmatrix} \tilde{y}_1(P+1) \cdots \tilde{y}_1(K) & \tilde{y}_2(P+1) \cdots \\ \tilde{y}_n(P+1) \cdots \tilde{y}_n(K) & c_0^T \end{bmatrix} \in \mathbb{R}^{1 \times (n(K-P)+M)}. \end{aligned}$$

Remark 3.4.1. Notice that in (3.68) we re-define the cost function (3.67) by introducing a multiplier constant $\eta > 0 \in \mathbb{R}$ and an additional cost function $\|c - c_0\|$. Since the generated data in Step i) may lead to large value of c , then the second term in (3.68) provides trade-off in seeking optimal solution between the original cost function (3.51) and the initial parameters of c .

Remark 3.4.2. Note that we use the discrete-time domain on describing the structure of the Laguerre filter (3.56) and Laguerre network (3.57). Since the tuning procedure involves utilization of the sampled data set, hence it is clearer to discuss the algorithm in this domain.

3.4.3 Selection of dynamics C_1, C_2, C_3 and C_4

From the structure of teleoperation in Fig. 3.2, defining $\Omega = C_1 + C_3 \hat{\mathcal{Z}}_m + C_3 F + C_3 C_m$ and $\Sigma = \hat{\mathcal{Z}}_m + F + C_m$, the hybrid matrix (3.4) consists of

$$h_{11} = \Sigma \cdot \Omega^{-1} (\hat{\mathcal{Z}}_{Lc} + C_m - C_3 C_4) + C_4 \quad (3.71)$$

$$h_{12} = -\Sigma \cdot \Omega^{-1} (\mathbf{I} - C_3 C_2) - C_2 \quad (3.72)$$

$$h_{21} = \Omega^{-1} (\hat{\mathcal{Z}}_{Lc} + C_m - C_3 C_4) \quad (3.73)$$

$$h_{22} = -\Omega^{-1} (\mathbf{I} - C_3 C_2) \quad (3.74)$$

To use the *Transparency-Optimized* architecture [3, 8] and towards attaining symmetry between the master and slave sides, we choose

$$C_1 = C_m, \quad C_2 = \mathbf{I}, \quad C_3 = \mathbf{I}, \quad C_4 = -C_m. \quad (3.75)$$

Since $C_2 = C_3 = \mathbf{I}$, we obtain $h_{22} = 0$ and $h_{12} = -\mathbf{I}$. Next, the properties of the dynamics h_{11} and h_{21} are stated in the following lemma.

Lemma 3.4.1. If the equalizer F is properly tuned and we can use (3.75), then $h_{21} = \mathbf{I}$, and

$$h_{11} = \hat{\mathcal{Z}}_m + F^*, \quad (3.76)$$

Proof. By optimally tuned equalizer F , we reach to $\hat{\mathcal{Z}}_m + F^* = \mathcal{Z}_{Lc}$. Substituting C_3, C_4 into (3.73), and to use $\Omega = \hat{\mathcal{Z}}_m + F^* + 2C_m = \hat{\mathcal{Z}}_{Lc} + 2C_m$, hence obviously $h_{21} = \Omega^{-1} \Omega = \mathbf{I}$. \square

Remark 3.4.3. For $h_{11} \neq 0$, the transmitted impedance is insensitive to \mathcal{Z}_e as $\mathcal{Z}_e \rightarrow 0$ due to \mathcal{Z}_T depends only on the ratio $h_{11} h_{21}^{-1}$ [8]. However, Zhu & Salcudean [2] pointed out that a complete transparency might not be desirable since for infinitely stiff and weightless mechanical manipulators would drift around if they are not con-

nected to any load and an operator. Hence, (3.76) is sufficient in our case. For this condition, the total impedance felt by the human operator will include the master impedance and equalizer such that $\mathcal{Z}_T = \hat{\mathcal{Z}}_m + F^* + \mathcal{Z}_e$.

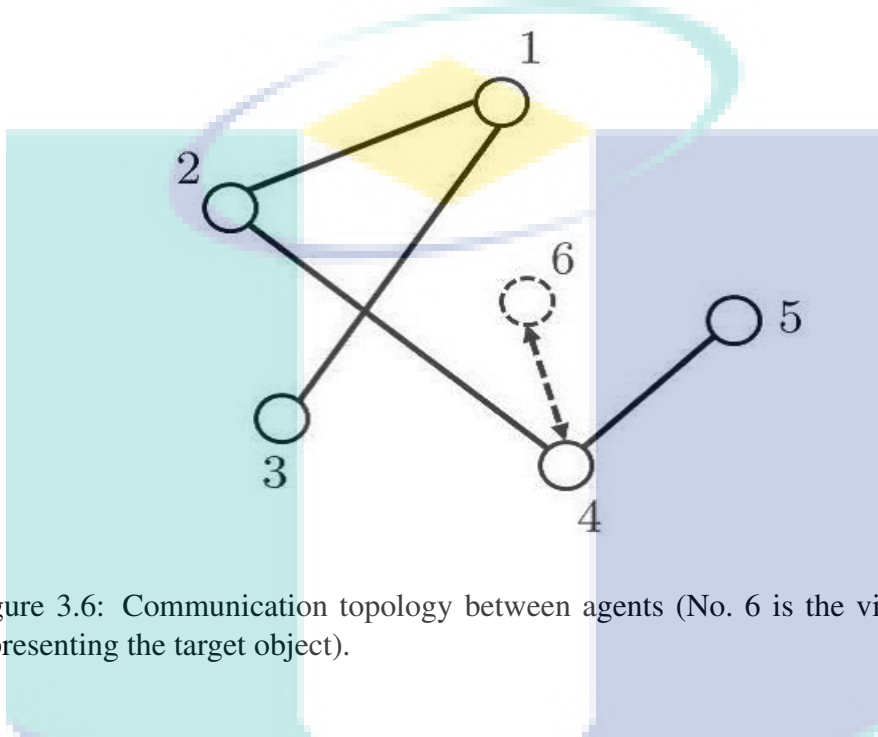


Figure 3.6: Communication topology between agents (No. 6 is the virtual agent representing the target object).

3.5 Numerical example

A numerical example to illustrate the effectiveness of our approach is presented in this section. Let the slave manipulators comprised of $N = 5$ agents with their communication topology as shown in Fig. 3.6. The dashed-arrow indicates that only agent 4 can measure the position and velocity of the target object (indicated by virtual agent 6). The mass of the master, slave agents and the environment were chosen as $[m_m, m_i, m_e] = [2.0, 0.5, 10]$ kg, $\forall i$. Meanwhile, the radius of the target object/environment was chosen as $R = 1$ m. To satisfy Lem. 3.3.1, the spring and damping constants in (3.17) were selected as $[k, b] = [1200 \text{ N/m}, 500 \text{ Ns/m}]$. With this selection, the dominant eigenvalue of the Shape system (3.31) has been obtained as $\lambda_{tele} = \lambda_{\min} = 2.4029$. For ease of analysis, we assume that the friction force, $F_f = 0$.

The initial positions of the master manipulator and the C.O.M of the target(environment) were set at $(0, 0)$ and being stationary at $t \in [0, T_{tele})$. Meanwhile, the slave agents' positions $p_i(0) \in \mathbb{R}^2, \forall i$ were initialized around the target in the region $[-10, 10] \times [-10, 10] \subseteq \mathbb{R}^2$, with zero velocity at $t = 0$ i.e., $\dot{p}_i(0) = 0, \forall i$. In Fig. 3.7(a), the agents' initial positions and trajectories towards their intended final positions on the object for $t \in [0, T_{tele})$ are illustrated. Subsequently, Fig. 3.7(b) depicts the trajectory of Shape system's velocity and position. It is clearly observed that the trajectories of the Shape system were asymptotically converging such that $\lim_{t \rightarrow T_{tele}} \mathbf{z}_e = \lim_{t \rightarrow T_{tele}} \dot{\mathbf{z}}_e = 0$. The estimated teleoperation time based on the given initial positions were obtained as $T_{tele} = 4.1331$ s.

The equalizer $\mathcal{H}(z)$ with order $P = 5$, has its poles and zeros as $p = 0.9689, -0.0989 \pm j0.4221, -0.3925, -0.0299, z = 0.5025 \pm j0.4343, 0.8725, 0.5767 \pm 0.2256$, which all lie inside the unit circle indicates that the tuned system is stable. Correspondingly, the velocity matching performance between $\mathcal{H}\dot{p}_m(k)$ and $\dot{z}_1(k)$ as presented in Fig. 3.8 verifies that there exist \mathcal{H} such that the cost function (3.49) is minimized.

For the selection of the equalizer $F(z)$, a truncated Laguerre network of size $M = 50$ was chosen. The parameters τ_1, τ_2, τ_3 and τ_4 used in (3.58)-(3.59) were obtained as $0.8868, -0.0442, 0.0499$, and 0.1033 , respectively. In Fig. 3.9, we exhibit the comparison between $f_{Lc}^0(k)$ and the response of fictitious signal (3.52) when the equalizer F with optimally tuned parameters was applied. It can be shown that these two signals were almost identical in both x and y directions in the sense that $\|\tilde{f}_{Lc}(k) - f_{Lc}^0(k)\|$ is minimized.

To further illustrate the intelligibility of our approach, we present the signal comparison on positions, velocities, and exerted forces, for the master and the slaves (Locked) manipulators before and after tuning. Clearly as can be seen in Fig. 3.10(a) that prior tuning, the transparency between master and slave was sluggish. As we performed the tuning procedure, the transparency has significantly improved. Therefore, from Fig. 3.10(b) it is observed that the (Locked) manipula-

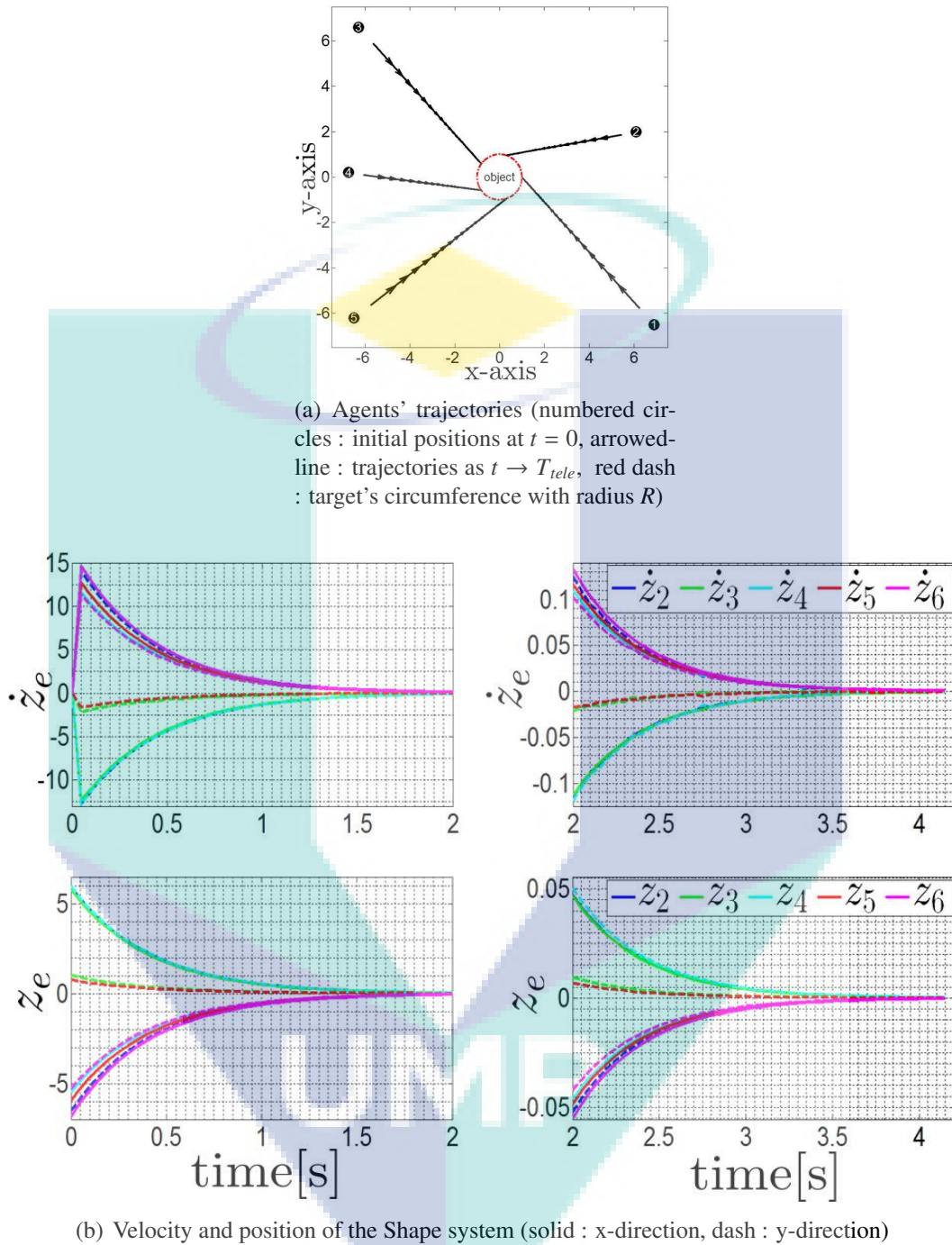


Figure 3.7: Asymptotic convergence of the agents onto their intended final positions on the target object as $t < T_{tele}$, with $\varphi(0) = 0$.

tor asymptotically tracked the master manipulator in both positions and velocities as well as the exerted force signals.

Notice that on the time interval $t \in [4.35, 4.45]$ s, the exerted forces f_m and f_{LC} were slightly larger as compared to the other time intervals. For $t \leq T_{tele}$, the master

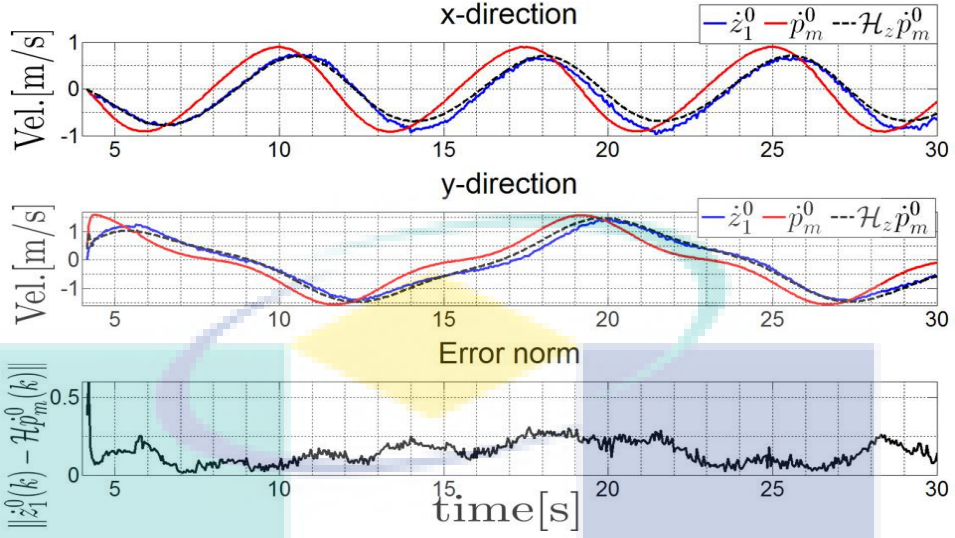


Figure 3.8: Velocity matching through gain $\mathcal{H}(z)$.

manipulator and the target object were both stationary. Therefore in the handling operation ($t > T_{tele}$), to move the manipulators from the stall positions requires for extra exerted forces than when the manipulators were already in motion.

In this example, we used of the intervenient impedances $C_{mc} = \mathbf{I}_2 \otimes \left(2 + \frac{20}{s}\right)$, $C_{sc} = \mathbf{I}_2 \otimes \left(20 + \frac{6}{s}\right)$, the controller $C_m = \mathbf{I}_2 \otimes \left(100 + \frac{1}{s}\right)$, $\mathcal{Z}_h = \mathbf{I}_2 \otimes \left(0.5s + 70 + \frac{2000}{s}\right)$, $\eta = 0.1$, and $T_{sim} = 30[\text{sec}]$, respectively.

3.6 Conclusion

In this chapter, we have proposed tuning algorithm to improve transparency through impedance matching between master and slave manipulators in the multilateral teleoperation system. The passive decomposition technique has provided substantial approach to convert the total dynamics of a multi-slave system into the bilateral teleoperation architecture so that the existing bilateral control technique can be used. Subsequently, from the result of decomposition and the initial states of all slave agents, the teleoperation time, T_{tele} that separated the two operations (grasping and teleoperation) has been estimated. In terms of equalizer tuning, we conclude that FRIT provides powerful algorithms since only a single-shot of measurement data

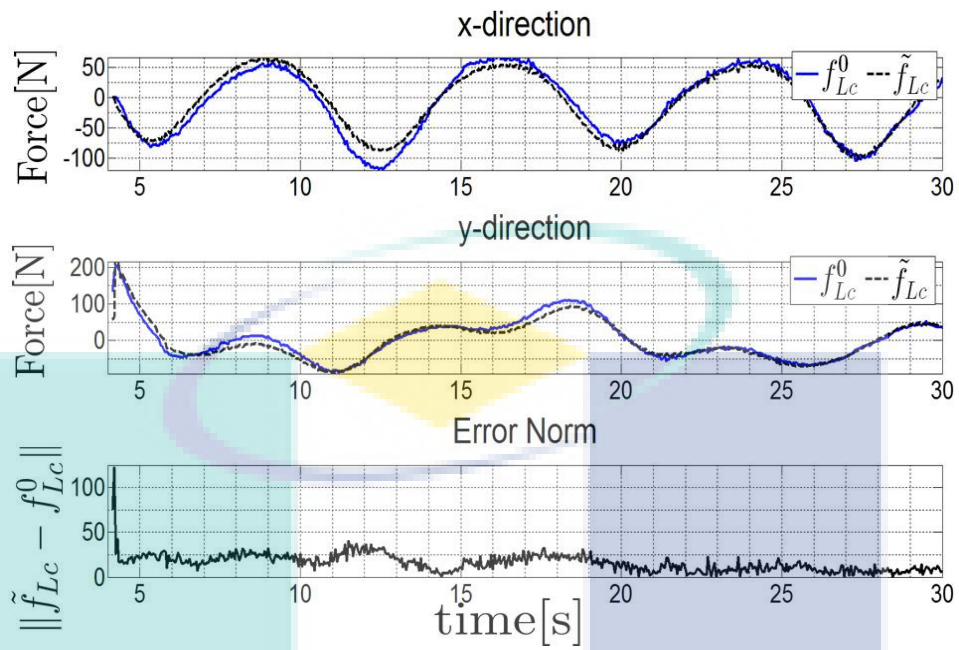
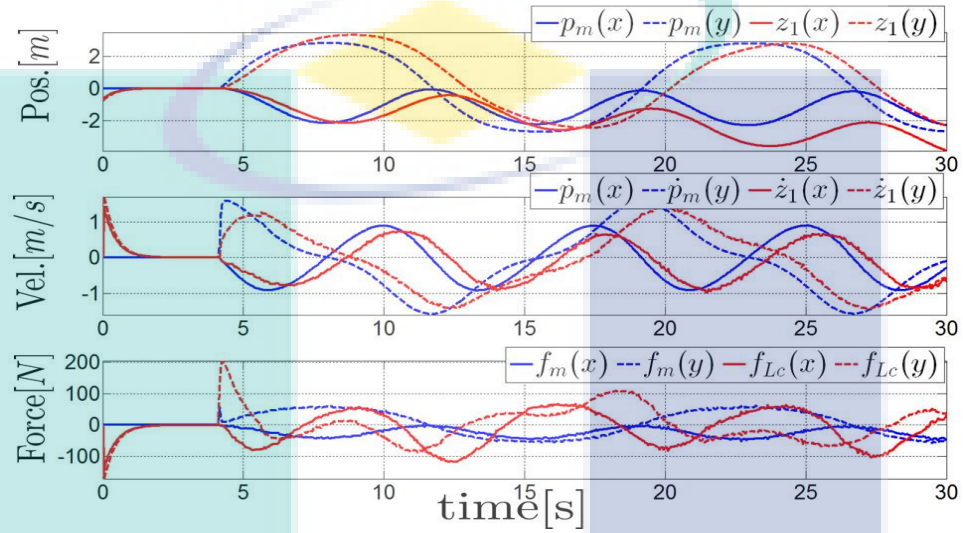
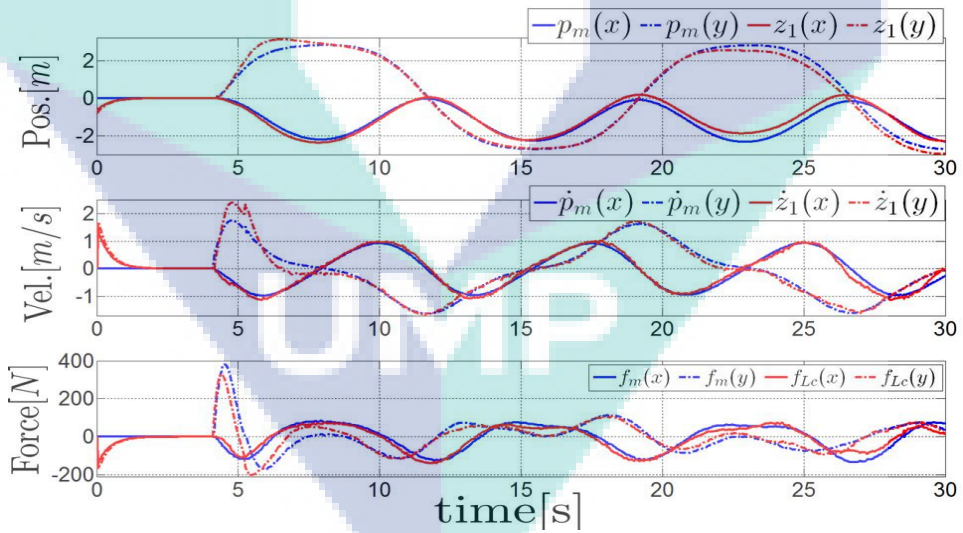


Figure 3.9: Comparison of optimized fictitious signal (3.52) with the initial f_{Lc} .

was required. The overall performance and comparison presented through numerical example has illustrated the applicability of the proposed tuning method.



(a) Before tuning



(b) After tuning

Figure 3.10: Signals comparison for positions, velocities and forces.

Chapter 4

A Fictitious Reference Iterative Tuning Method for Buck Converter-Powered Motor Control System

4.1 Introduction

The usage of a DC motor system can be found in many applications such as home appliances[36], robotics[37], industrial machinery and equipment[38, 39]. There were many studies have been conducted by researchers to design an effective and efficient mechanism to control this system. In general, the commonly used methods for controlling the speed of the motor shaft of a DC motor can be divided into two approaches. For the first approach, the studies focus on the investigation of the topologies of the buck-converter design. For instances, Ortigoza et al., [40] and Beevi & Noufal [41] proposed the hierarchical control of the buck converter. Meanwhile, a bidirectional DC/DC buck converter system that will allow the motor shaft to rotate in both directions was considered in [42]. For the second approach, the

studies are intensified on identifying the control algorithms to efficaciously control the switching signals of the buck converter circuit. One way of achieving this is by controlling the Pulse Width Modulation (PWM) signals, where PWM works in reducing the average power delivered by the electrical signal, by effectively chopping it up into discrete parts.

Having said that, the second method of controlling the DC motor by controlling the PWM signal is more prominent. This is due to the simplicity of the buck-converter structure, and the ease implementation of the control algorithm where only the duty ratio of PWM is to be manipulated. Some related studies that focus on designing the control algorithm to control the duty cycle of PWM switching can be found in [43] where the authors proposed PI-type Fuzzy Logic Control structure; in [44] where the sliding mode controller was investigated; and in [45] where the neural network control structure has been considered. However, these model-based methods require accurate modeling of the plant for controller design.

A model-free or data-driven approach in controller design, on the other hand, has recently attracted the interest of the researchers in the field of control theory. Since the model-based controller design may not work well if the plant model does not fall into the assumed model, there is an added advantage if the modeling requirement can be eradicated in the design procedure. Some of the model-free design techniques found in the literatures are the simultaneous-perturbation-stochastic-approximation (SPSA) methods[46], model-free adaptive control (MFAC)[47], unfalsified control(UC)[48], iterative-feedback tuning (IFT)[49], and virtual-reference-feedback tuning (VRFT)[50]. To add further to the list, the fictitious-reference-iterative-tuning (FRIT) also falls into the category of the model-free design approach. First introduced by Kaneko et. al[51], FRIT only requires the set of recorded input-output data in designing the fictitious reference signals, which availed in formulating the cost function for optimization. Comparing FRIT to VRFT, the key difference between them is that the cost function to be minimized in FRIT fo-

cuses on the output while that in VRFT focuses on the input. Therefore, FRIT is more intuitively understandable than VRFT from a practical point of view. Some examples of the FRIT applications are the controller design for a non-minimum phase system[31], and impedance matching in multilateral teleoperation system[17]. In these works, they had considered the utilization of FRIT in tuning the Laguerre expansion network which forms part of the controller. In [52], the authors provided detail surveys on the comparison between the model-based control and data-driven control.

In this work, we employed the Simulated Kalman Filter (SKF) algorithm[53] in minimizing the formulated cost function to obtain the optimal PID controller's parameters. The SKF is an estimation-based metaheuristic optimization algorithm which relies on the collection of agents to look for the near optimum solution within a reasonable computational effort[54]. By parameterizing the controller and assigning the agents' position as the controller's gain, the algorithm seeks for the best solutions which correspond to the global minimum of the fitness function.

The rest of the chapter is organized as follows. In Section 4.2, we discuss our problem formulation and the modeling of the buck converter-powered DC motor system. Meanwhile, in Section 4.3 we elucidate our proposed methods. A numerical example is presented in Section 4.4. Finally, our main conclusion is drawn in Section 4.5.

Mathematical Notation: Let \mathbb{R} and \mathbb{R}^n denote the set of a real number and real vector with dimension n respectively. We denote the vector norm as $\|v\| = \sqrt{v^T v}$ and $\|v(k)\|_K^2$ implies $\|v(k)\|_K^2 := \sum_{k=1}^K \|v(k)\|^2$.

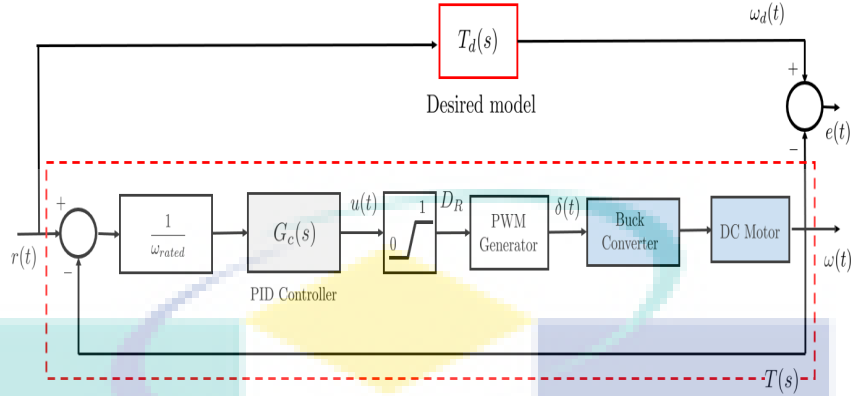


Figure 4.1: Block diagram of the closed system

4.2 Problem Statements

Consider the block diagram of the closed system of a buck converter-powered DC motor control system shown in Fig. 4.1. The design objective is to obtain the optimal PID controller $G_c(s)$ such that for any set point reference input $r(t)$, the angular velocity of is able to track the trajectory of $r(t)$ in minimizing the error $e(t)$, to satisfy the condition $\lim_{t \rightarrow \infty} e(t) = 0, \forall t$. Practically, this can be achieved by having the dynamic of the closed system $T(s)$ to be identical to the desired model $T_d(s)$. Let $\omega_{rated} \in \mathbb{R}$ is the maximum attainable speed when the control input $u(t) = 1$ is applied. This is considered as the saturation point of the angular velocity and is needed to ensure that the error signal fed into the controller will be bounded between 0 to 1.

The saturation block takes the input $u(t)$ to satisfy

$$D_R = \begin{cases} 1 & u(t) \geq 1 \\ u(t) & 0 < u(t) < 1 \\ 0 & u(t) \leq 0, \end{cases} \quad (4.1)$$

where $D_R \in \mathbb{R}$ is the duty ratio to control switching of the PWM output signal $\delta(t) \in \mathbb{R}$. The chosen PID controller structure is defined by $G_c(s) = K \left(1 + \frac{1}{T_i} + T_d \frac{1}{1 + \frac{1}{N_f s}} \right)$ where $K \in \mathbb{R}$, $T_i \in \mathbb{R}$, $T_d \in \mathbb{R}$ and $N_f \in \mathbb{R}$ are the proportional gain, the integral

time constant, the derivative time constant and filter coefficient, respectively.

To achieve $T(s) \equiv T_d(s)$, the controller $G_c(s)$ must be properly tuned. This implies that there exist optimal values of K , T_i , T_d and N_f such that the cost function

$$J_1 = \frac{1}{t_f - t_0} \int_{t_0}^{t_f} e^2(t) dt = \frac{1}{t_f - t_0} \int_{t_0}^{t_f} (T_d(s)r(t) - \omega(t)) dt \quad (4.2)$$

is minimized.

4.2.1 Buck-converter powered dc motor model

This section provides a brief description of the modeling of the buck-converter-driven DC motor system which forms the basis for the simulation analysis presented in this paper. Figure 4.2 delineates the schematic diagram of the DC motor system fed by a buck converter (as indicated in the blue box model in Fig. 4.1). The dynamic of the overall system can be described as follows [40, 41]

$$L \frac{di}{dt} = -v + E\delta(t) \quad (4.3)$$

$$C \frac{dv}{dt} = i - i_a \quad (4.4)$$

$$L_a \frac{di_a}{dt} = v - R_a i_a - K_e \omega \quad (4.5)$$

$$J \frac{d\omega}{dt} = K_m i_a - B\omega - T_L \quad (4.6)$$

where i is the converter input current, i_a is the DC motor armature current, v is the converter output voltage, ω is the motor angular velocity, T_L is the load torque, K_m is the torque constant, K_E is the back-emf constant, J is the moment of inertia, and B is the coefficient of friction. Meanwhile L_a , R_a , and L , R are the armature inductance & resistance and converter inductance & resistance, respectively. The signal $\delta(t)$ is the control input which takes the form of the PWM signals based on the duty ratio of equation (4.1).

Remark 1: It should be noted that even though the mathematical modeling of the

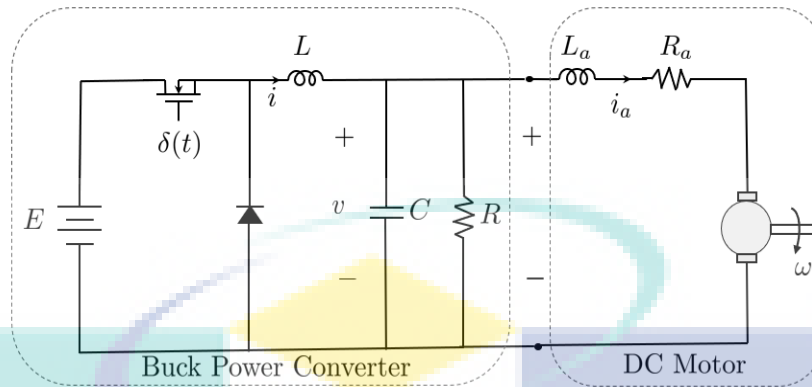


Figure 4.2: Schematic of the buck converter powered DC motor system

system is provided in this paper, it is not a necessity as our proposed method requires only the input-output data of the plant for controller tuning. The modeling is supplied to provide insights and for results comparison between the model-based technique and our proposed solutions in controller design.

4.3 Algorithm for Controller Tuning

4.3.1 A brief review of SKF algorithm

In this section, we provide a brief review of the Simulated Kalman Filter (SKF) algorithm which was used in obtaining the optimal controller parameters. First introduced by R.E Kalman in 1960[55], the Kalman Filter is a well-established state estimation method of a dynamic system that is excited by a stochastic process and measurement noise. Improved by Ibrahim et.al.,[53, 54], SKF algorithm consists for three main stages namely, Stage 1: Initialization, Stage 2: Fitness Evaluation, and Stage 3: Predict, measure and Estimate.

In the initialization stage, the algorithm starts with random initialization of agents' estimated state, $x(0) \in \mathbb{R}^N$, within the search space. At the same instant, the initial value of error covariance estimate, $P(0) \in \mathbb{R}$, the process noise, $Q \in \mathbb{R}$, measurement noise, $R \in \mathbb{R}$ and the maximum number of iterations, t_{Max} are all to be

initialized. As reported in [54], the best values of $P(0)$, Q and R are 1000, 0.5 and 0.5, respectively.

Next, in the second stage, the iteration begins with the fitness calculation of i th agent, $fit_i(x(t))$. The $x_{best}(t) \in \mathbb{R}$ is updated to satisfy the following minimization problem of

$$x_{best}(t) = \min_{i \in \{1, 2, \dots, N\}} fit_i(x(t)). \quad (4.7)$$

Then, the true value, $x_{true} \in \mathbb{R}$ which represents the best solutions-so-far will be updated. This value is updated if there exists a better solution, i.e. $x_{best}(t) < x_{true}$.

Finally, in the third stage, the SKF search strategy implements three simple steps; predict-measure-estimate. In the prediction step, the time update equations are used to obtain a *priori* estimates for the next time step. After the measurement process, measurement-update equations are used to obtain improved *posterior* estimates. The prediction of the state and error covariance estimates given the prior estimated are updated based on the following time-update equations:

$$x_i(t | t + 1) = x_i(t) \quad (4.8)$$

$$P(t | t + 1) = P(t) + Q. \quad (4.9)$$

The next step is the measurement, which acts as a feedback to the estimation process. The measurement of each individual agent is simulated based on the following equation:

$$z_i(t) = x_i(t | t + 1) + \sin(\text{rand} \times 2\pi) \times |x_i(t | t + 1) - x_{true}|. \quad (4.10)$$

The final step is the estimation. Here, the Kalman gain $K(t)$ is computed based

on the following equation:

$$K(t) = \frac{P(t | t + 1)}{P(t | t + 1) + R}. \quad (4.11)$$

Then, the following measurement-update equation are used to improve a *posteriori* estimates from a *priori* estimates:

$$x_i(t + 1) = x_i(t | t + 1) + K(t) \times (z_i(t) - x_i(t | t + 1)) \quad (4.12)$$

$$P(t + 1) = (1 - K(t)) \times P(t | t + 1). \quad (4.13)$$

Each agent updates the optimal estimate for that corresponding iteration based on the measured position which was used as feedback and influenced by the gain value, $K(t)$. The iteration continues until the maximum number of iterations t_{Max} is reached. Further details on the algorithm can be found in [54].

4.3.2 Fictitious Reference Iterative Tuning

The FRIT technique only utilizes the recorded input and output data of the plant to obtain the optimal parameters of the controller. Hence, this approach eliminates the needs of the mathematical model of the plant, as commonly practiced by the model-based control designer. Thus, the FRIT is totally a model-free approach.

Reconsider the closed loop block diagram shown in Fig. 4.1. Suppose the PID controller can be parameterized in ρ such that $G_c(\rho)$. Redefine the controller gains as $G_c(s) = K_p + \frac{K_i}{s} + K_d \frac{1}{1 + N_f s}$ where $K_p = K$, $K_i = K/T_i$ and $K_d = KT_d$, respectively. The initial arbitrary controller values are first to be selected, i.e. $\rho^0 := [K_p^0, K_i^0, K_d^0, N_f^0] \in \mathbb{R}^4$. Then, the one-shot of experiments has to be performed, in which the input data u^0 and ω^0 are measured and recorded. These recorded data can then be used to design and formulate the fictitious refer-ence input signal. In Fig. 4.3, we illustrate the general concept of defining the fictitious signal where the

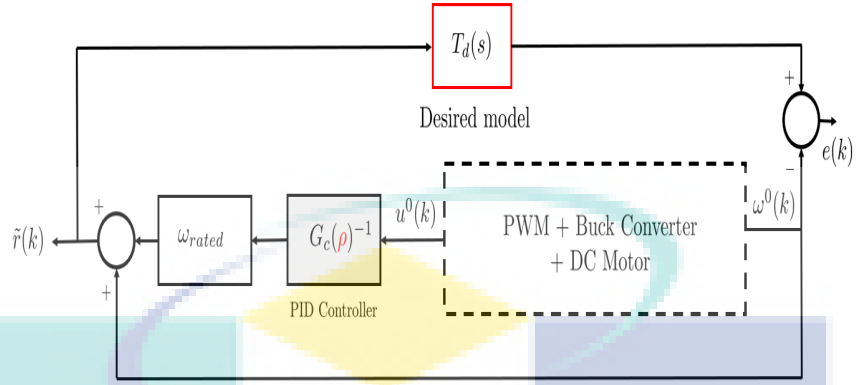


Figure 4.3: Fictitious signal $\tilde{r}(k)$ derivation

signal is formulated as follows:

$$\tilde{r}(k) = \omega_{rated} G_c(\rho)^{-1} u^0(k) + \omega^0(k). \quad (4.14)$$

Here, $u^0(k)$ and $\omega^0(k)$ are the recorded input-output data at the time-instant k , and $G_c(\rho)^{-1} = 1/G_c(\rho)$. Note that in formulating the fictitious signal (4.14), the subsystems consist of the PWM, buck converter and DC motor (as indicated in the dashed box of Fig. 4.3), are no longer required for signal generation.

By the selection of the fictitious signal (4.14), the optimization problem can be re-formulated. Instead of minimizing the cost function of equation (4.2), we can now define a new cost function of

$$\begin{aligned} J_2 &= \frac{1}{M} \|e(k)\|_M^2 = \frac{1}{M} \|T_d(s)\tilde{r}(k) - \omega^0(k)\|_M^2 \\ &= \frac{1}{M} \|T_d(s)(\omega_{rated} G_c(\rho)^{-1} u^0(k) + \omega^0(k)) - \omega^0(k)\|_M^2, \end{aligned} \quad (4.15)$$

where M is the total number of sampled-data taken from the time interval $t \in [t_0, t_f]$.

Thus, the new control objective is to find a set of optimal parameters such that

$$\rho^* = \arg \min_{\rho} J_2. \quad (4.16)$$

The following algorithm has been implemented in our work to attain the optimal parameter ρ^* .

- Step 1** : By arbitrary selection of ρ^0 , run one-shot experiment to generate the input-output data of u^0 and ω^0 .
- Step 2** : Initialize the SKF agents' position, $x(0)$ within the search space. Then, assigning $\rho := [K_p, K_i, K_d, N_f] = x$.
- Step 3** : Assigning the cost function J_2 of equation (4.15) as the SKF fitness function in equation (4.7).
- Step 4** : Iterate the SKF algorithm till t_{Max} to attain x_{true} .
- Step 5** : Assigning the final value of x_{true} at t_{Max} as the optimal parameters. This implies $\rho^* := x_{true} = \arg \min_{\rho} J_2$.
- Step 6** : Validate the performance of the closed-loop system. If the results are unsatisfying, repeat the procedure from **Step 2**.

4.4 Numerical Example

To demonstrate the effectiveness of our proposed method, we present a numerical example and the related results. The Matlab Simulation package has been utilized to perform the simulation analysis. We use the same parameters reported in [46] as follows: $L_a = 8.9 \times 10^{-3}$ H, $R_a = 6 \Omega$, $K_E = 0.0517$ Vs/rad, $K_M = 0.0517$ Vs/rad, $J = 7.95 \times 10^{-6}$ kgm², $R = 0.2 \Omega$, $L = 1.33 \times 10^{-6}$ H, $C = 470 \times 10^{-6}$ F, and $E = 24$ V. Meanwhile, the rated speed is obtained $w_{rated} = 464.22$. As reported in [46] and [43], we use a similar desired trajectory reference signal given by

$$r(t) = 75 (\tanh(30(t - 0.1) + 1)). \quad (4.17)$$

The dynamic model of the desired transfer function was chosen as a first order system of $T_d(s) = \frac{1}{0.01s+1}$. The PWM frequency was set to 1 kHz, with the selected sample-time $t_s = 0.1$ ms. The initial controller gains $\rho^0 = [0.5, 1.0, 0.25, 0.5]$ were used in generating the initial input-output data u^0 and ω^0 . Figure 4.4 depicts the angular velocity and duty cycle of the untuned system when we use the gain ρ^0 . These data were then adopted to form the fictitious reference signal $\tilde{r}(k)$ of (4.14).

Apart from the parameter setting of the buck-converter power DC motor system, the parameters of the SKF algorithm used in this work are as follows. The best values of P , Q and R as suggested in [54] are 1000, 0.5, and 0.5 respectively. Whereas, the number of agents is selected as $N = 1000$, which are bounded in the region of $x \in [1, 100]$. Figure 4.5 illustrates the convergence of the cost function (4.15) when we run the SKF algorithm with a maximum number of iterations $t_{Max} = 300$. It can be seen that the cost function already converged to 0.0751 when $k = 100$ and remained on this value for the rest of iterations. The optimal parameters that minimized J_2 were obtained $\rho^* = [1.3983, 96.0201, 1.0158, 1.0578]$. This implies the optimal PID parameters were $K^* = 1.3983$, $T_i^* = 0.0146$ s, $T_d^* = 0.7265$ s and $N_f^* = 1.5078$, respectively.

For performance comparison with a model-based controller, let the plant of the buck converter powered DC motor system be denoted as

$$G_p(s) = \frac{\omega(s)}{u(s)} := \left[\begin{array}{c|c} A & B \\ \hline C & D \end{array} \right] \quad (4.18)$$

$$\text{where } A = \begin{bmatrix} 0 & -\frac{1}{L} & 0 & 0 \\ \frac{1}{C} & 0 & -\frac{1}{C} & 0 \\ 0 & \frac{1}{L_a} & -\frac{R_a}{L_a} & -\frac{K_e}{L_a} \\ 0 & 0 & \frac{K_m}{J} & -\frac{B}{J} \end{bmatrix}, B = \left[\frac{1}{L} \quad 0 \quad 0 \quad 0 \right]^T, C = \left[0 \quad 0 \quad 0 \quad 1 \right], \text{ and}$$

$D = 0$. By choosing a State Feedback Controller with Integral Control (SFCI) in the form of $u(t) = -KX(t) + K_n \int e(t)$, where $X(t) := [i(t), v(t), i_a(t), \omega(t)]^T$ are the

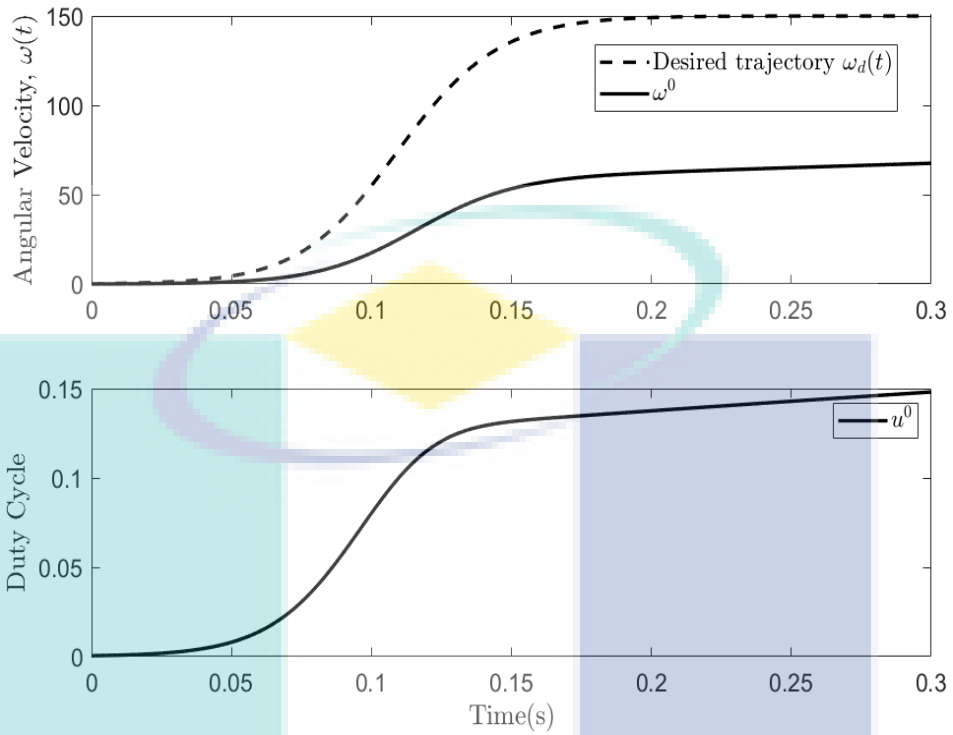


Figure 4.4: Angular velocity and duty responses for $\rho^0 = [0.5, 1, 0.25, 0.5]$ captured in a time interval $t_0 = 0$ s and $t_f = 0.3$ s.

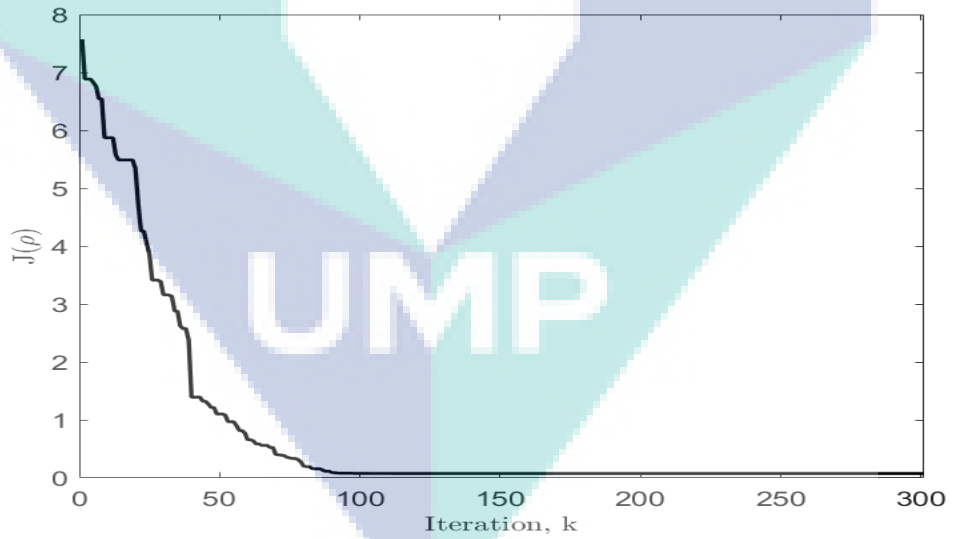


Figure 4.5: The convergence of the cost function J_2 .

state variables, $K^T \in \mathbb{R}^4$ is the state feedback gain, $K_n \in \mathbb{R}$ is the integral gain, and $e(t) = r(t) - CX(t)$ is the error. We employed the pole-placement method based on Bass & Gura's approach as discussed in [56] to obtain the controller gains K and K_n . It is worth mentioning that since the desired transfer function $T_d(s)$ was chosen

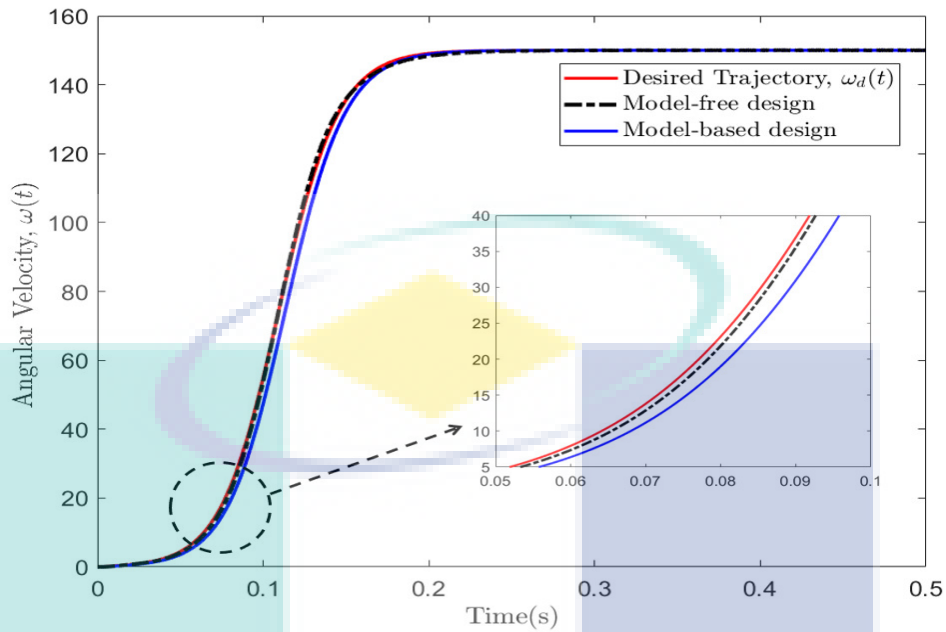


Figure 4.6: Performance comparison between the model-free design (PID controller tuned with FRIT and SKF) and model-based design (SFCI controller designed by pole-placement method).

as a first-order dynamic, slight modification has been performed to ensure the suitability of the selected model in obtaining the state feed-back gains. By doing so, the desired pole locations were chosen as the roots of the denominator polynomial of the transfer function $\tilde{T}_d(s) = T_d(s) \frac{(s+1000)^4}{(s+1000.01)^4}$. It can be clarified that the order of the desired model is raised from first order to the fifth order, but the dynamic of the output response is retained. With this approach, we obtained the values of the gains of the SFCI controller as $[K, K_n] = [4.5564, 1.3839, 6.0122, 1.0745, 85.5526]$.

Figure 4.6 exhibits the output responses of the closed system, utilizing the PID controller tuned by SKF and the SFCI controller designed by the pole placement method. Meanwhile, Fig. 4.7 depicts the comparison of the duty ratio output between the two controllers. Evidently, it can be observed that the output response of the PID controller tuned by FRIT and SKF exhibited better and faster performance as compared to the SFCI controller. This yields to the cost values J_1 of 0.1703 and 3.3659 for PID and SFCI controllers, respectively.

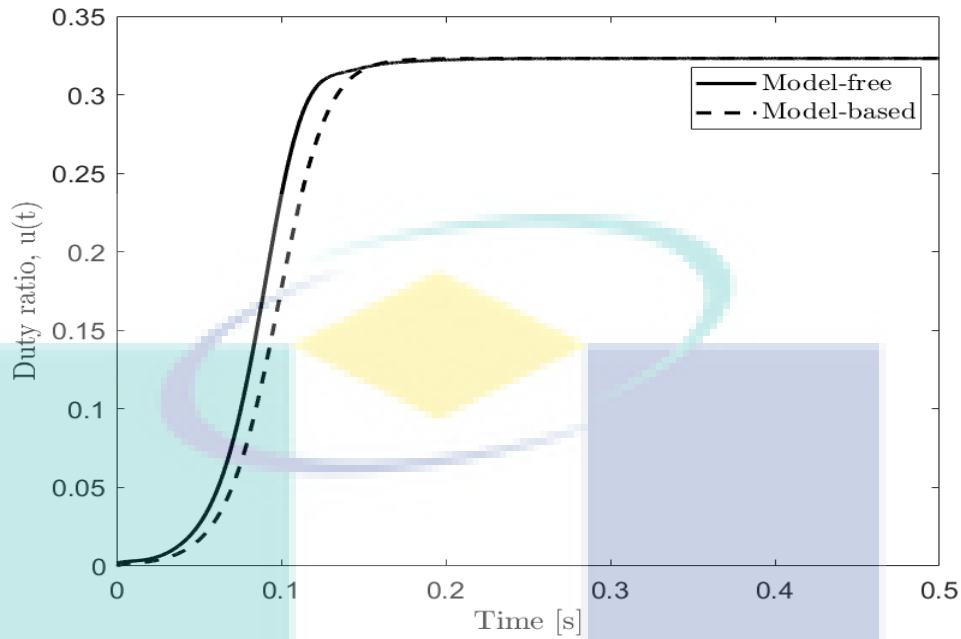


Figure 4.7: Performance comparison in terms of duty ratio between the two controllers.

4.5 Conclusion

In this chapter, we present the PID controller tuning method employing FRIT and SKF algorithm. Our presented model-free technique only utilized the set of input-output data to design the fictitious reference signal for the cost function minimization procedure. The performance of the controller has been investigated and validated through numerical simulation on a buck converter-powered DC motor system. A simple comparison with a state feedback controller designed using a model-based approach was also presented. It can be concluded that the PID controller tuned using the FRIT and SKF exhibits a better angular velocity trajectory tracking response as compared to the SFCI controller designed using the pole placement method. Furthermore, this approach is superior since it eliminates the needs for the mathematical modeling of the system-to-be-controlled in contrast to model-based controller design.

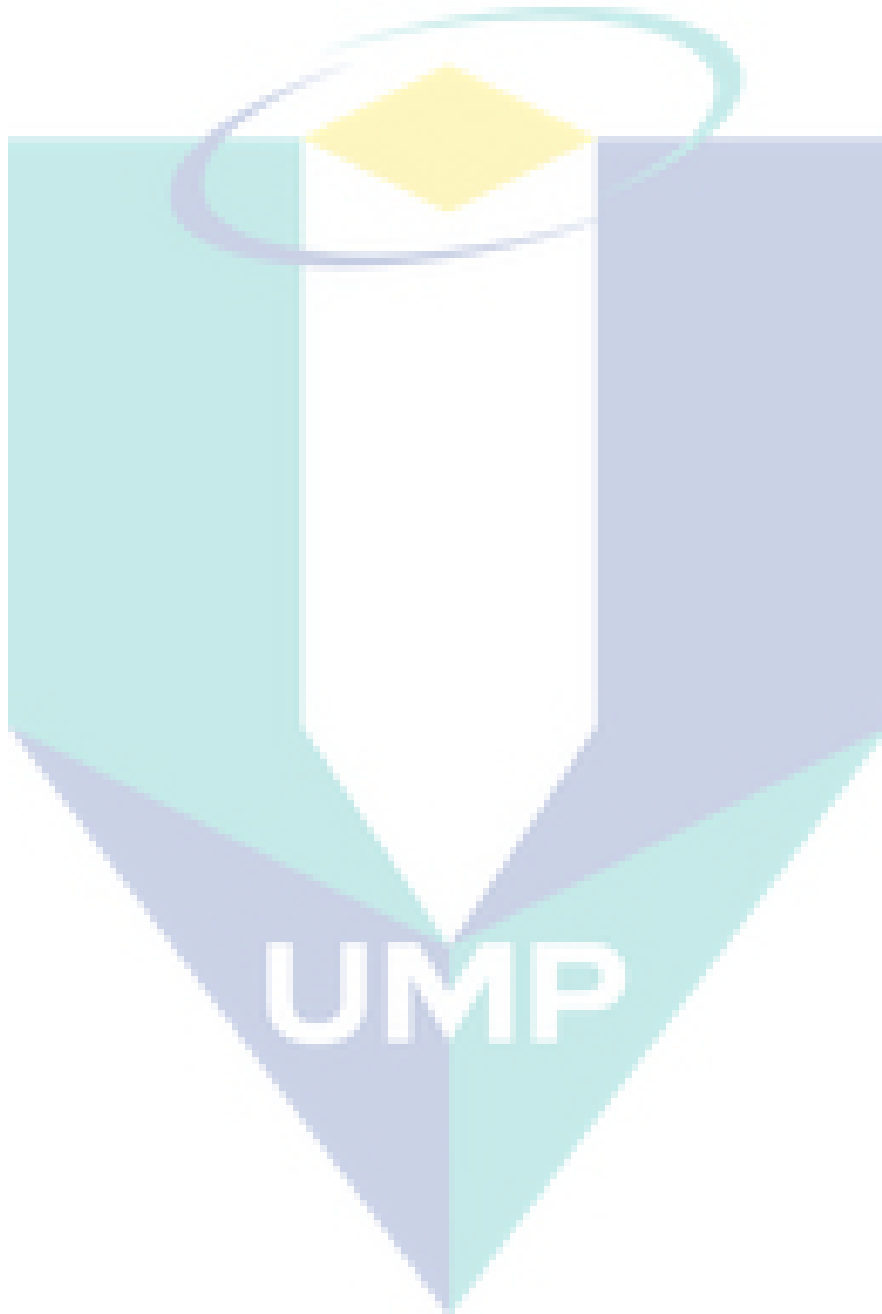
Chapter 5

Conclusion and Future Work

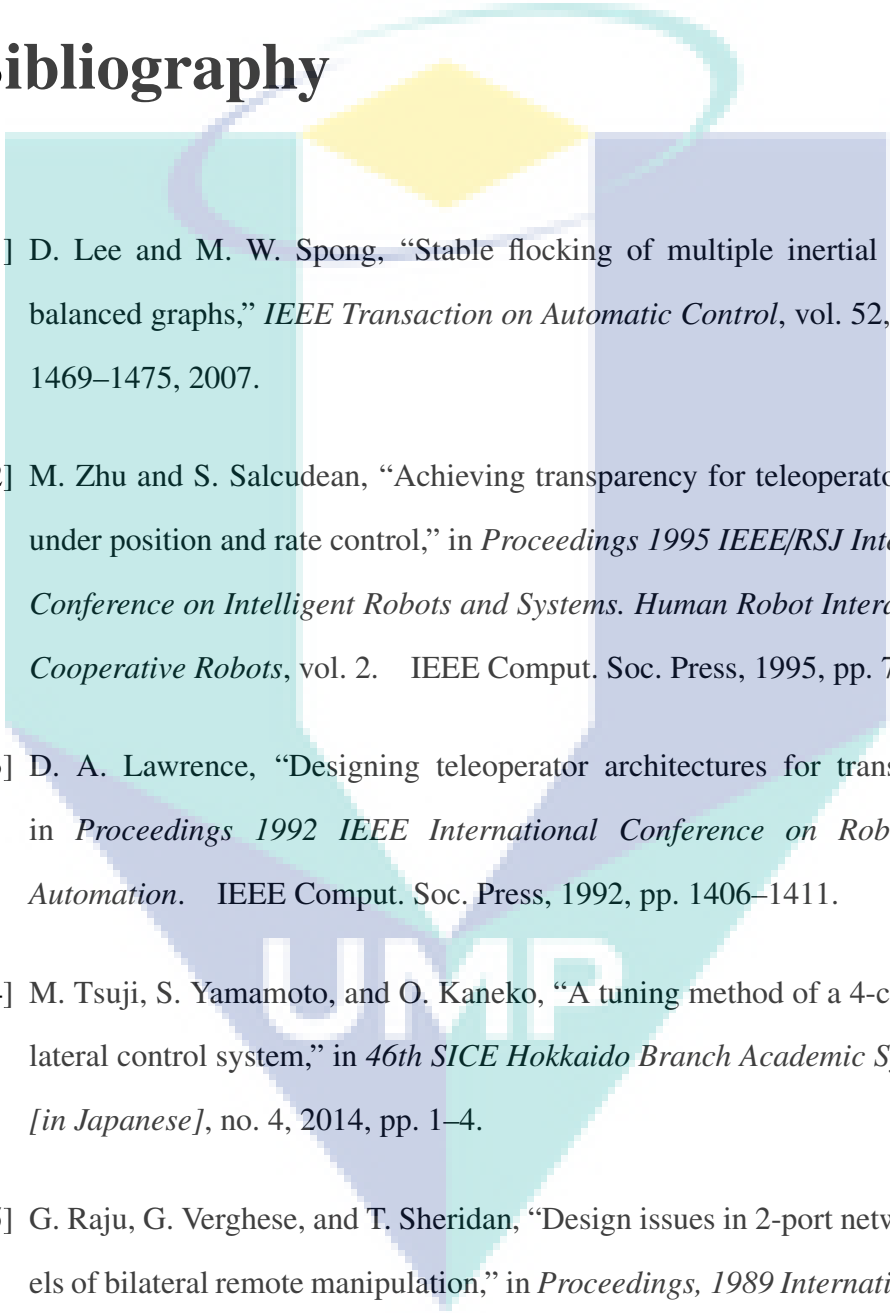
This project focus on investigating the feasible control techniques to attain a dynamical symmetric between the master and slave manipulators of a teleoperation systems. By introducing an equalizer or controller connected in-feedback loop to the master manipulator, it was found that a matched impedance between both sides of the system can be achieved. It was proposed that the Laguerre network structure to be chosen as the feasible controller, since it requires tuning only on the coefficients that formed the basis of the network.

Two different cases had been investigated in this project. For the first case where we aimed to attain a matched impedance between a single-master and single-slave manipulator, the Particle Swarm Optimization and FRIT had been utilized in tuning the chosen controller. Then in the later case, we considered the teleoperation system comprised of a single-master and multi-slave manipulators. Here, the passive decomposition and least square technique were the main findings in our work.

As for the current studies, we limit our investigation on the teleoperation system without the time delay. Since from practical point-of-view, there always exist some delays in the transmission of information from one subsystem to another. Hence, the effects of the time delay shall be taken into account in the future as part of the continuation of work from this project.



Bibliography

- 
- [1] D. Lee and M. W. Spong, “Stable flocking of multiple inertial agents on balanced graphs,” *IEEE Transaction on Automatic Control*, vol. 52, no. 8, pp. 1469–1475, 2007.
- [2] M. Zhu and S. Salcudean, “Achieving transparency for teleoperator systems under position and rate control,” in *Proceedings 1995 IEEE/RSJ International Conference on Intelligent Robots and Systems. Human Robot Interaction and Cooperative Robots*, vol. 2. IEEE Comput. Soc. Press, 1995, pp. 7–12.
- [3] D. A. Lawrence, “Designing teleoperator architectures for transparency,” in *Proceedings 1992 IEEE International Conference on Robotics and Automation*. IEEE Comput. Soc. Press, 1992, pp. 1406–1411.
- [4] M. Tsuji, S. Yamamoto, and O. Kaneko, “A tuning method of a 4-channel bilateral control system,” in *46th SICE Hokkaido Branch Academic Symposium [in Japanese]*, no. 4, 2014, pp. 1–4.
- [5] G. Raju, G. Verghese, and T. Sheridan, “Design issues in 2-port network models of bilateral remote manipulation,” in *Proceedings, 1989 International Conference on Robotics and Automation*, 1989, pp. 1316–1321.
- [6] N. D. Do and T. Namerikawa, “Four-channel force-reflecting teleoperation with impedance control,” *International Journal of Advanced Mechatronics Systems*, vol. 2, no. April 2009, pp. 318–329, 2010.

- [7] S. Sirouspour, "Modeling and control of cooperative teleoperation systems," *IEEE Transactions on Robotics*, vol. 21, no. 6, pp. 1220–1225, dec 2005.
- [8] D. Lawrence, "Stability and transparency in bilateral teleoperation," *IEEE Transactions on Robotics and Automation*, vol. 9, no. 5, pp. 624–637, 1993.
- [9] T. Namerikawa and H. Kawada, "Symmetric impedance matched teleoperation with position tracking," in *Proceedings of the 45th IEEE Conference on Decision and Control*, 2006, pp. 4496–4501.
- [10] K. Mohammadi, H. A. Talebi, and M. Zareinejad, "A novel position and force coordination approach in four channel nonlinear teleoperation," *Computers and Electrical Engineering*, vol. 56, pp. 688–699, 2016.
- [11] J. Zhang, W. Li, J. Yu, Q. Zhang, S. Cui, Y. Li, S. Li, and G. Chen, "Development of a virtual platform for telepresence control of an underwater manipulator mounted on a submersible vehicle," *IEEE Transactions on Industrial Electronics*, vol. 64, no. 2, pp. 1716–1727, 2017.
- [12] R. Saltaren, A. R. Barroso, and O. Yakurangi, "Robotics for seabed teleoperation: Part-1-Conception and practical implementation of a hybrid seabed robot," *IEEE Access*, vol. 6, pp. 60 559–60 569, 2018.
- [13] P. Berthet-Rayne, K. Leibrandt, G. Gras, P. Fraise, A. Crosnier, and G.-Z. Yang, "Inverse kinematics control methods for redundant snakelike robot teleoperation during minimally invasive surgery," *IEEE Robotics and Automation Letters*, vol. 3, no. 3, pp. 2501–2508, 2018.
- [14] J. Y. Chen and M. J. Barnes, "Robotics operator performance in a multi-tasking environment," in *Human-Robot Interactions in Future Military Operations*, 2008, pp. 293–314.

- [15] D. Sun, F. Naghdy, and H. Du, "Application of wave-variable control to bilateral teleoperation systems: A survey," *Annual Reviews in Control*, vol. 38, no. 1, pp. 12–31, 2014.
- [16] T. Kanno and Yasuyoshi Yokokohji, "Multilateral teleoperation control over time-delayed computer networks using wave variables," in *Haptics Symposium (HAPTICS), 2012 IEEE*, 2012, pp. 125–131.
- [17] M. S. Ramli and H. Ahmad, "Data-driven impedance matching in multilateral teleoperation systems," *Indonesian Journal of Electrical Engineering and Computer Science*, vol. 10, no. 2, pp. 713–724, 2018.
- [18] O. Kaneko, S. Soma, and T. Fujii, "A fictitious reference iterative tuning (FRIT) in the two-degree of freedom control scheme and its application to closed loop system identification," in *Proceedings of the 16th IFAC World Congress*, vol. 16, no. 1, 2005, pp. 626–631.
- [19] J. Kennedy and R. Eberhart, "Particle swarm optimization," in *Proceedings of ICNN'95 - International Conference on Neural Networks*, 1995, pp. 1942–1948.
- [20] Q.-c. Wang and J.-z. Zhang, "Wiener model identification and nonlinear model predictive control of a pH neutralization process based on Laguerre filters and least squares support vector machines," *Journal of Zhejiang University- SCIENCE C (Computers & Electronics)*, vol. 12, no. 1, pp. 25–35, 2011.
- [21] G. Wang, L. Zhang, D. Chen, D. Liu, and X. Chen, "Modeling and Simulation of Multi-legged Walking Machine Prototype," *2009 International Conference on Measuring Technology and Mechatronics Automation*, pp. 251–254, 2009.
- [22] N. D. Do and T. Namerikawa, "Four-channel force-reflecting teleoperation with impedance control," *International Journal of Advanced Mechatronic Systems*, vol. 2, no. 5/6, pp. 318–329, 2010.

- [23] L. Marton, Z. Szanto, P. Haller, H. Sandor, and T. Szabo, "Bilateral teleoperation of wheeled mobile robots working in common workspace," *IAES International Journal of Robotics and Automation*, vol. 3, no. 1, pp. 62–74, 2014.
- [24] D. D. Nam, Y. Yamashina, and T. Namerikawa, "Bilateral teleoperation of multiple cooperative robots with time-varying delay," *2010 IEEE International Conference on Control Applications*, pp. 2053–2058, sep 2010.
- [25] P. F. Hokayem and M. W. Spong, "Bilateral teleoperation: An historical survey," *Automatica*, vol. 42, no. 12, pp. 2035–2057, dec 2006.
- [26] C. Zervos, P. Bélanger, and G. Dumont, "On PID controller tuning using orthonormal series identification," *Automatica*, vol. 24, no. 2, pp. 165–175, 1988.
- [27] Q. G. Zhou and E. Davison, "A simplified algorithm for balanced realization of Laguerre network models," in *Proceedings of the 39th IEEE Conference on Decision and Control*, vol. 5, 2000.
- [28] T. O. e Silva, "Optimality conditions for truncated Laguerre networks," *IEEE Transactions on Signal Processing*, vol. 42, no. 9, pp. 2528–2530, 1994.
- [29] O. Kaneko, Y. Yamashina, and S. Yamamoto, "Fictitious reference tuning for the optimal parameter of a feedforward controller in the two-degree-of-freedom control system," *Proceedings of the IEEE International Conference on Control Applications*, vol. 4, no. 1, pp. 59–64, 2010.
- [30] S. Yamamoto and K. Okano, "Direct controller tuning based on data matching," in *SICE-ICASE International Joint Conference*, vol. 4028, no. C, 2006, pp. 4028–4031.
- [31] H. T. Nguyen, O. Kaneko, and S. Yamamoto, "Data-driven IMC for Non-Minimum Phase Systems - Laguerre Expansion Approach -," in *50th IEEE*

- Conference on Decision and Control and European Control Conference*, 2011, pp. 476–481.
- [32] M. Mesbahi and M. Egerstedt, *Graph theoretic methods in multiagent networks*. Princeton University Press, 2010.
- [33] H. Kawakami and T. Namerikawa, “Cooperative target-capturing strategy for multi-vehicle systems with dynamic network topology,” in *American Control Conference*, 2009, pp. 635–640.
- [34] P. Aadaleesan and P. Saha, “Nonlinear System Identification Using Laguerre Wavelet Models,” in *International Conference on Modelling and Simulation*, vol. 3, 2007, pp. 189–194.
- [35] B. Wahlberg, “System identification using Laguerre models,” *IEEE Transactions on Automatic Control*, vol. 36, no. 9143255, pp. 551–562, 1991.
- [36] F. Parasiliti, M. Villani, and M. Castello, “PM Brushless DC Motor with exterior rotor for high efficiency household appliances,” in *Proceedings - 2014 International Conference on Electrical Machines, ICEM 2014*. IEEE, 2014, pp. 623–628.
- [37] C. Hwang, P. Li, C. Liu, and C. Chen, “Design and analysis of a brushless DC motor for applications in robotics,” *IET Electric Power Applications*, vol. 6, no. 7, p. 385, 2012.
- [38] D. Rajesh, D. Ravikumar, S. K. Bharadwaj, and B. K. S. Vastav, “Design and control of digital DC drives in steel rolling mills,” in *Proceedings of the International Conference on Inventive Computation Technologies, ICICT 2016*, vol. 2016. IEEE, 2016, pp. 1–5.
- [39] B. D. Hall, “Notes on complex measurement uncertainty – part 1,” no. November, 2010.

- [40] R. Silva-Ortigoza, V. M. Hernández-Guzmán, M. Antonio-Cruz, and D. Muñoz-Carrillo, "DC/DC buck power converter as a smooth starter for a DC motor based on a hierarchical control," *IEEE Transactions on Power Electronics*, vol. 30, no. 2, pp. 1076–1084, 2015.
- [41] A. Beevi and M. Noufal, "Hierarchical Control For a Buck Converter Driven DC Motor," *International Journal of Advanced Research in Electrical Electronics and Instrumentation Engineering*, vol. 5, no. 9, pp. 7218–7224, 2016.
- [42] E. Hernandez-Marquez, R. Silva-Ortigoza, S. H. Dong, V. H. Garcia-Rodriguez, G. Saldana-Gonzalez, and M. Marcelino-Aranda, "A New DC/DC Buck-Boost converter-DC motor system: Modeling and simulation," in *Proceedings - 2016 International Conference on Mechatronics, Electronics, and Automotive Engineering, ICMEAE 2016*, 2016, pp. 101–106.
- [43] M. Ahmad, R. Raja Ismail, and M. Ramli, "Control Strategy of Buck Converter Driven Dc Motor: a Comparative Assessment," *Australian Journal of Basic and Applied Sciences*, vol. 4, no. 10, pp. 4893–4903, 2010.
- [44] J. Linares-Flores and H. Sira-Ramírez, "Sliding Mode-Delta Modulation GPI Control of a DC Motor through a Buck Converter," in *IFAC Proceedings Volumes*, vol. 37, no. 21, 2017, pp. 405–410.
- [45] M. A. Kamarposhti, T. Tayebbifar, M. Shaker, and P. Nouri, "The control of buck boost DC-DC converters for DC motor drives on variable DC voltage by using neural network," *Life Science Journal*, vol. 10, no. 5, pp. 236–240, 2013.
- [46] M. A. Ahmad and R. M. Ismail, "A data-driven sigmoid-based PI controller for buck-converter powered DC motor," in *ISCAIE 2017 - 2017 IEEE Symposium on Computer Applications and Industrial Electronics*, 2017, pp. 81–86.

- [47] G. Li and L. Liu, "Robust Adaptive Coordinated Attitude Control Problem with Unknown Communication Delays and Uncertainties," *Procedia Engineering*, vol. 29, pp. 1447–1455, jan 2012.
- [48] G. Battistelli, D. Mari, D. Selvi, and P. Tesi, "Unfalsified approach to data-driven control design," in *Proceedings of the IEEE Conference on Decision and Control*, vol. 2015-Febru, no. February. IEEE, 2014, pp. 6003–6008.
- [49] O. Saleem and M. Rizwan, "Performance optimization of LQR-based PID controller for DC-DC buck converter via iterative-learning-tuning of state-weighting matrix," *International Journal of Numerical Modelling: Electronic Networks, Devices and Fields*, no. December 2018, pp. 1–17, 2019.
- [50] G. Rallo, S. Formentin, C. R. Rojas, and S. M. Savaresi, "Robust Experiment Design for Virtual Reference Feedback Tuning," in *Proceedings of the IEEE Conference on Decision and Control*. IEEE, 2018, pp. 2271–2276.
- [51] O. Kaneko, S. Soma, and T. Fujii, "A fictitious reference iterative tuning (FRIT) in the two degree of freedom control scheme and its application to closed loop system identification," in *IFAC Proceedings Volumes*, vol. 38, no. 1. IFAC, 2005, pp. 626–631.
- [52] Z. S. Hou and Z. Wang, "From model-based control to data-driven control: Survey, classification and perspective," *Information Sciences*, vol. 235, pp. 3–35, 2013.
- [53] Z. Ibrahim, N. H. A. Aziz, N. A. A. Aziz, S. Razali, M. I. Shapiai, S. W. Nawawi, and M. S. Mohamad, "A Kalman filter approach for solving uni-modal optimization problems," *ICIC Express Letters*, vol. 9, no. 12, pp. 3415–3422, 2015.
- [54] Z. Ibrahim, N. H. Abdul Aziz, N. A. Nor, S. Razali, and M. S. Mohamad, "Simulated Kalman Filter: A novel estimation-based metaheuristic optimiza-

tion algorithm,” *Advanced Science Letters*, vol. 22, no. 10, pp. 2941–2946, 2016.

[55] R. Kalman, “A new approach to Linear Filtering and Prediction Problems,” *Transactions of the ASME—Journal of Basic Engineering*, vol. 82, no. D, pp. 35–45, 1960.

[56] M. S. Ramli and M. F. Rahmat, “Servomotor Control Using Direct Digital Control and State Space Technique,” *Jurnal Teknologi*, vol. 49, no. D, pp. 45–60, 2008.

